DENDRIMERS FOR CANCER THERAPY AND DIAGNOSTIC IMAGING

DENDRIMERS FOR CANCER THERAPY AND DIAGNOSTIC IMAGING

By

MATTHEW CRAIG PARROTT

B.Sc. (University of Western Ontario, London) 2002

A Thesis

Submitted to the School of Graduate Studies

In Partial Fulfillment of the Requirements

for the Degree of

Doctor of Philosophy

in

Chemistry

McMaster University

DOCTOR OF PHILOSOPHY	McMaster University
(Chemistry)	Hamilton, Ontario

TITLE:	Dendrimers for Cancer Therapy and Diagnostic Imaging
AUTHOR:	Matthew Craig Parrott, B.Sc. (University of Western Ontario, London)
SUPERVISOR:	Professor Alex Adronov
NUMBER OF PAGES:	xvi, 175

Abstract

The enhanced permeation and retention (EPR) effect is a phenomenon that allows macromolecular (or polymeric) structures to passively concentrate in tumour tissue. The large size and high molecular weight of macromolecular-drug conjugates increase their blood circulation time, which allows for significant accumulation in tumor tissue over an extended period of time. Linking chemotherapeutic agents to the backbone of water-soluble polymers has resulted in a number of polymer therapeutics currently in clinical trials.

A growing number of researchers are utilizing the EPR effect to develop new macromolecular-drug conjugates for the treatment and/or diagnostic imaging of diseased tissue. We have added to this research by constructing three novel carborane containing dendrimers for drug delivery. We were able to synthesize these materials using a bifunctional carborane synthon bearing a carboxylic acid and protected alcohol functionality. This bifunctional synthon could be integrated into an aliphatic polyester dendrimer using esterification conditions followed by further dendronization. This approach led to three water soluble dendrimers that contain 4, 8, and 16 hydrophobic carborane cages within their interior. The sensitive balance between the hydrophobic nature of the carborane cages and hydrophilic nature of the dendrimer scaffolds led to materials that had a lower critical solution temperature (LCST), a phenomenon where material precipitates from solution at high temperatures. The final dendrimers had a high molecular weight, were water soluble, and had a large concentration of boron encapsulated within the dendritic interior. These characteristics are ideal for potential agents for Boron Neutron Capture Therapy (BNCT), a well known treatment for cancer and rheumatoid arthritis. However, the inability to track each dendrimer in vivo and determine its biodistribution was a major drawback.

To overcome this limitation we synthesized three additional dendrimers. These dendrimers were synthesized to a high molecular weight using a unique orthogonal protecting group strategy. Following the removal of a toluene sulfonyl ethanol protecting group located at the core of the dendrimer, we were able to introduce a metal chelating ligand using standard amidation chemistry. This ligand was comprised of a tri-nitrogen bis-pyridyl moiety known to chelate an atom of radioactive technetium-99m with high affinity. Technetium-99m is the most widely used radionuclide in diagnostic nuclear medicine due to its ideal nuclear properties, low cost, widespread availability, and its ability to be tracked in vivo using Single Photon Emission Computed Tomography (SPECT). By placing the radioactive nuclide at the core of the dendrimer we were able to provide a unique environment that maintained overall dendrimer solubility characteristics, provided protection from the external environment, and minimized the interaction between the metal/ligand complex and biological tissues. These were the first dendritic compounds to utilize the core functionality for radioactive labeling, and the first dendritic compounds to chelate radioactive technetium-99m. Real-time dynamic SPECT and three dimensional SPECT-CT were performed on all three radioactive dendrimers, and an in depth biodistribution study was performed on the largest macromolecule.

This work opens the possibility for combining carborane-containing dendrimers with the ^{99m}Tc-label, allowing the potential development of a dendrimer that can 1) passively target diseased tissue via the EPR effect, 2) be tracked and imaged in vivo by SPECT, and finally 3) be used to treat diseased tissue by way of BNCT.

Acknowledgements

First and foremost I would like to thank my supervisor Prof. Alex Adronov for his constant encouragement, generous support, and for his mentorship. I know that the time spent in his laboratory and under his supervision has made me a better chemist and a better scientist.

Thank you to Prof. John Valliant for the time and effort he put into this project. As my co-supervisor, he provided a wealth of knowledge throughout the course of my studies.

A special thanks to Prof. Brian McCarry for his continued interest and helpful comments during committee meetings.

To all the members of the Adronov and Valliant groups, who have contributed to this work, thank you. All of you have made my time at McMaster extremely enjoyable and full of great memories. I wish you all the best and great success in the upcoming years.

This thesis could not have been possible without the love and support of my family. Both Sharron and Craig Parrott have always supported my decisions and helped me when the times were tough. Greg Bahun, although you are not my biological brother, no one has talked with me, fought with me, and laughed with me as much as you. I can not think of anyone I would rather call my best friend. Last and certainly not least, I would like to thank Dr. Rahima Benhabbour. I never thought I would find love in the lab, but you instantly took my attention away from column chromatography and showed me the sweeter side of life. You are a blessing in my life and I am better person when you are around. I look forward to our future together, and I promise to love and support you as much as you loved and supported me throughout this thesis.

Table of Contents

Page

List of Figures and Schemes

List of Figures **Page**

List of Schemes **Page**

Chapter 1 - Introduction

1.1. Introduction to Dendrimers

Dendrimers are perfect, monodisperse macromolecules with a regular and highly branched three dimensional architecture.[1] Similar structures containing branching patterns can be found in nature. For example, the branching patterns visible in lightning, the branches and root systems found in trees, and the detailed and symmetrical branching found in a snowflake. Interestingly, through evolutionary processes animals and humans have developed exceedingly complex dendritic solutions to enhance properties, including the dendritic network of bronchioles in lungs to increase oxygenation of blood, the perfusion of blood through a dendritic arterial network, and a dendritic central nervous system that can transport information from our surroundings to our brain.[2]

Polymer chemists have attempted to mimic this branching phenomenon for decades in the hopes that they may improve or even discover new polymer properties. The quest for branched polymeric architectures have led to the discovery of a number of novel structures, which include graft polymers, branched polymers, hyper-branched polymers, and dendrimers (Figure 1.1).

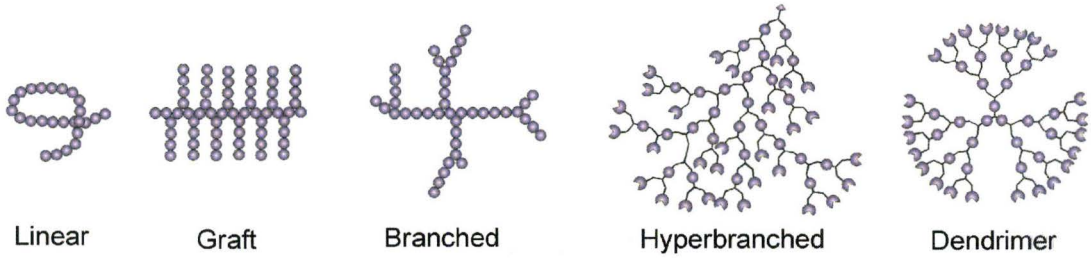

Figure 1.1. A schematic diagram of a linear polymer and the four major branched polymers.

Dendrimers are a unique class of branched polymer due to their structural control and perfection. The aforementioned polymer architectures contain numerous branching points, but the synthesis of each polymer is relatively uncontrolled, which leads to a mixture of similar compounds with a distribution of molecular weights. Dendrimers, on the other hand, are easily controlled and yield perfect molecules with one molecular weight.

1.2. Dendrimer Structure

In general, a dendrimer is comprised of three distinct components: (1) a core, (2) generations of branched repeat units (or monomers) radiating from the core, and (3) the outer layer of surface functionality (Figure 1.2). The surface functionalities dominate the dendrimers solubility characteristics, chemical reactivity, and glass transition temperature and are the boundary between the dendrimer and its macroscopic environment. The branching points provide a 3-dimensional structure, stability, and a site to increase the

number of surface functionalities. At the core, there is a unique environment that can encapsulate guest molecules and provide protection from the outside environment.[3]

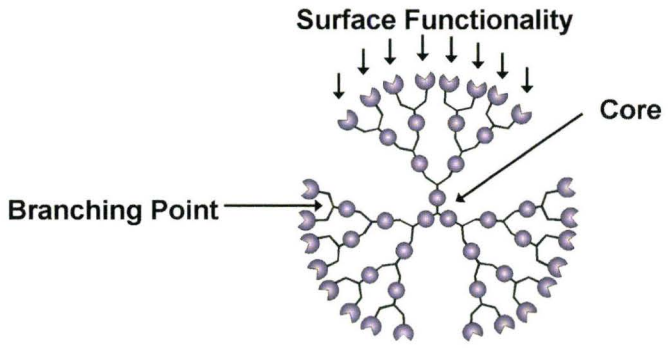

Figure 1.2. The three parts of the dendrimer: (1) the core, (2) branching points, and (3) surface functionality.

1.3. Dendrimers: A brief History

P.J. Flory made the following statement in 1952, and since this publication numerous research groups have focused on the creation of new branched-polymeric structures.

> "Highly branched polymer molecules may be synthesized through the use of a single monomer comprised of one functional group (A) and two or more of another functional group (B) capable of reacting with one another."[4]

A representative schematic of this can be seen in Figure 1.3, where a monomer comprised of one functional group (A) and two separate functional groups (B) can

be reacted to form the random and highly disperse hyperbranched polymer or the synthetically perfect and monodisperse dendrimer.

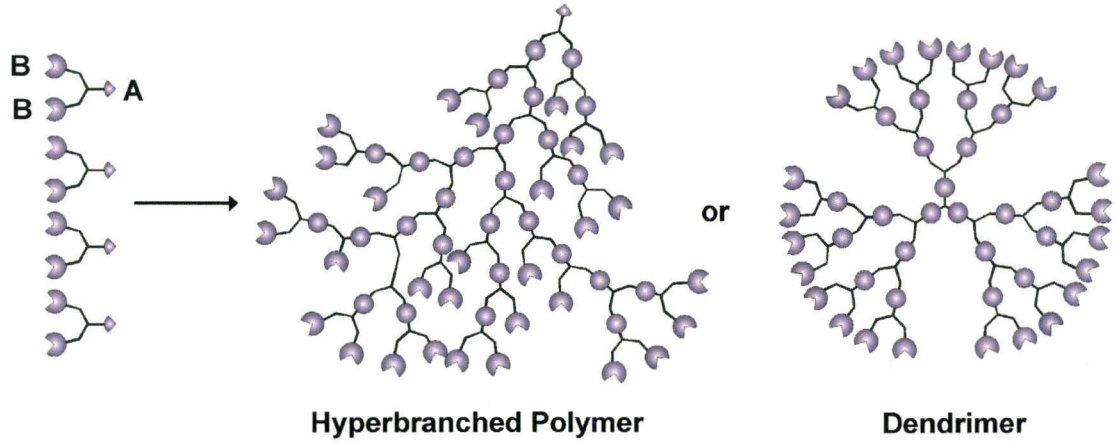

Figure 1.3. The polymers architectures predicted by Flory using an AB2 monomer.

The development of a synthetically pure, monodisperse, 3-dimensional polymer has taken over 20 years and required a number of advances to succeed.

The first milestone came in 1978 when Vogtle became the first chemist to design and synthesize low molecular weight branched polymers.[5] The stepwise process began with a Michael addition reaction with an amine and excess acrylonitrile, followed by a reduction of the nitrile moieties with Co(III) and sodium borohydride ($NaBH_4$) (Figure 1.4). These cascade polymers were the beginnings of dendritic macromolecules, but were plagued with low yields and difficult purification steps.[6]

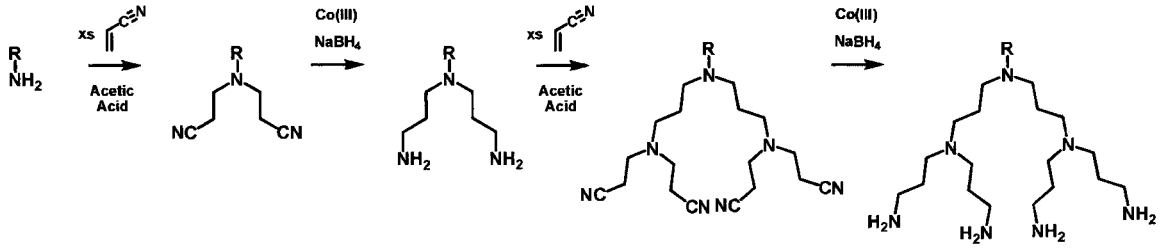

Figure 1.4. The stepwise synthesis of low molecular weight branched polymers.

In 1985, the first paper using the term dendrimer was published by Tomalia.[7] This seminal work detailed the intricate and laborious chemistry required to synthesize large macromolecular dendrimers. The iterative methodology also utilized a Michael addition reaction with ammonia and methyl acrylate followed by an amidation reaction between the methyl esters and a large excess of ethylenediamine (Figure 1.5). This synthesis afforded the first family of dendrimers with molecular weights ranging between several hundred to over 1 million Daltons.[6] Due to the success and high fidelity of this synthesis these dendrimers, coined polyamidoamine (PAMAM) dendrimers, are produced commercially and are the most widely used material in dendrimer chemistry.

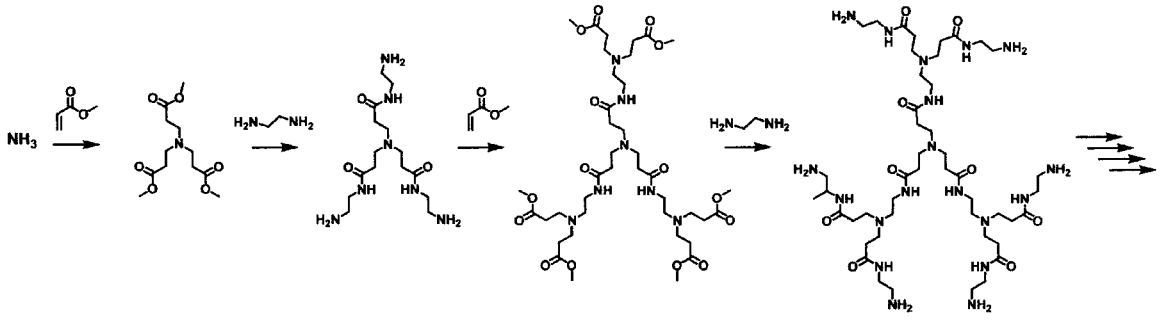

Figure 1.5. The stepwise synthesis of polyamidoamine (PAMAM) dendrimers.

Further optimization of the Vogtle cascade polymers was performed by Meijer in 1993.[8] Similar to the cascade synthesis, polypropylene imine (PPI) dendrimers were synthesized by an iterative combination of a Michael addition reaction with 1,4-diaminobutane and acrylonitrile, followed by a hydrogenation of the nitrile moieties with Raney cobalt and hydrogen gas (Figure 1.6). The resulting PPI dendrimers are the second most widely used in dendrimer research, and the high purity and high yielding synthesis allows these materials to be made on an industrial scale.

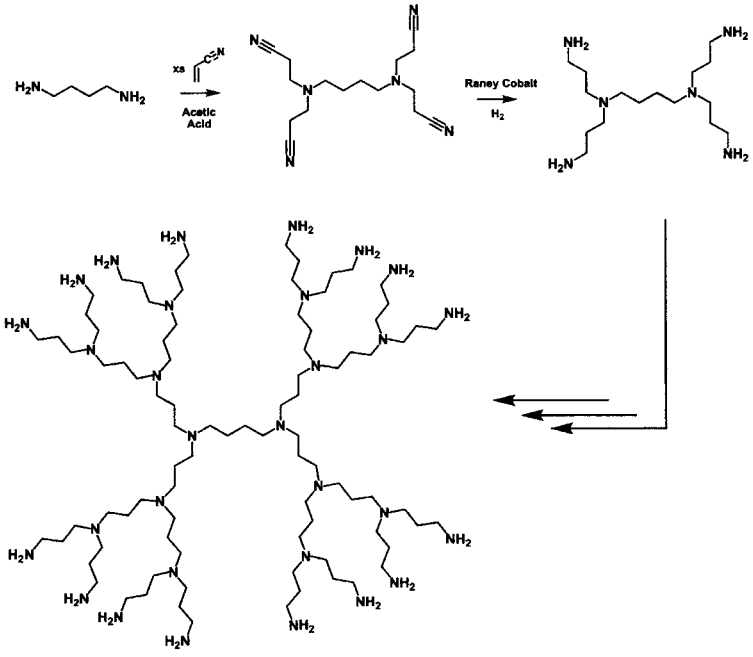

Figure 1.6. The stepwise synthesis of polypropyleneimine (PPI) dendrimers.

The final breakthrough in dendrimer chemistry came from Hawker and Fréchet in 1990.[9, 10] Up to that point all dendrimers were synthesized using a divergent synthesis where each layer or generation radiates from a central core outward (more details can be seen in Section 1.4.1). The Fréchet convergent method introduced a second synthetic

strategy where the process is started at the periphery and moves inward towards the core. The convergent dendrimer synthesis provided greater structural control due to the low number of reactions, and it also provided the ability to precisely place functional groups throughout the structure and more importantly it yielded extremely pure and defect free dendrimers. This will be elaborated on in Section 1.4.2.

1.4. Dendrimer Synthesis

As mentioned above, there are two general methods used to synthesize a dendrimer, either by a divergent approach or by a convergent approach.

1.4.1. Divergent Synthesis

The divergent dendrimer synthesis was first introduced by Tomalia,[7] Newkome,[11] and Vogtle[5] and was the first synthetic strategy employed. The divergent approach originates from a central core and is built up generation by generation (Figure 1.7). Dendrimer growth proceeds when functional groups on a core molecule are coupled with complementary reactive moieties on monomers. By using an excess of monomer, the dendrimer growth reaction can be driven to completion to yield a new layer on the core molecule, or a first generation (G1) dendrimer. Peripheral functional groups are typically blocked or protected to prevent uncontrolled hyper-branched polymerization during the dendrimer growth. Therefore, following the dendrimer growth reaction an activation reaction is required to unblock or deprotect these peripheral functionalities. The activation step provides the necessary functionality for a subsequent dendrimer growth

reaction, and the iterative process of dendrimer growth followed by peripheral activation can be continued to produce monodisperse, multi-layered dendrimers.

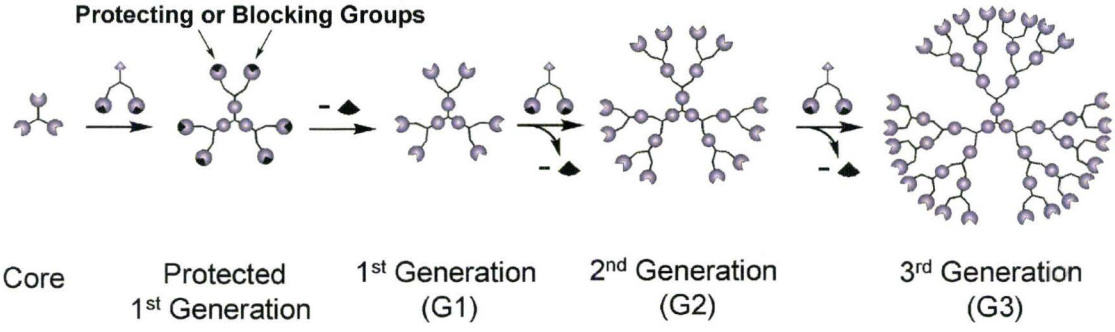

Figure 1.7. The divergent approach to dendrimer synthesis.

Dendrimers developed utilizing this strategy are easily separated from smaller starting materials by distillation, filtration and precipitation.[3] In addition, the molecular weight of these materials, and therefore the amount of dendrimer synthesized, doubles with each generation making this approach ideal for commercial applications. This strategy is limited due to the exponential increase of peripheral functionality. If, for example, the core starts with 3 functional groups, then generations 1 through 5 will have 6, 12, 24, 48, and 96 surface functional groups respectively. The increase in surface functionality also increases the number of reactions that must occur in order to produce a dendrimer of the next generation in pure form. The exponential increase in peripheral reactions amplifies the likelihood of incomplete reactions of the end groups and typically leads to significant amounts of structural imperfections at high generations.

1.4.2. Convergent Synthesis

As mentioned in Section 1.3, the convergent approach was first introduced by Hawker and Fréchet,[9, 10] and later by Miller and Neenan.[12, 13] Unlike the divergent methodology where the dendrimer is synthesized from the core outward, the convergent growth begins at the exterior and moves inward toward a central core (Figure 1.8). Two peripheral branching monomers are reacted with one central monomer through complementary functional groups. This forms a dendritic wedge known as a dendron. The dendron is activated at one single point, and reacted with an additional monomer. Like the divergent synthesis, this method uses an iterative stepwise sequence of growth reactions followed by activation steps. To complete the synthesis, the dendrons are reacted with a central core to form the desired dendrimer.

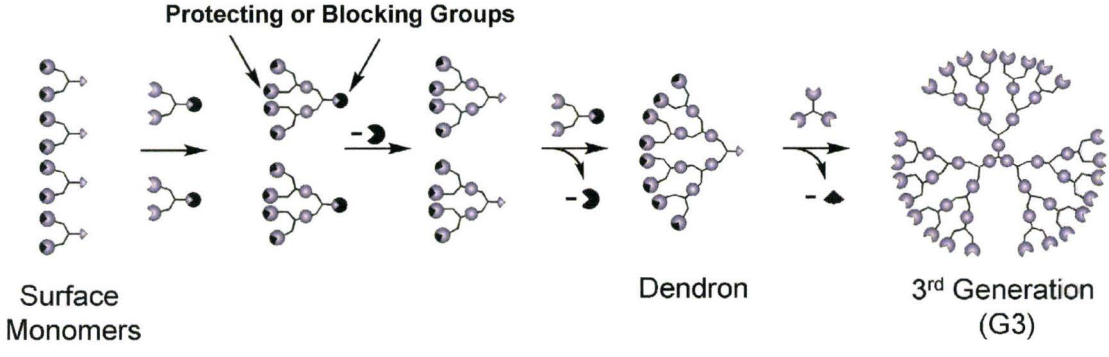

Figure 1.8. The convergent approach to dendrimer synthesis.

This method leads to dendrimers that are synthetically pure and monodisperse. The high purity in which these dendrimers can be prepared is attributed to the small number of reactions required at each generation growth step (typically two or three

dendrons are coupled to a monomer or core unit). Therefore, if a single coupling reaction does not occur, the imperfect product will have a molecular weight approximately half that of the fully coupled product, allowing facile purification by column chromatography. However, the convergent synthesis has several limitations, including the need for extensive purification at each generation, which results in lost time and decreased yields. In addition, as the dendrons increase in generation, the reactivity to the next generation or to the core decreases due to the steric bulk around the single interior functionality. Finally, unlike for the divergent synthesis, as the dendrimer generation increases, the overall yield and mass of the product decreases dramatically relative to the starting material.

1.5. Material Applications

Due to the number of synthetic steps and the high cost of multi-step syntheses there are a limited number of commercial applications for dendrimers. Academia has revealed several applications that utilize the unique 3-dimensional shape, core microenvironment, and the abundant surface functionalities found in dendrimers. From early on, dendrimers were seen to be similar to globular proteins and enzymes, and this vision prompted researchers to investigate a number of similar functions including molecular transport and encapsulation, energy transfer and storage, and catalysis (Figure 1.9). This led to the discovery of the "dendritic box",[14] where guest molecules can be encapsulated within a dendrimer and released in a controlled fashion (Figure 1.9A).[15] This also encouraged researchers to synthetically mimic the 3-dimensional, multi-

chromophore containing,[16] photosynthetic system for light harvesting[17] and energy transfer (Figure 1.9B).[18-20] Additional applications for catalysis were investigated and led to dendrimers that could attract reactants toward a catalytic core and following a reaction, could expel the products away from the structure (Figure 1.9C).[21, 22]

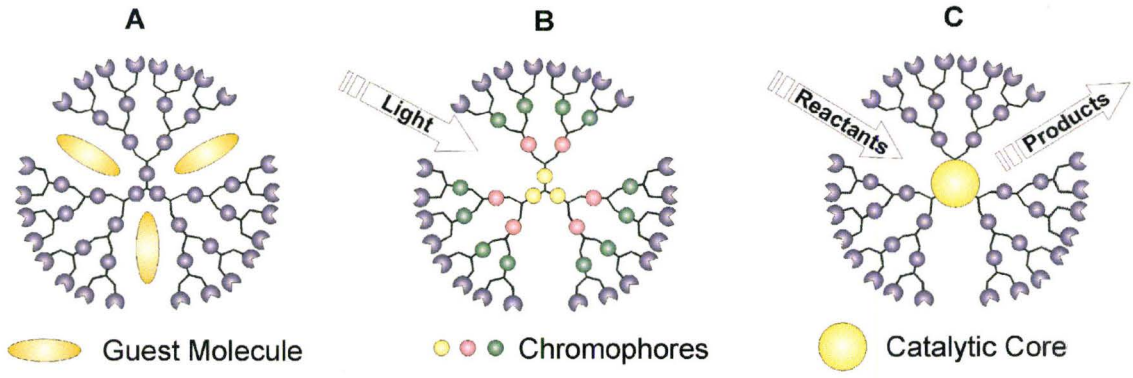

Figure 1.9. Representative images of dendrimers for guest molecule encapsulation (A), light harvesting and energy storage (B), and catalysis (C).

1.6. Polymer Therapeutics

By far, the largest effort in dendrimer chemistry over the past 30 years has focused on biological applications. The integration of polymer science and pharmaceutical science, coined polymer therapeutics, has rapidly advanced from a laboratory curiosity to a significant area of research and development.[23, 24] Specifically, a drug conjugated to a water-soluble, biocompatible polymer has been found to enhance a drug's plasma half-life, stability against degradation, solubility, and targeting efficiency while reducing drug clearance and immunogenicity.[25] Several polymeric drug delivery

agents for cancer chemotherapy, especially in targeting solid tumours, are now in clinical trials.[26]

Furthermore, large polymeric scaffolds (size > 5 nm, molecular weight > 50 kDa)[26, 27] are also known to provide a means to passively target tumour tissue.[28] Due to the rapid growth of a tumour, the vasculature is typically highly permeable or "leaky". Leaky vasculature allows macromolecular polymers to cross the endothelial layer and penetrate into the tumour. In addition, the rapid growth also minimizes the lymphatic drainage, which effectively traps the polymer within the diseased tissue. Combined, these factors lead to the selective accumulation of macromolecules in a tumour, a phenomenon known as the enhanced permeation and retention (EPR) effect (Figure 1.10).[24, 28, 29] This phenomenon has resulted in polymer-drug conjugates that accumulate 10-100 times more efficiently into tumours than the native drug.[30]

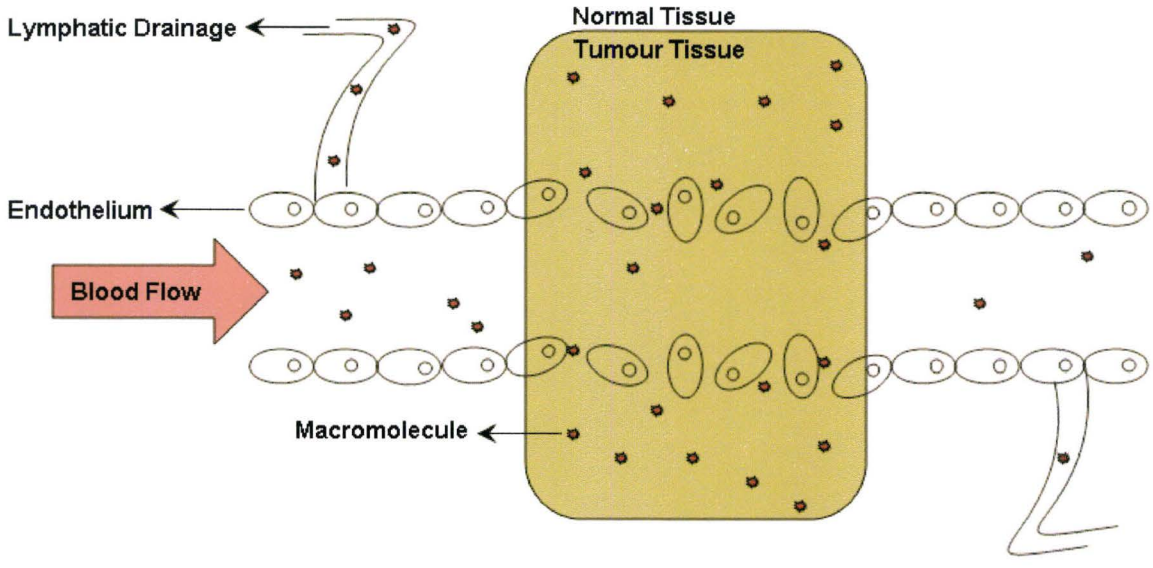

Figure 1.10. A representation of the enhanced permeability and retention (EPR) effect.

1.7. Dendrimers vs. Linear Polymers for Biological Applications

By comparing the dendritic architecture against the linear polymer architecture, one can see a number of advantages present in dendrimers that are not present in linear polymers. Aside from the 3-dimensional shape, core microenvironment, and the abundant surface functionalities already mentioned, dendrimers provide a means to increase the synthetic control over the number and placement of targeting moieties, drug moieties, and solubilizing groups. In addition, dendrimers provide a globular structure that closely resembles proteins and enzymes, and finally the low polydispersity of dendrimers should provide reproducible pharmacokinetic and pharmacodynamic performance.[31]

1.8. Biocompatible Dendrimers

Commercially available PAMAM, and PPI dendrimers have been widely studied for biological applications.[32, 33] However, due to abundant amines throughout the structure, these dendrimers become polycationic in vivo, are known to accumulate in the liver and are highly toxic.[32, 34] For dendrimers to be applicable for biological processes they must fulfill the following criteria: they must be water soluble, non-toxic, non-immunogenic, able to cross biological barriers (intestine, blood-tissue interfaces, cell membranes etc.), remain in circulations for the desired clinical application to take effect, and be able to target specific tissues.[35]

To meet these requirements several new classes of biologically relevant dendrimers have been developed. Of these, one promising example is an aliphatic polyester dendrimer structure that was first synthesized by Hult[36] and later modified by

Fréchet.[37, 38] The synthesis is based on 2,2-bis-(hydroxylmethyl)propionic acid (bis-MPA) and leads to a water soluble, biocompatible, and biodegradable system that is useful in anticancer drug delivery systems.[39-41] Other elegant dendritic systems have been able to incorporate monomers that are found in various metabolic pathways. Grinstaff has been able to design two dendrimer families that degrade into glycerol and succinic acid,[42, 43] or glycerol and lactic acid,[44] and both have been used for tissue engineering and tissue repair. Moreover, a number of groups have investigated polypeptide dendrimers to imitate proteins. The most well known polypeptide dendrimer is synthesized solely from the amino acid lysine, and provides a potential candidate for vaccines, antiviral medication, and antibacterial medication.[45, 46]

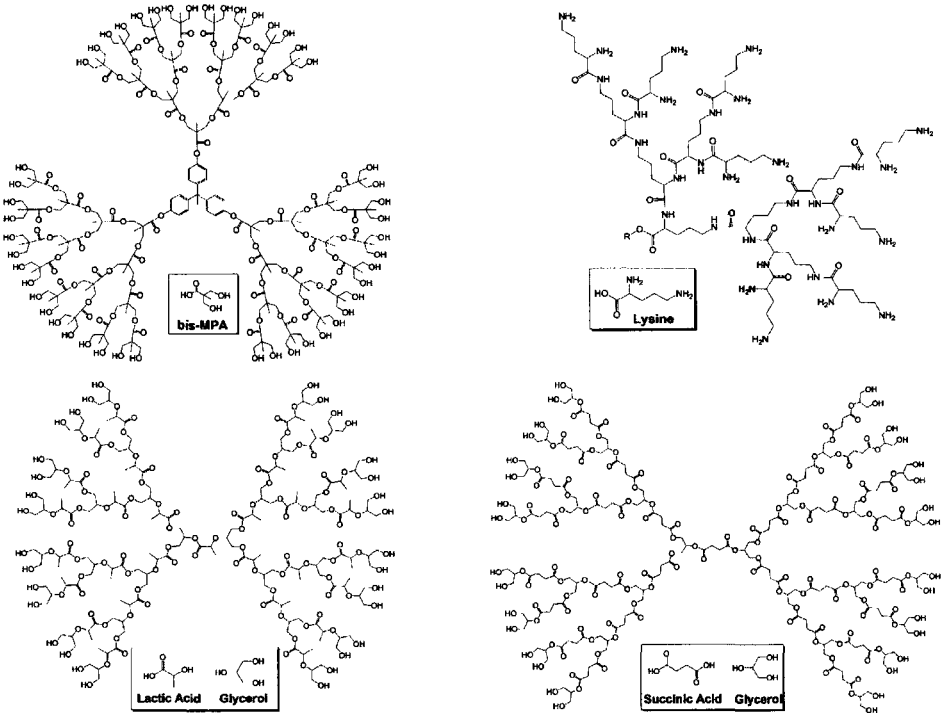

Figure 1.11. Biologically compatible dendrimers based on bis-MPA, lysine, lactic acid and glycerol, and succinic acid and glycerol.

1.9. Dendrimers for Biological Applications

The large number of biological applications of dendrimers documented in the literature has given rise to numerous reviews,[2, 27, 31, 35] and a detailed description of them all is beyond the scope of this thesis. In general, most biological applications fall under three categories (1) the delivery of non-covalently encapsulated therapeutics (eg. 5-fluorouracil,[47] methotrexate,[48] doxorubicin[48]) via the dendritic box; (2) the delivery of covalently-bound therapeutics (eg. cisplatin,[49] cytarabine,[50] methotrexate[51]) forming a dendrimer-drug conjugate and (3) the use of dendrimers for tissue engineering and tissue repair using biodegradable and biocompatible monomers.[52-54]

This thesis will focus on the following biological applications found in dendrimer chemistry: (1) the covalent attachment of boron-10 within a dendrimer to provide a potential polymer therapeutic for boron neutron capture therapy (BNCT), and (2) the development and synthesis of dendrimers for *in vivo* diagnostics for single photon emission computed tomography (SPECT).

1.10. Boron Neutron Capture Therapy (BNCT)

Following the discovery of the neutron[55] and the detection of a neutron capture event that occurs for boron-10,[56, 57] Locher proposed the potential use of boron-10 as a treatment for cancer, in 1935.[58] The treatment was named Boron Neutron Capture Therapy or BNCT, and to this day it is believed that this binary approach can be an effective technique for cancer treatment.[59] The two components of this binary approach are slow thermal neutrons and ^{10}B nuclei. Separately, these components are non-toxic *in*

vivo, however, when a stable ^{10}B nucleus (20% natural abundance) is irradiated with slow thermal neutrons it produces an unstable ^{11}B species that undergoes an instantaneous nuclear fission reaction, producing high energy alpha particles (^{4}He) and ^{7}Li atoms (Figure 1.12).

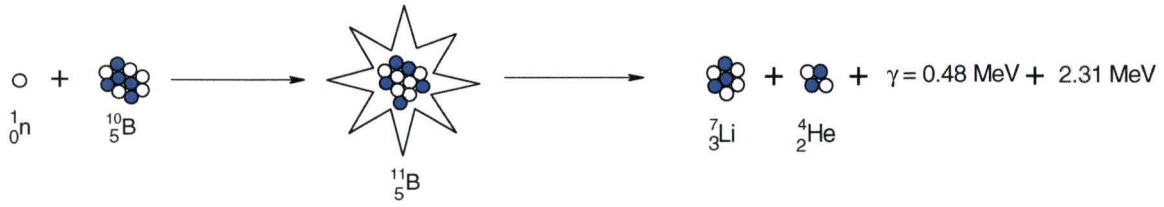

Figure 1.12. Representation of the neutron capture event for boron-10.

These charged particles have destructive path-lengths equal to one cell diameter and therefore leave most of their energy within cells containing boron. If ^{10}B nuclei are selectively delivered to tumour cells and low-energy neutrons reach this diseased tissue, the tumour cells can be selectively annihilated by the $^{10}B(n,\alpha)\ ^{7}Li$ nuclear reaction. In theory, BNCT offers a mechanism for a nuclear reaction to occur within specific diseased cells, while sparing any damage to healthy tissue.

1.11. Requirements for an Ideal BNCT Agent

The three vital criteria for clinically relevant BNCT agents include: (1) high boron concentration; (2) aqueous solubility; and (3) selective targeting to tumours. A high concentration of boron is required to decrease the probability of other light nuclei capturing neutrons. Other light nuclei that undergo neutron capture events are ^{1}H, ^{14}N and

^{35}Cl which have a neutron capture cross-section of 0.332, 1.82, and 32.68 barns, respectively.[60] Boron has the highest neutron capture cross-section of all light elements measuring 3,838 barns.[60] By introducing a minimum concentration of 10 μg of boron per gram of tumour tissue, the relative ability of the other light elements (within the tumour) to capture neutrons becomes negligible.[61] In order to achieve such high loadings of boron within tissues, the development of chemical structures containing a high number of boron atoms has been investigated over the past 60 years.

1.12. Early Examples of BNCT Agents

Initially, highly boronated compounds like sodium borate and boric acid derivatives were used (Figure 1.13).[62-64] However, due to the lack of slow-thermal neutron sources at the time and inadequate tumour selectivity these compounds were found to be ineffective as BNCT agents. In the mid 1950s, Hawthorne and co-workers discovered the polyhedral boron anions, $B_{10}H_{10}^{2-}$ and $B_{12}H_{12}^{2-}$.[65-67] This discovery led to a second generation of BNCT agents, which also failed clinical trails due to elevated boron concentration in the blood and therefore poor tumour selectivity. Within the last three decades, the neutral and isoelectronic analog of the $B_{12}H_{12}^{2-}$ anion, namely di-carbo-dodecaboranes ($C_2B_{10}H_{12}$), commonly known as carboranes, have attracted attention because of their organic nature, their high boron content, their size, their stability *in vivo*, and finally their ability to be chemically modified.[68]

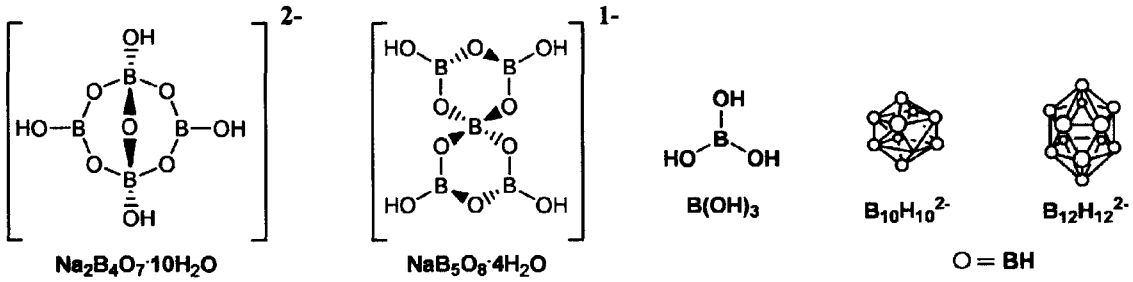

Figure 1.13. Early Examples of Boronated Compounds for BNCT (from left to right) borax, pentaborate, boronic acid, and polyhedral boron ions.

1.13. Isomers of Di-carbo-dodecaboranes or Carboranes ($C_2B_{10}H_{12}$)

The majority of carborane research is based on the 1,2-$C_2B_{10}H_{12}$ (ortho) isomer, however, an increase in the use of the 1,7-$C_2B_{10}H_{12}$ (meta) isomer and the 1,12-$C_2B_{10}H_{12}$ (para) isomer (Figure 1.14) has occurred because of the enhanced stability of these isomers toward degradation by various bases.[60]

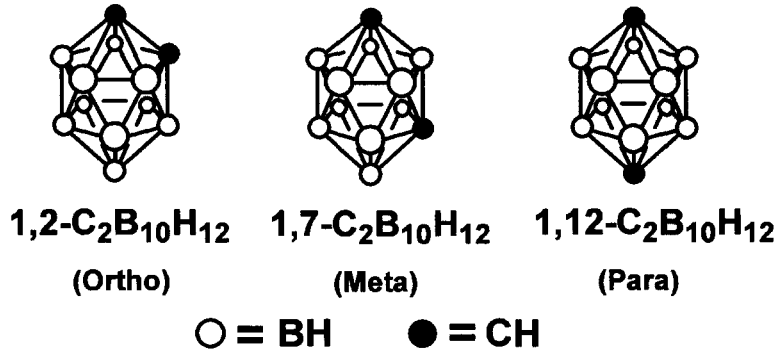

Figure 1.14. The ortho, meta and para isomers of di-carbo-dodecaboranes ($C_2B_{10}H_{12}$).

The aforementioned characteristics of these isomers substantiate that carboranes are versatile synthons for BNCT, however, the major disadvantage of carborane moieties is that they are extremely hydrophobic (comparable to the adamantyl group in lipophilicity)[69] and therefore not compatible with circulation within the blood stream.

1.14. Dendrimers for BNCT

Dendrimers present a highly adaptable polymeric architecture for the delivery of boron. First and foremost, dendrimers provide control over the amount of boron that can be charged within the structure. In addition, dendrimers can provide control over the molecular weight, a means to add targeting moieties on the periphery, and most importantly, dendrimers provide a scaffold that can take an extremely hydrophobic carborane and make it soluble in water.

Numerous research efforts have utilized these characteristics to produce highly boronated dendrimers for BNCT. The earliest dendrimer to incorporate carborane moieties was developed by Yamamoto, where he combined ortho-carborane clusters with a cascade-type tetraol to increase water solubility.[70] Additional dendritic structures containing carborane cages followed and included the well known PAMAM,[71] PPI,[72] and polylysine[73] dendrimers as well as metallo-dendrimers,[74] carbosilane-dendrimers[75] and Hawthorne's closomers.[76] Interestingly, only the PAMAM and polylysine dendrimers exhibited adequate water solubility, although neither dendrimer proved to be a viable BNCT agent due to the toxicity associated with the PAMAM dendrimers and the decrease in water solubility of the polylysine dendrimers when functionalized with

carborane cages.[73] The introduction of peripheral sulfate moieties on a hydrocarbon-based dendrimer yielded a highly water soluble dendrimer over a wide pH range, however, the biocompatibility of this hydrocarbon-based dendrimer was not reported.[77]

All of these examples include methodologies on incorporating a high boron concentration, and a few even illustrate how to incorporate water solubility. However, the remaining parameter for an ideal clinical BNCT is to selectively target tumours, and little effort has been invested in determining how these highly boronated dendrimer systems interact with biological tissue *in vivo*.

1.15. Dendrimers for Diagnostic Imaging

Simple modifications of dendritic structures have led to a number of materials that can be monitored *in vivo* using modern imaging techniques. *In vivo* imaging is an increasingly useful tool in biomedicine, as it is noninvasive and provides a wealth of information regarding the native states of a variety of tissues.[27] Images can be produced either by measuring the absorption of externally applied radiation (eg. magnetic resonance imaging (MRI), x-ray computed tomography (CT), and ultrasound) or by administering a small amount of radioactive material and detecting the radiation escaping from the body (eg. positron emission tomography (PET) and single photon emission computed tomography (SPECT)).[78] All of these techniques are routinely applied in hospitals, and have been utilized to monitor dendrimers as the progress through biological tissue. These techniques have provided information on circulation times,

biodistribution in various organs and tissues, and the localization of dendrimers within tumour tissues.

1.16. MRI and CT

The first technique,[79, 80] and the most widely used technique for *in vivo* imaging of dendrimers has been magnetic resonance imaging (MRI). Direct conjugation of gadolinium atoms to PAMAM[80, 81] and PPI[82] dendrimers via diethylenetriaminepentaacetic acid (DTPA) chelating agents gives macromolecular devices useful for the imaging of tumour structures, specific organs, and the lymphatic system.[83] The effect of molecular weight on tissue accumulation of these dendrimer-gadolinium conjugates has been determined. In general, dendrimer-gadolinium conjugates with molecular weights less than 60 kDa are excreted rapidly from the kidney.[80, 81] Larger (> 60 kDa), hydrophilic dendrimer-gadolinium conjugates have been shown to have long circulation times *in vivo,* while large, hydrophobic variants localize within the liver.[80, 81, 84] Based on size and polarity of the dendrimer-gadolinium conjugates, one can synthesize an agent capable of imaging the kidneys, the liver, circulating blood, and if conjugated with folate or monoclonal antibodies these conjugates can also be used to image tumour tissues.[85-87]

Similar strategies using PAMAM[88] and polylysine[89] dendrimers doped with a high concentration of iodine are currently being investigated as potential agents for x-ray computed tomography (CT). To date, an increase in blood circulation of large (>50 kDa) dendrimers has been observed,[89] however, there is limited information reported on the biodistribution of these materials.

1.17. Radioactive Dendrimers for Biodistribution

As the number of dendrimer chemistries used for biological applications increases, the ability to quantify how dendrimers navigate, and accumulate within biological tissues becomes progressively more important. The majority of researchers utilize radioactive iodine-125 due to the long half-life (60 days) and low γ-ray emission (35 keV).[90] The attachment of radioactive ^{125}I to dendrimers provides a method to monitor how radioactive macromolecules progress through a subject, and a means to quantify the amount of radioactivity distributed within various tissues.

The first example of radio-iodinated dendrimers utilized PAMAM structures with a large range of molecular weights (6.3 to 53 kDa).[32] These materials were rapidly cleared from circulation, and the majority of the radioactivity (60-90%) was found to localize in the liver. Biocompatible dendrimers based on bis-MPA, were also radio-iodinated with ^{125}I. The biodistribution of a fourth generation bis-MPA dendrimer (3.8 kDa) and a fourth generation bis-MPA dendrimer having tri(ethylene glycol) units tethered to the periphery (11.5 kDa) was studied.[41] Unlike the polycationic PAMAM dendrimers, this system remained uncharged and resulted in no visible toxicity *in vitro* and *in vivo*. It was observed that the majority of the radioactivity was rapidly eliminated through the kidney and excreted within 30 minutes.

Strategies to increase the bulk of the bis-MPA dendrimers led to the synthesis of a number of polymer-dendrimer hybrids called "bow-ties".[31, 91] The increase of molecular weight (M.W. = 45 - 160 kDa) and the overall size of these materials resulted in circulation half lives between 30 and 50 hours. Less than 4% of the radioactive dose was

found in the urine for these polymers, indicating that their effective sizes were above the threshold for renal filtration. Furthermore, these materials were radio-iodinated and injected into tumoured mice, and it was observed that 10-15% of the total radioactivity passively targeted the tumour after 48 hours.

These examples establish that valuable quantitative data can be collected and used to interpret how dendrimers progresses through biological tissues. The biggest shortcoming of this technique is that it requires the sacrifice of numerous animals and the time consuming harvesting of individual organs of interest. In addition, the radio-iodination typically occurs via a phenol-functionalized derivative on the surface of the dendrimer, which increases liver uptake and effectively alters the true biodistribution of the original dendrimer.[39, 41, 92]

1.18. Technetium-99m and Single Photon Emission Computed Tomography (SPECT)

Radioactive technetium-99m and single photon emission computed tomography (SPECT) offer a non-invasive alternative to the cut-and-count technique used for ^{125}I. Technetium-99m (^{99m}Tc) has become the most widely used radionuclide in diagnostic nuclear medicine and is employed in the majority of the diagnostic scans performed each year.[93] Its wide use is due to its ideal half-life (6 h), a γ-energy (140 keV) that can pass through internal organs without depositing a high dose of radiation within the patient, and the commercial availability of $^{99}Mo/^{99m}Tc$-generators at a relatively low cost.[94] These properties make ^{99m}Tc the preferred radionuclide in SPECT.

SPECT is a non-lethal radioimaging technique that is reliant upon the detection of γ-rays arising from the radioactive decay of technetium-99m.[95] Implementation of multiple gamma cameras (or detectors) around a subject allows researchers to acquire in real-time, and in 3-dimensions, *in vivo* images of the radioactive material as it navigates through the body. While a number of clinically useful chelators for ^{99m}Tc have been developed and applied to the imaging of tumours, organs, vasculature, and numerous other tissues, its use in tracing the pharmacokinetics and pharmacodynamics[94] of dendrimers as macromolecular drug delivery agents has received very little attention.

1.19. Goals of the Thesis

The goal of this thesis was to synthesize novel dendrimers based on 2,2-bis-(hydroxylmethyl)propionic acid (bis-MPA) that could be used for medicinal applications. The synthesis and full spectroscopic characterization of carborane-containing dendrimers is described in Chapter 2. Several key advancements were demonstrated and include the development and synthesis of a bifunctional carborane synthon, the utilization of this synthon to insert 4, 8, or 16 carborane cages within three different dendrimers, and the aqueous solubility of each structure. A number of these carborane-containing dendrimers were found to exhibit a reversible precipitation at elevated temperatures in aqueous solution. Experiments on the how the cloud point temperatures varied as a function of dendrimer generation, solution pH, and the number of heating/cooling cycles were investigated and are described in Chapter 3.

The remaining Chapters 4 and Chapter 5 describe the synthesis and full spectroscopic characterization of technetium-99m labeled dendrimers. These chapters detail a new orthogonal synthetic strategy to produce high-generation dendrons using the toluene sulfonyl ethyl (TSe) ester as a removable protecting group, enabling further core modification. Furthermore, the introduction of a bis-pyridyl ligand at the dendrimer core, capable of binding various isotopes of Tc and Re, along with optimal ^{99m}Tc radiolabeling conditions is discussed in these chapters. A radio-imaging experiment utilizing SPECT-CT for three dendrimers, followed by a detailed biodistribution of a seventh generation dendrimer will be discussed.

1.20. References

(1) Bosman, A. W.; Janssen, H. M.; Meijer, E. W. *Chemical Reviews* **1999**, *99*, 1665-1688.

(2) Boas, U.; Christensen, J. B.; Heegaard, P. M. H. *Journal of Materials Chemistry* **2006**, *16*, 3786-3798.

(3) Grayson, S. M.; Frechet, J. M. J. *Chemical Reviews* **2001**, *101*, 3819-3867.

(4) Flory, P. *Journal of the American Chemical Society* **1952**, *74*, 2718.

(5) Buhleier, E.; Wehner, W.; Vogtle, F. *Synthesis-Stuttgart* **1978**, 155-158.

(6) Tomalia, D. A.; Frechet, J. M. J. *Journal of Polymer Science Part a-Polymer Chemistry* **2002**, *40*, 2719-2728.

(7) Tomalia, D. A.; Baker, H.; Dewald, J.; Hall, M.; Kallos, G.; Martin, S.; Roeck, J.; Ryder, J.; Smith, P. *Polymer Journal* **1985**, *17*, 117-132.

(8) Brabander-van den Berg, E. M. M.; Meijer, E. W. *Angewandte Chemie-International Editiion* **1993**, *32*, 1308-1310.

(9) Hawker, C. J.; Frechet, J. M. J. *Journal of the American Chemical Society* **1990**, *112*, 7638-7647.

(10) Hawker, C. J.; Frechet, J. M. J. *Journal of the Chemical Society-Chemical Communications* **1990**, 1010-1013.

(11) Newkome, G. R.; Yao, Z. Q.; Baker, G. R.; Gupta, V. K. *Journal of Organic Chemistry* **1985**, *50*, 2003-2004.

(12) Miller, T. M.; Neenan, T. X. *Chemistry of Materials* **1990**, *2*, 346-349.

(13) Kwock, E. W.; Neenan, T. X.; Miller, T. M. *Chemistry of Materials* **1991**, *3*, 775-777.

(14) Jansen, J. F. G. A.; Debrabandervandenberg, E. M. M.; Meijer, E. W. *Science* **1994**, *266*, 1226-1229.

(15) Jansen, J. F. G. A.; Meijer, E. W.; Debrabandervandenberg, E. M. M. *Journal of the American Chemical Society* **1995**, *117*, 4417-4418.

(16) Serin, J. M.; Brousmiche, D. W.; Frechet, J. M. J. *Chemical Communications* **2002**, 2605-2607.

(17) Adronov, A.; Frechet, J. M. J. *Chemical Communications* **2000**, 1701-1710.

(18) Gilat, S. L.; Adronov, A.; Frechet, J. M. J. *Angewandte Chemie-International Edition* **1999**, *38*, 1422-1427.

(19) Adronov, A.; Gilat, S. L.; Frechet, J. M. J.; Ohta, K.; Neuwahl, F. V. R.; Fleming, G. R. *Journal of the American Chemical Society* **2000**, *122*, 1175-1185.

(20) Brousmiche, D. W.; Serin, J. M.; Frechet, J. M. J.; He, G. S.; Lin, T. C.; Chung, S. J.; Prasad, P. N. *Journal of the American Chemical Society* **2003**, *125*, 1448-1449.

(21) Hecht, S.; Frechet, J. M. J. *Journal of the American Chemical Society* **2001**, *123*, 6959-6960.

(22) Piotti, M. E.; Rivera, F.; Bond, R.; Hawker, C. J.; Frechet, J. M. J. *Journal of the American Chemical Society* **1999**, *121*, 9471-9472.

(23) Duncan, R. *Anti-Cancer Drugs* **1992**, *3*, 175-210.

(24) Maeda, H.; Wu, J.; Sawa, T.; Matsumura, Y.; Hori, K. *Journal of Controlled Release* **2000**, *65*, 271-284.
(25) Twaites, B.; Alarcon, C. D.; Alexander, C. *Journal of Materials Chemistry* **2005**, *15*, 441-455.
(26) Duncan, R. *Nature Reviews Drug Discovery* **2003**, *2*, 347-360.
(27) Lee, C. C.; MacKay, J. A.; Frechet, J. M. J.; Szoka, F. C. *Nature Biotechnology* **2005**, *23*, 1517-1526.
(28) Matsumura, Y.; Maeda, H. *Cancer Research* **1986**, *46*, 6387-6392.
(29) Seymour, L. W. *Critical Reviews in Therapeutic Drug Carrier Systems* **1992**, *9*, 135-187.
(30) Duncan, R. *Nature Reviews Cancer* **2006**, *6*, 688-701.
(31) Gillies, E. R.; Frechet, J. M. J. *Drug Discovery Today* **2005**, *10*, 35-43.
(32) Malik, N.; Wiwattanapatapee, R.; Klopsch, R.; Lorenz, K.; Frey, H.; Weener, J. W.; Meijer, E. W.; Paulus, W.; Duncan, R. *Journal of Controlled Release* **2000**, *68*, 299-302.
(33) Esfand, R.; Tomalia, D. A. *Drug Discovery Today* **2001**, *6*, 427-436.
(34) Jevprasesphant, R.; Penny, J.; Jalal, R.; Attwood, D.; McKeown, N. B.; D'Emanuele, A. *International Journal of Pharmaceutics* **2003**, *252*, 263-266.
(35) Boas, U.; Heegaard, P. M. H. *Chemical Society Reviews* **2004**, *33*, 43-63.
(36) Ihre, H.; Soderlind, E.; Hult, A. *Abstracts of Papers of the American Chemical Society* **1995**, *210*, 187-Pmse.
(37) Ihre, H.; De Jesus, O. L. P.; Frechet, J. M. J. *Journal of the American Chemical Society* **2001**, *123*, 5908-5917.
(38) Ihre, H. R.; De Jesus, O. L. P.; Szoka, F. C.; Frechet, J. M. J. *Bioconjugate Chemistry* **2002**, *13*, 443-452.
(39) Gillies, E. R.; Dy, E.; Frechet, J. M. J.; Szoka, F. C. *Molecular Pharmaceutics* **2005**, *2*, 129-138.
(40) Ihre, H.; De Jesus, O. L. P.; Szoka, F. C.; Frechet, J. M. J. *Bioconjugate Chemistry* **2002**, *13*, 443-452.
(41) De Jesus, O. L. P.; Ihre, H. R.; Gagne, L.; Frechet, J. M. J.; Szoka, F. C. *Bioconjugate Chemistry* **2002**, *13*, 453-461.
(42) Smeds, K. A.; Luman, N. R.; Grinstaff, M. W. *Abstracts of Papers of the American Chemical Society* **2002**, *224*, U430-U430.
(43) Carnahan, M. A.; Grinstaff, M. W. *Macromolecules* **2001**, *34*, 7648-7655.
(44) Carnahan, M. A.; Grinstaff, M. W. *Journal of the American Chemical Society* **2001**, *123*, 2905-2906.
(45) Tam, J.; Lu, Y.; Yang, J. *European Journal of Biochemistry* **2002**, *269*, 923-932.
(46) Berstein, D.; Stanberry, L.; Sacks, S.; Ayis, N.; Gong, Y.; Ireland, J.; Mumper, R. J.; Holan, G.; Matthews, B.; McCarthy, T.; Bourne, N. *Antimicrobial Agents and Chemotherapy* **2003**, *47*, 3784-3788.
(47) Bhadra, D.; Bhadra, S.; Jain, S.; Jain, N. K. *International Journal of Pharmaceutics* **2003**, *257*, 111-124.
(48) Kojima, C.; Kono, K.; Maruyama, K.; Takagishi, T. *Bioconjugate Chemistry* **2000**, *11*, 910-917.

(49) Malik, N.; Evagorou, E. G.; Duncan, R. *Anti-Cancer Drugs* **1999**, *10*, 767-776.
(50) Choe, Y. H.; Conover, C. D.; Wu, D. C.; Royzen, M.; Gervacio, Y.; Borowski, V.; Mehlig, M.; Greenwald, R. B. *Journal of Controlled Release* **2002**, *79*, 55-70.
(51) Kono, K.; Liu, M. J.; Frechet, J. M. J. *Bioconjugate Chemistry* **1999**, *10*, 1115-1121.
(52) Sontjens, S. H. M.; Nettles, D. L.; Carnahan, M. A.; Setton, L. A.; Grinstaff, M. W. *Biomacromolecules* **2006**, *7*, 310-316.
(53) Sontjens, S. H. M.; Nettles, D. L.; Carnahan, M. A.; Setton, L. A.; Grinstaff, M. W. *Abstracts of Papers of the American Chemical Society* **2004**, *228*, U443-U443.
(54) Middleton, C.; Carnahan, M. A.; Kim, J.; Kang, P.; Kim, T.; Grinstaff, M. W. *Investigative Ophthalmology & Visual Science* **2002**, *43*, U1185-U1185.
(55) Chadwick, J. *Nature* **1932**, *129*, 312.
(56) Fermi, E.; Amaldi, E.; D'Agostino, O.; Rasetti, F.; Serge, E. *E. Proc. Roy. Soc.* **1934**, *A146*, 483.
(57) Taylor, H. J.; Goldhaber, M. *Nature* **1935**, *135*, 341.
(58) Locher, G. L. *Am. J. Roentgenol. Radium Ther.* **1936**, *36*, 1.
(59) Barth, R. F. *Journal of Neuro-Oncology* **2003**, *62*, 1.
(60) Soloway, A. H.; Tjarks, W.; Barnum, B. A.; Rong, F. G.; Barth, R. F.; Codogni, I. M.; Wilson, J. G. *Chemical Reviews* **1998**, *98*, 1515.
(61) Javid, M.; Brownell, G. L.; Sweet, W. H. *J. Clin. Invest.* **1952**, *31*, 604.
(62) Locksley, H. B.; Farr, L. E. *J. Pharmacol. Exp. Ther.* **1955**, *114*, 4.
(63) Farr, L. E.; Sweet, W. H.; Locksley, H. B.; Robertson, J. S. *Am. Neurol. Assoc.* **1954**, *79*, 110.
(64) Farr, L. E.; Sweet, W. H.; Robertson, J. S.; Foster, C. G.; Locksley, H. B.; Sutherland, D. L.; Mendelsohn, M. L.; Stickley, E. E. *Am. J. Roentgenol. Radium Ther.* **1954**, *71*, 279.
(65) Pitochelli, A. R.; Hawthorne, M. F. *Journal of the American Chemical Society* **1960**, *82*, 3228.
(66) Lipscomb, W. N.; Pitochelli, A. R.; Hawthorne, M. F. *Journal of the American Chemical Society* **1959**, *81*, 5833.
(67) Hawthorne, M. F.; Pitochelli, A. R. *Journal of the American Chemical Society* **1959**, *81*, 5519.
(68) Valliant, J. F.; Guenther, K. J.; King, A. S.; Morel, P.; Schaffer, P.; Sogbein, O. O.; Stephenson, K. A. *Coordination Chemistry Reviews* **2002**, *232*, 173.
(69) Fauchere, J. L.; Do, K. Q.; Jow, P. Y. C.; Hansch, C. *Experientia* **1980**, *36*, 1203.
(70) Nemoto, H.; Cai, J. P.; Yamamoto, Y. *Journal of the Chemical Society-Chemical Communications* **1994**, 577-578.
(71) Barth, R. F.; Adams, D. M.; Soloway, A. H.; Alam, F.; Darby, M. V. *Bioconjugate Chemistry* **1994**, *5*, 58-66.
(72) Yao, H. J.; Grimes, R. N.; Corsini, M.; Zanello, P. *Organometallics* **2003**, *22*, 4381-4383.
(73) Qualmann, B.; Kessels, M. M.; Musiol, H. J.; Sierralta, W. D.; Jungblut, P. W.; Moroder, L. *Angewandte Chemie-International Edition in English* **1996**, *35*, 909-911.

(74) Armspach, D.; Cattalini, M.; Constable, E. C.; Housecroft, C. E.; Phillips, D. *Chemical Communications* **1996**, 1823-1824.
(75) Nunez, R.; Gonzalez, A.; Vinas, C.; Teixidor, F.; Sillanpaa, R.; Kivekas, R. *Organic Letters* **2005**, *7*, 231-233.
(76) Thomas, J.; Hawthorne, M. F. *Chemical Communications* **2001**, 1884-1885.
(77) Newkome, G. R.; Moorefield, C. N.; Keith, J. M.; Baker, G. R.; Escamilla, G. H. *Angewandte Chemie-International Edition in English* **1994**, *33*, 666-668.
(78) Dilworth, J. R.; Parrott, S. J. *Chemical Society Reviews* **1998**, *27*, 43-55.
(79) Margerum, L. D.; Campion, B. K.; Koo, M.; Shargill, N.; Lai, J. J.; Marumoto, A.; Sontum, P. C. *Journal of Alloys and Compounds* **1997**, *249*, 185-190.
(80) Wiener, E. C.; Brechbiel, M. W.; Brothers, H.; Magin, R. L.; Gansow, O. A.; Tomalia, D. A.; Lauterbur, P. C. *Magnetic Resonance in Medicine* **1994**, *31*, 1-8.
(81) Sato, N.; Kobayashi, H.; Hiraga, A.; Saga, T.; Togashi, K.; Konishi, J.; Brechbiel, M. W. *Magnetic Resonance in Medicine* **2001**, *46*, 1169-1173.
(82) Kobayashi, H.; Saga, T.; Kawamoto, S.; Sato, N.; Hiraga, A.; Ishimori, T.; Konishi, J.; Togashi, K.; Brechbiel, M. W. *Cancer Research* **2001**, *61*, 4966-4970.
(83) Kobayashi, H.; Brechbiel, M. W. *Molecular Imaging* **2003**, *2*, 1-10.
(84) Kobayashi, H.; Sato, N.; Kawamoto, S.; Saga, T.; Hiraga, A.; Ishimori, T.; Konishi, J.; Togashi, K.; Brechbiel, M. W. *Magnetic Resonance in Medicine* **2001**, *46*, 579-585.
(85) Wiener, E. C.; Konda, S.; Shadron, A.; Brechbiel, M.; Gansow, O. *Investigative Radiology* **1997**, *32*, 748-754.
(86) Konda, S. D.; Aref, M.; Brechbiel, M.; Wiener, E. C. *Investigative Radiology* **2000**, *35*, 50-57.
(87) Kobayashi, H.; Kawamoto, S.; Saga, T.; Sato, N.; Ishimori, T.; Konishi, J.; Ono, K.; Togashi, K.; Brechbiel, M. W. *Bioconjugate Chemistry* **2001**, *12*, 587-593.
(88) Yordanov, A. T.; Lodder, A. L.; Woller, E. K.; Cloninger, M. J.; Patronas, N.; Milenic, D.; Brechbiel, M. W. *Nano Letters* **2002**, *2*, 595-599.
(89) Fu, Y. J.; Nitecki, D. E.; Maltby, D.; Simon, G. H.; Berejnoi, K.; Raatschen, H. J.; Yeh, B. M.; Shames, D. M.; Brasch, R. C. *Bioconjugate Chemistry* **2006**, *17*, 1043-1056.
(90) Loveland, W.; Morrissey, D. J.; Seaborg, G. T. *Modern Nuclear Chemistry*, 1st ed.; Wiley: Hoboken, N.J., 2006.
(91) Gillies, E. R.; Frechet, J. M. J. *Journal of the American Chemical Society* **2002**, *124*, 14137-14146.
(92) Lee, C. C.; Yoshida, M.; Frechet, J. M. J.; Dy, E.; Szoka, F. C. *Bioconjugate Chemistry* **2005**, *16*, 535-541.
(93) Banerjee, S. R.; Maresca, K. P.; Francesconi, L.; Valliant, J.; Babich, J. W.; Zubieta, J. *Nuclear Medicine and Biology* **2005**, *32*, 1-20.
(94) Jurisson, S. S.; Lydon, J. D. *Chemical Reviews* **1999**, *99*, 2205-2218.
(95) Lyons, S. K. *Journal of Pathology* **2005**, *205*, 194-205.

Chapter 2 - Synthesis and Properties of Carborane-Functionalized Aliphatic Polyester Dendrimers

Abstract

The incorporation of multiple p-carborane cages within an aliphatic polyester dendrimer was accomplished through the preparation of a bifunctional carborane synthon. A p-carborane derivative having an acid and a protected alcohol functionality was found to efficiently couple to peripheral hydroxyl groups of low-generation dendrimers under standard esterification conditions. Deprotection of carborane hydroxyl groups allowed for further dendronization through a divergent approach using the highly reactive anhydride of benzylidene protected 2,2-bis(hydroxymethyl)propanoic acid. This approach was used to prepare fourth and fifth generation dendrimers that contain 4, 8, and 16 carborane cages within their interior. Upon peripheral deprotection to liberate a polyhydroxylated dendrimer exterior, these structures exhibited aqueous solubility as long as a minimum of 8 hydroxyl groups per carborane were present. Several of the water-soluble structures were found to exhibit a lower critical solution temperature. Additionally, irradiation of these materials with thermal neutrons resulted in emission of gamma radiation that is indicative of boron neutron capture events occurring within the carborane-containing dendrimers. This chapter has been reproduced in part with permission from *Journal of the American Chemical Society* **2005**, 12081-12089.

2.1. Introduction

Boron-10 delivery to biological tissues has been the subject of longstanding research due to the potential of Boron Neutron Capture Therapy (BNCT) in the treatment of diseases such as cancer.[1, 2] BNCT is a binary method for radiation therapy that involves the irradiation of ^{10}B nuclei with thermal neutrons. Upon neutron capture, the ^{10}B nucleus undergoes fission resulting in the localized emission of high linear energy transfer (LET) particles (^{4}He and ^{7}Li)[3] having a penetration range of less than 10 μm in biological tissues, which amounts to approximately one cell diameter.[4] Therefore, if high concentrations of ^{10}B are achieved in tumour cells relative to surrounding healthy tissues, neutron irradiation should result in selective tumour annihilation. Considering the high neutron capture cross-section of ^{10}B relative to other light elements,[2] BNCT is theoretically an ideal method for targeted delivery of radiation doses capable of selective tissue destruction. However, the principal obstacle to mainstream application of BNCT for cancer treatment has been the selective delivery of adequate boron concentrations, requiring a minimum of 10^9 ^{10}B atoms per cell within the target tissues.[5] To address this issue, polyhedral borane clusters, such as closo-$[B_{10}H_{10}]^{2-}$, closo-$[B_{12}H_{12}]^{2-}$, and the isoelectronic icosahedral family of carboranes, closo-$C_2B_{10}H_{12}$, have attracted significant attention due to the high boron content within each molecular cage (Figure 2.1).[1] Carboranes are particularly attractive due to their high stability, charge neutrality, and the relative ease with which they can be chemically modified.[6] For these reasons, the conjugation of carboranes to small biologically relevant molecules, such as nucleic acids, amino acids, sugars, and lipids has been extensively investigated.[2] However, many of

these studies have been plagued by the modification of biomolecule structure resulting from the introduction of the carborane, which causes a loss of function and/or receptor recognition of the hybrid compounds.[5] More recently, the need for high cellular ^{10}B concentrations has prompted the conjugation of multiple carboranes with biological and synthetic macromolecules capable of specifically targeting cancer cells. For example, direct conjugation of monoclonal antibodies with carboranes and carborane-functionalized polylysine resulted in heterostructures bearing greater than 1300 boron atoms.[7] Again, the success of this approach was limited due to decreased *in vivo* antigen specificity and decreased water solubility, resulting in greatly diminished tumour-localizing capability.[7] Additional promising methods have also been reported, including boron-rich oligomeric phosphate diesters[8] and carborane-loaded unilamellar liposomes.[9]

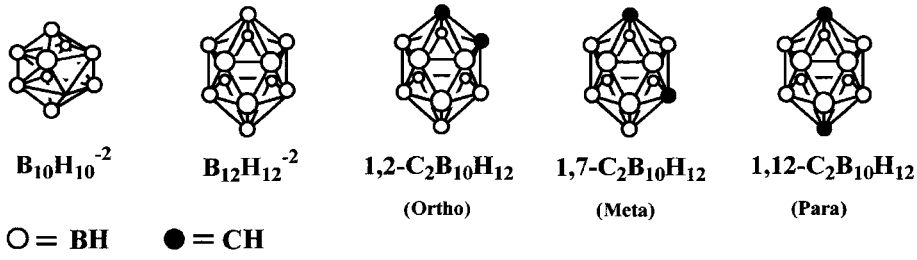

Figure 2.1. Structures of some common polyhedral boranes.

Over the past two decades, the use of synthetic macromolecules as drug-delivery agents has gained increasing momentum. The idea of using water-soluble polymers to mimic transport proteins was first introduced by Ringsdorf[10, 11] and Kopecek,[12, 13] and has led to clinical trials of several polymer therapeutic agents for cancer chemotherapy.[14]

Polymer-based drug delivery agents exhibit improved solubility and increased vascular circulation time due to a decreased rate of renal filtration, a process that is abated by increasing the molecular size of the delivery system.[15, 16] This prolonged circulation time enables macromolecular drug delivery systems to passively target tumour tissues as a result of increased permeability of tumour vasculature to macromolecules and the limited lymphatic drainage away from a tumour.[17] Combined, these two factors allow the selective accumulation of macromolecules in tumour tissue, a phenomenon known as the enhanced permeation and retention (EPR) effect.[18-20]

Within the area of polymer therapeutics, dendritic macromolecules exhibit several distinct advantages over their linear counterparts. These include their precisely controlled architecture, monodispersity, and the ability to incorporate specific functional groups at the periphery or the interior of the molecule.[21-25] Dendrimers can therefore serve as highly versatile drug delivery vehicles, allowing for control over solubility, molecular weight, multiplicity of therapeutic agents, and potentially the incorporation of active targeting moieties.[17, 26] In light of these advantages, several research groups have already investigated the incorporation of carboranes within a dendritic polymer architecture. Perhaps the first example was Yamamoto's ortho-carborane coupled to a cascade-type tetraol that exhibited enhanced water solubility over the non dendron-functionalized starting material.[27, 28] Following this, other groups investigated the coupling of multiple carborane cages to the peripheral groups of various dendrimers, including PAMAM,[29] poly(propylene imine),[30] carbosilane,[31] polylysine,[32] metallodendrimers,[33] and the dendrimer-like closomers.[34] Of these, only the PAMAM and polylysine structures

exhibited some degree of aqueous solubility, though neither one proved to be an ideal boron delivery agent. PAMAM dendrimers have been found to be cytotoxic due to their polycationic nature,[35] and the polylysine scaffold, while clearly biocompatible, exhibited diminished aqueous solubility upon carborane introduction, requiring aqueous-organic solvent mixtures for bioconjugation reactions.[32] A more successful approach to producing water soluble carborane functionalized dendrimers, reported by Newkome and co-workers, involved the reaction of alkyne moieties with decaborane to form ortho-carborane cages within the interior of cascade macromolecules.[36] Aqueous solubility over a wide pH range was provided by peripheral sulphate groups, resulting in a unimolecular micelle-type structure. However, the biocompatibility and biodegradability of this hydrocarbon-based dendrimer has not been reported.

Based on these studies, it is clear that internal dendrimer functionalization is advantageous, allowing peripheral hydrophilic groups to impart aqueous solubility and effectively mask the presence of hydrophobic carborane cages within the macromolecule. Additionally, the dendrimer scaffold must be chosen such that it imparts the required solubility features while also maintaining biocompatibility. Recently, Fréchet and co-workers developed an efficient divergent synthesis of aliphatic polyester dendrimers based on 2,2-bis(hydroxymethyl)propanoic acid (bis-MPA),[37] originally prepared by Ihre et al. in a convergent manner.[38, 39] These structures were found to be promising as drug delivery agents, as they are biocompatible, non-immunogenic, non-toxic, water soluble, and well-tolerated *in vivo*.[26, 40] We have therefore undertaken the development of similar aliphatic polyester dendrimers that incorporate an easily controllable number of

carboranes within the interior of the dendrimer structure. Critical to this approach was the development of a bifunctional carborane synthon that matches the dual functionality of the bis-MPA monomer, allowing it to be inserted within the dendrimer synthesis at any generation using traditional carbodiimide esterification reactions. This flexibility in the position of carborane insertion provides control over the boron concentration within a specific dendrimer target compound. Here, we report the synthesis and properties of this novel class of carborane-functionalized dendrimers.

2.2. Results and Discussion

2.2.1. Dendrimer Synthesis

The general procedure for the divergent synthesis of aliphatic poly(ester) dendrimers, utilizing readily available and inexpensive 2,2-bis(hydroxymethyl) propionic acid (bis-MPA) as the monomer, involves coupling of a highly reactive bis-MPA anhydride with nucleophiles such as alcohols or amines.[37] The bis-MPA anhydride (**2.1**) was prepared in two steps, according to literature procedures.[37] This anhydride was reacted with the 1,1,1-tris(hydroxyphenyl)ethane core using a catalytic amount 4-dimethylaminopyridine (DMAP) in 96% yield (Scheme 2.1). We have found that using a 3:2 mixture of CH_2Cl_2 and pyridine, and a two-fold excess of **2.1** relative to each alcohol functionality are optimal conditions for all generations. The excess anhydride (**2.1**) was quenched with water, and the pure first generation dendrimer was obtained after extraction and washing with $NaHSO_4$ (1 M), Na_2CO_3 (10% w/v), and brine. The benzylidene protecting groups of **2.3** were quantitatively removed by hydrogenolysis

using a catalytic amount of 10% (w/w) Pd/C and H_2 to produce **2.4**. Iteration of these steps allowed the production of a series of hydroxy-terminated dendrimer generations, from G-1 to G-4.

Scheme 2.1. Synthesis of 2,2-bis(hydroxymethyl) propionic acid (bis-MPA) dendrimer.

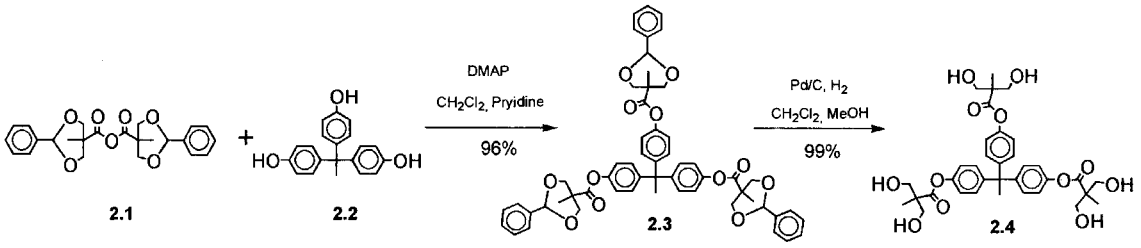

The general strategy for the incorporation of carborane cages into the polyester dendrimer synthesis involved the preparation of a bifunctional carborane bearing a carboxylic acid and a protected alcohol. The carboxylic acid of such a bifunctional structure could be coupled to the peripheral alcohols of the deprotected polyester dendrimer at any generation, and the protected alcohols of the resulting product would subsequently be deprotected to regenerate peripheral alcohol functionalities (Figure 2.2). The new array of peripheral alcohols would then be reacted with the bis-MPA anhydride (**2.1**) again to produce higher generation dendrimers. By doing this, the modified carborane cage acts as a spacer between generations, and can be inserted at any stage of the dendrimer synthesis.

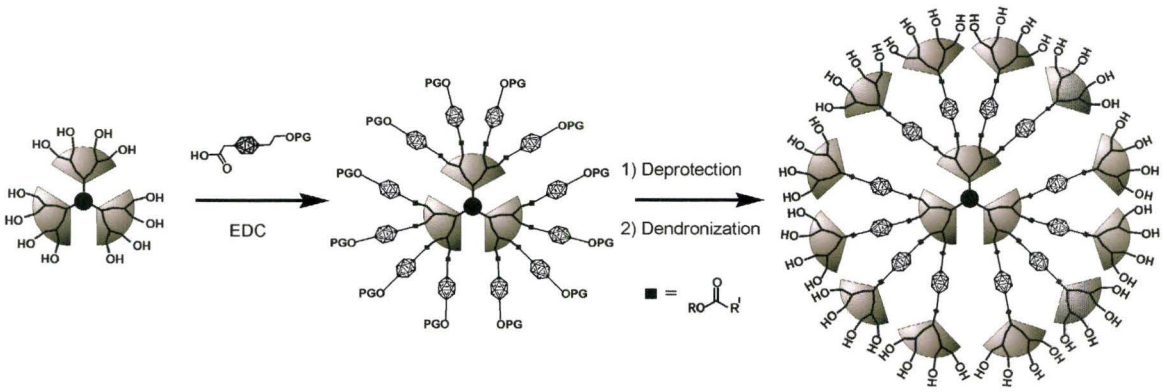

Figure 2.2. Schematic describing the strategy for incorporation of a carborane synthon into the polyester dendrimer.

Preparation of the bifunctional carborane cage was accomplished by utilizing the relative acidity of the proton on the carbon vertices (pKa = 26.8).[41] A simple deprotonation of para-carborane with one equivalent of n-butyllithium (n-BuLi) was performed in dry THF (Scheme 2.2), leading to the formation of a statistical mixture of three species, including a monoanion, a dianion, and the starting material. The anions generated from this reaction were treated with 1 equiv. of trimethylene oxide resulting in a hydroxypropyl group coupled directly to the cage.[42] The reaction was quenched with HCl (1 M) and the product was purified by column chromatography in dichloromethane giving **2.5** in 50% yield. It is important to note that the unreacted starting material (25%) could be recovered and reused, while the diol by-product (25%) was a useful synthon in other reactions (vide infra). The resulting alcohol (**2.5**) was subsequently protected using *t*-butyldiphenylsilyl chloride (TBDPS-Cl) to form **2.6** in 98% yield. Compound **2.6** was deprotonated with n-BuLi and the resulting anion was quenched with CO_2 to produce the

desired carboxylate functionality. Acidic workup, followed by column chromatography in 9:1, DCM : methanol resulted in acid **2.7** (84% yield).

Scheme 2.2. Synthesis of bifunctional carborane 2.7.

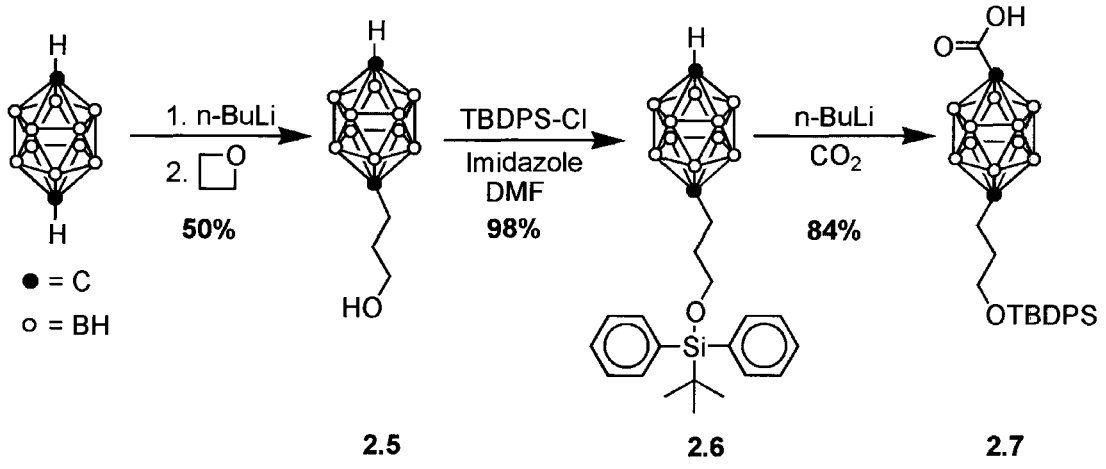

2.5 **2.6** **2.7**

To investigate the esterification chemistry between acid **2.7** and the eventual hydroxyl functionalized dendrimer, a model study was performed using benzylated bis-MPA (**2.8**) as a dendrimer mimic (Scheme 2.3). Compound **2.8** was prepared in a single quantitative step by reacting bis-MPA with benzyl bromide in the presence of DMAP.[39] Unfortunately, all attempts to couple **2.7** and **2.8** using carbodiimide chemistry were unsuccessful, resulting only in the isolation of starting material. The apparent lack of reactivity is likely due to steric hindrance of the proximal acid group caused by the bulky carborane cage. To reduce this deactivating effect, it was necessary to introduce a spacer between the carborane cage and the acid functionality.

Scheme 2.3. Model coupling of 2.7 to 2.8.

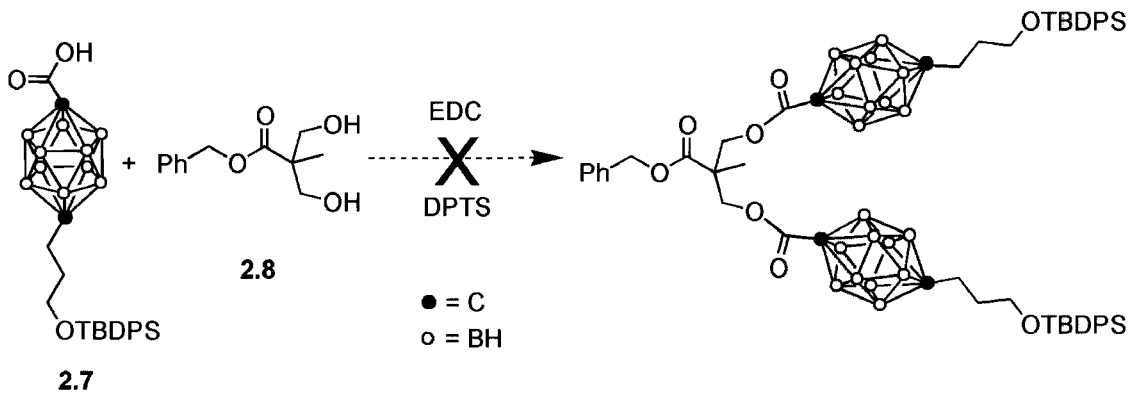

The original synthesis of the bifunctional carborane was easily modified by deprotonating the protected alcohol **2.6** using n-butylithium and reacting with a second equivalent of trimethylene oxide (Scheme 2.4). After an acidic workup, compound **2.9** was purified by column chromatography using 100% DCM as the eluent and was isolated in 87% yield. Alcohol **2.9** was then oxidized using iodobenzene diacetate (IBDA) and TEMPO in dichloromethane under ambient conditions.[43] This nitroxyl radical mediated oxidation was chosen for its mild and selective oxidation of primary alcohols, allowing us to avoid the more aggressive chromium (VI) oxides that are known to deprotect the TBDPS group.[44] Compound **2.10** was precipitated from hexanes and isolated in 85% yield. The reactivity of acid **2.10** was tested by coupling to **2.8** using EDC and DPTS.[45] This reaction produced **2.11** in quantitative yield, indicating that the spacer between the carborane and the acid group was indeed required to impart the necessary acid reactivity in the carbodiimide mediated esterification. The bifunctional carborane **2.10** was

subsequently used as a synthon in the preparation of carborane functionalized dendrimers.

Scheme 2.4. Synthesis of bifunctional carborane 2.10 and model coupling of 2.10 to 2.8.

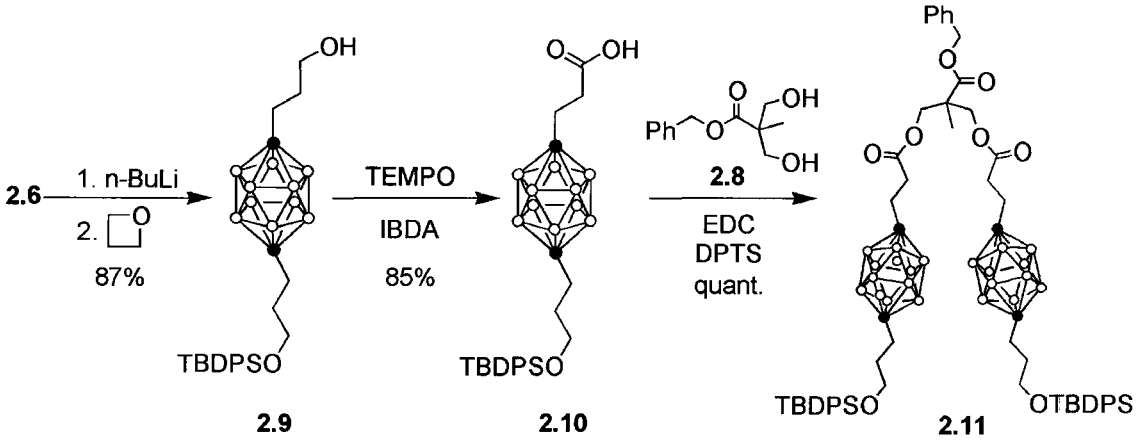

The EDC/ DPTS couplings between **2.10** and the 1,1,1-tris(hydroxyphenyl)ethane core **2.2**, the first generation bis-MPA dendrimer **2.4**, and second generation bis-MPA dendrimer **2.12** were carried out in 93%, 84%, and 79% yield, respectively (Scheme 2.5). In each case a small excess of the carborane acid **2.10** was used (1.25 equiv. per alcohol) to ensure complete functionalization. Compounds **2.13**, **2.14**, and **2.15** were easily purified by column chromatography using various mixtures of hexanes and ethyl acetate as the eluent. These structures were fully characterized by ^{1}H NMR, ^{13}C NMR, and MALDI-TOF MS to ensure that complete functionalization of all peripheral alcohols on the dendritic precursors was obtained. In each case, lower mass structures corresponding to incompletely carborane-functionalized dendrimers were not observed, indicating that the coupling of **2.10** to the dendrimer periphery is a highly efficient process

Scheme 2.5. Coupling of 2.10 to 1,1,1-tris(hydroxyphenyl)ethane, G-1 and G-2 dendrimers.

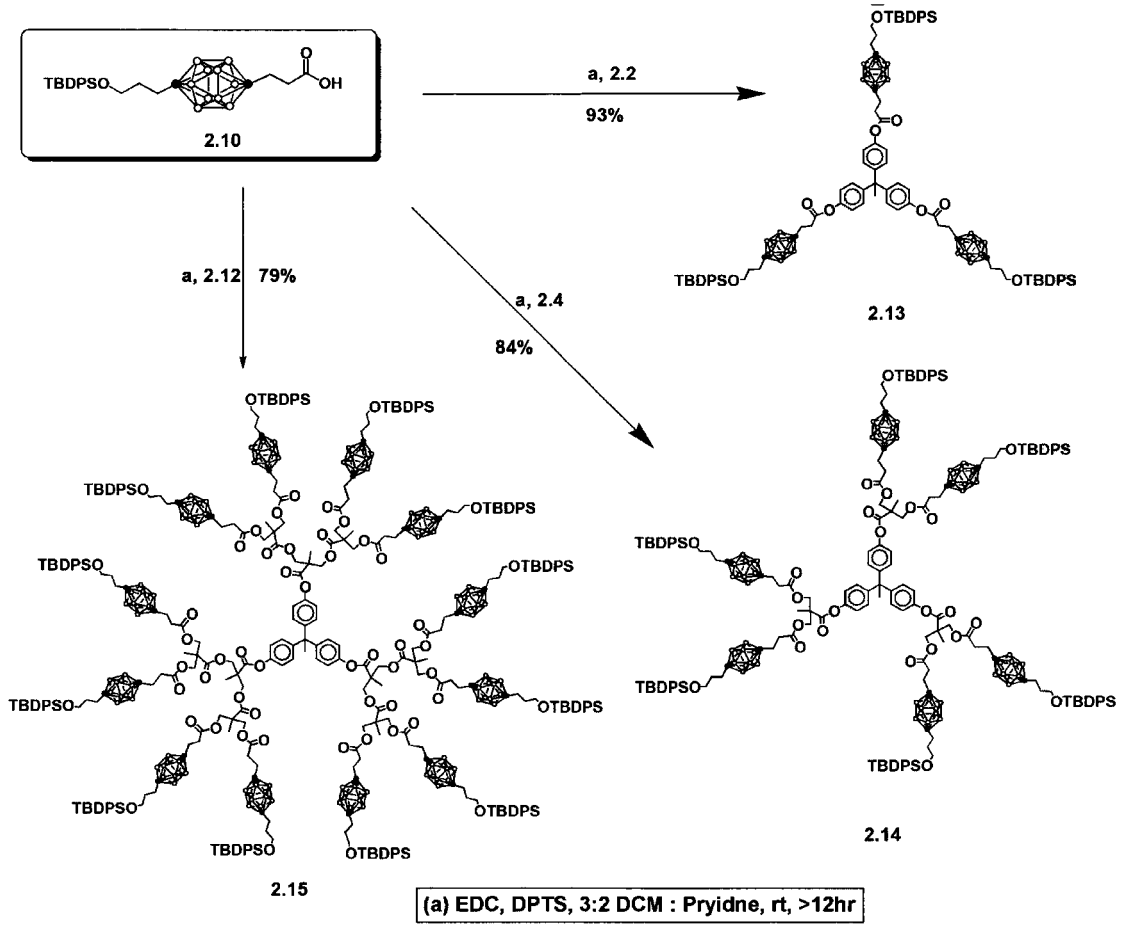

In order to add dendrimer generations at the periphery of these molecules, it was necessary to remove the TBDPS protecting groups, followed by coupling with anhydride **2.2**. Deprotection of the TBDPS groups was attempted under standard conditions using tetrabutylammonium fluoride (TBAF) in THF. However, both thin layer chromatography and ^{1}H NMR indicated extensive degradation of the dendrimers during the course of this

deprotection reaction. It was postulated that the alkoxides generated from removal of the TBDPS groups attacked the various esters in the dendrimer backbone, especially the relatively labile phenolic ester linkages between the core and the dendrons.

To avoid the TBAF deprotection and the ensuing degradation of the dendrimer, we decided to utilize a benzyl ether group to mono-protect the carborane diol **2.16** (Scheme 2.6). The benzyl ether was chosen for its stability to slightly acidic and basic media and for its mild and efficient deprotection conditions. Considering that benzyl ethers are quantitatively removed by hydrogenolysis with a catalytic amount of 10% (w/w) Pd/C and H_2,[44] identical to the conditions used to remove the benzylidene protecting groups of the dendrimer, this deprotection is convenient and highly compatible with the dendrimer synthesis.

Starting with para-carborane, deprotonation of both carbon verticies using two equivalents of n-butyllithium (n-BuLi) was followed by ring opening of trimethylene oxide to produce diol **2.16** in 92% yield after acidic workup and crystallization from $CHCl_3$. This diol was mono-protected using benzyl bromide under basic conditions to produce **2.17** in 48% yield. The remaining free alcohol of **2.17** was subsequently oxidized using TEMPO and IBDA to yield acid **2.18** in 91% yield.

Scheme 2.6. Synthesis of bifunctional carborane 2.18.

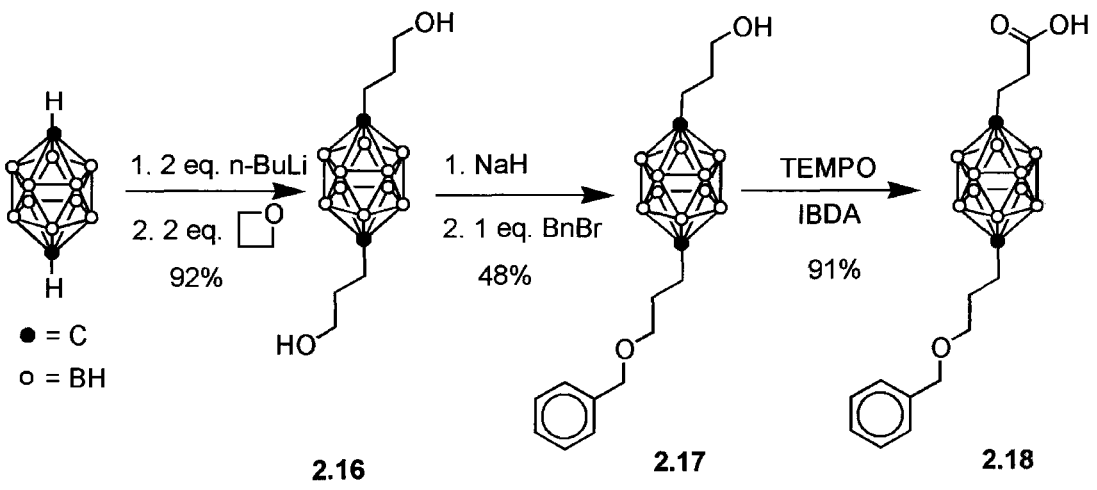

As an additional precaution in the dendrimer synthesis, it was decided to substitute the 1,1,1-tris(hydroxyphenyl) ethane core with pentaerythritol. This modification not only eliminates the weak phenolic ester linkages between the core and the dendrons, but also increases the number of dendrons, and therefore the number of carboranes, within each dendrimer. The G-1 and G-2 protected dendrimers (**2.19** and **2.20**, respectively) having pentaerythritol cores were easily prepared in high yields using the aforementioned procedures. As depicted in Scheme 2.7, carbodiimde coupling reactions were carried out on pentaerthritol, the G-1 bis-MPA dendrimer (**2.19**), and the G-2 bis-MPA dendrimer (**2.20**) in 99%, 93%, and 93% yield, respectively. In each of these reactions, a small excess of the carborane acid **2.18** (1.25 equiv. per alcohol) was required for complete functionalization. Compounds **2.21**, **2.22** and **2.23** were easily purified by column chromatography.

The ^{1}H NMR spectra for dendrimers **2.21-2.23** exhibit all of the expected resonances attributed to the branched polyester core, the carborane linker, and the

peripheral protecting groups (Figure 2.3). The broad carborane B-H resonances observable in these spectra prevent accurate integration of signals in the range of 0.8 – 3.8 ppm. However, the appearance of methyl and methylene signals at 1.1 – 1.3 ppm and 4.0 – 4.3 ppm (J, L and I, K, respectively) provides a clear indication of dendrimer growth (Figure 2.3).

Scheme 2.7. Coupling of 2.18 to pentaerythritol, G-1 and G-2 dendrimers.

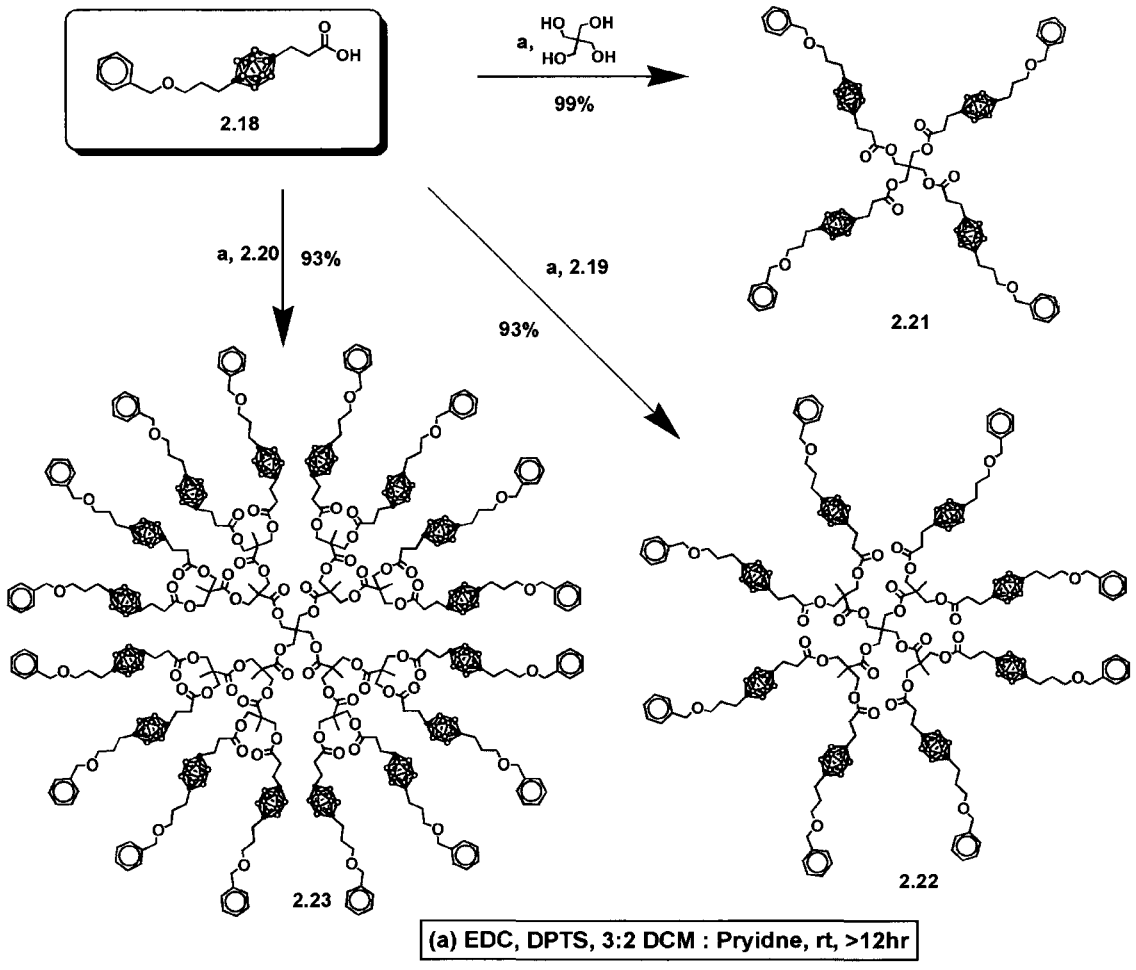

MALDI-TOF MS provided the critical evidence for successful preparation of compounds **2.21**, **2.22**, and **2.23** (Figure 2.4). The mass of the observed molecular ion clearly corresponded to the Na^+ adducts of each respective dendrimer, with no observable lower molecular weight fragments or incompletely functionalized materials. Again, this illustrates the efficiency of the esterification between of the carborane acid **2.18** and the multitude of hydroxyl groups at the dendrimer periphery.

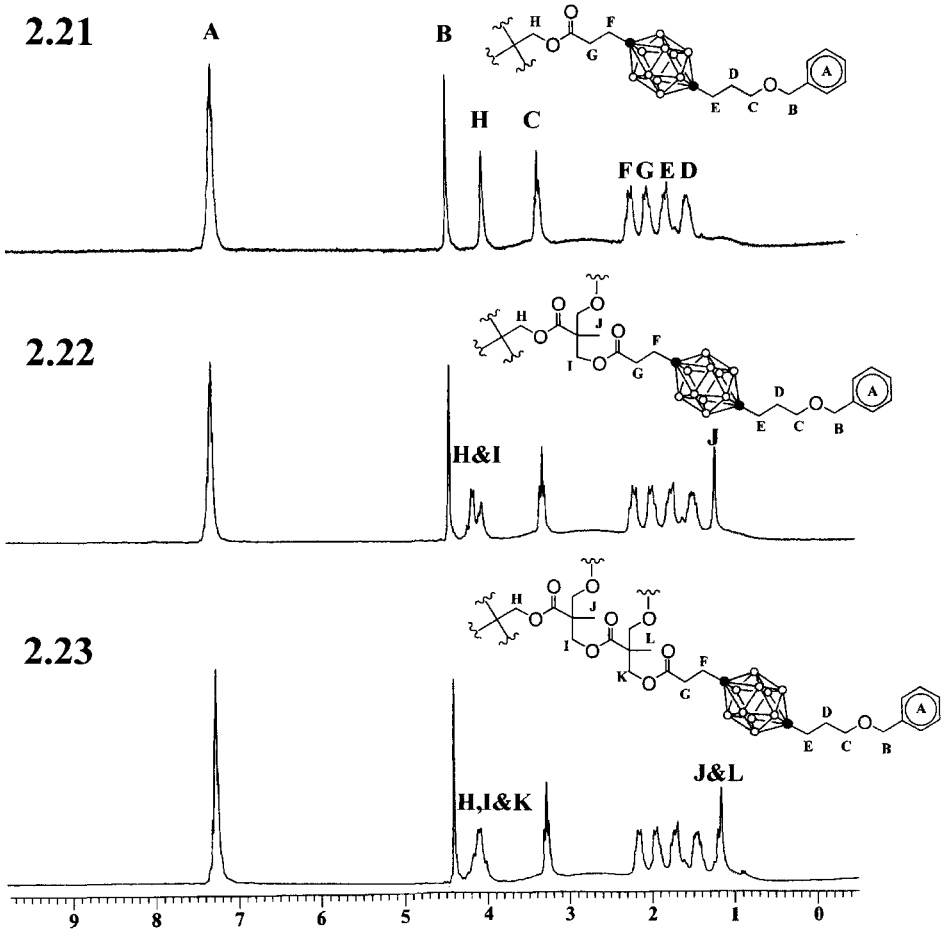

Figure 2.3. ^1H NMR spectra of 2.21, 2.22 and 2.23.

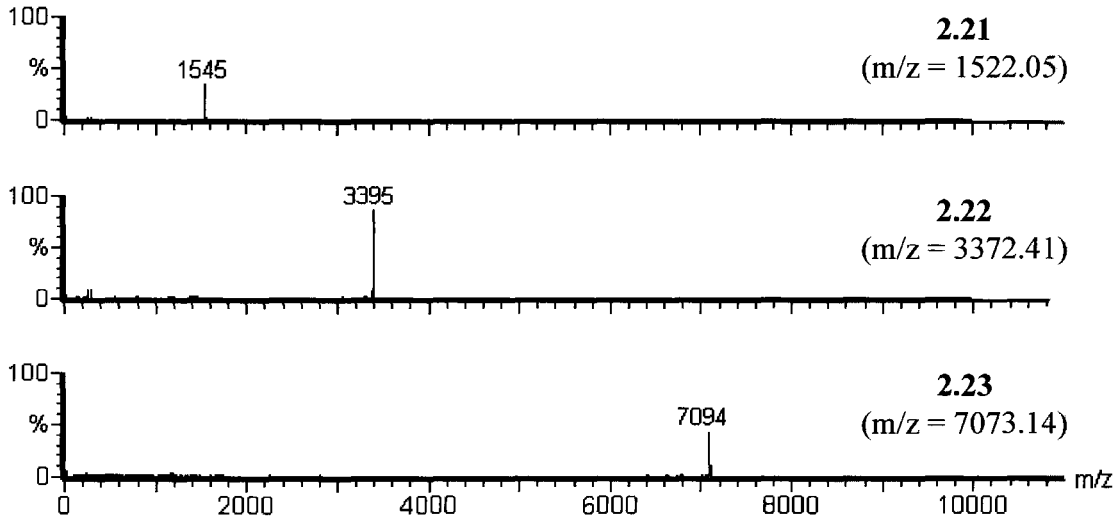

Figure 2.4. MALDI-TOF MS of 2.21, 2.22 and 2.23 with calculated m/z values in parentheses.

Deprotection of the peripheral benzyl ether groups was accomplished quantitatively by hydrogenolysis using a catalytic amount of 10% (w/w) Pd/C and H_2 (Scheme 2.8). The reaction conditions were essentially identical to those of the benzylidene deprotections discussed above. The success of this reaction was easily confirmed by ^1H NMR due to complete disappearance of the aromatic signals at 7.2 – 7.4 ppm as well as the benzylic proton signals at 4.4 ppm. As an example, the ^1H NMR spectra of **2.23** and **2.24** are depicted in Figure 2.5. It can clearly be seen that the strong aromatic signals at 7.3 ppm and the methylene protons at 4.4 ppm completely disappear, while the signals due to the dendrimer backbone remain unchanged. This result was significant as it confirmed that the deprotection reaction occurred without any degradation of the dendritic backbone, unlike the analogous reaction with TBDPS protecting groups.

Scheme 2.8. Deprotection of the peripheral benzyl ether groups on 2.23.

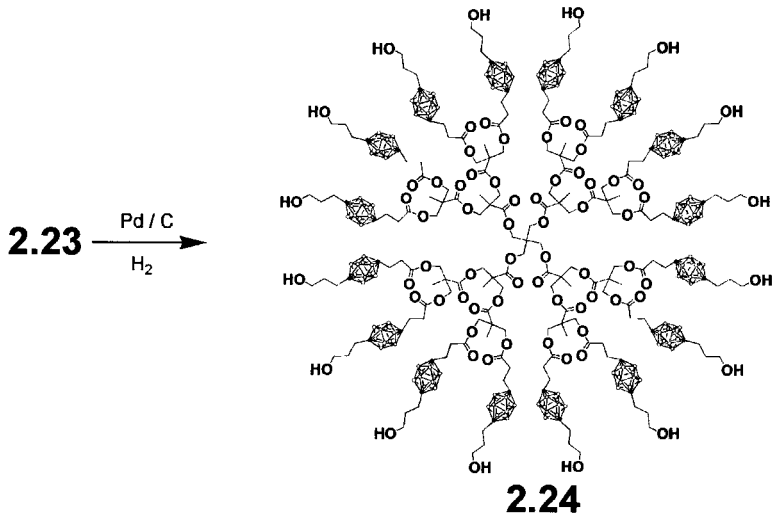

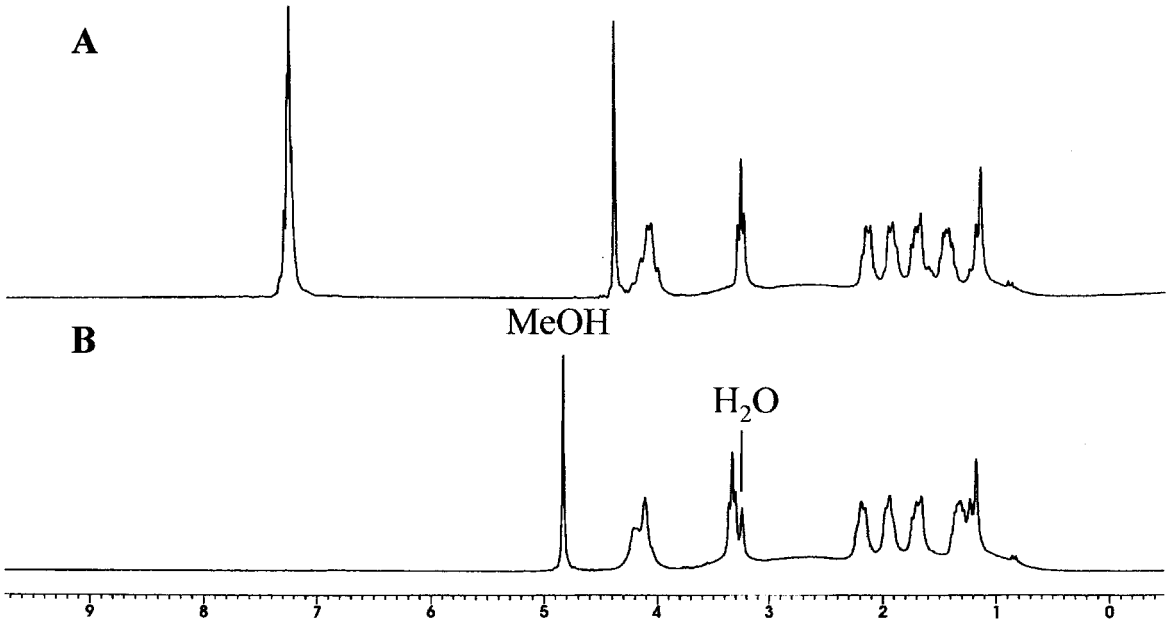

Figure 2.5. ^{1}H NMR before (A) and after (B) benzyl ether deprotection of 2.23. Solvents used for spectra A and B were $CDCl_3$ and CD_3OD, respectively.

Successful deprotection of the benzyl ether groups resulted in the regeneration of peripheral alcohols on the dendrimer, allowing for further divergent growth. These peripheral functionalities were reacted with the bis-MPA anhydride **2.1** to further dendronize each molecule, allowing the carborane cages to be internalized within higher generation dendrimers. Scheme 2.9 depicts the deprotection and dendronization of **2.21** to the third-generation deprotected structure. Similar reaction sequences were used to produce hydroxyl-terminated dendrimers of varying generation containing 8 and 16 carborane cages. The structures of the largest members of these two dendrimer families are given in Figure 2.6. To name each of these molecules, we refer to the number of carborane cages, the overall dendrimer generation number, and the total number of peripheral functional groups. Thus, a structure containing 8 carboranes attached to a first generation core and G-4 dendrons coupled to each of the carboranes would be named 8-[G-5]-OH_{128}, as depicted in Figure 2.6.

Scheme 2.9. Iterative synthesis of 4-[G-4]-OH_{64} from 2.21.

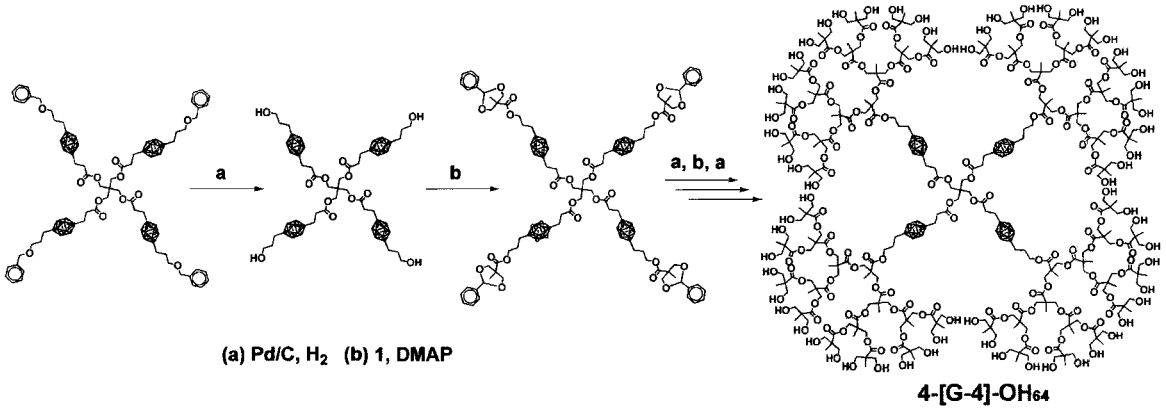

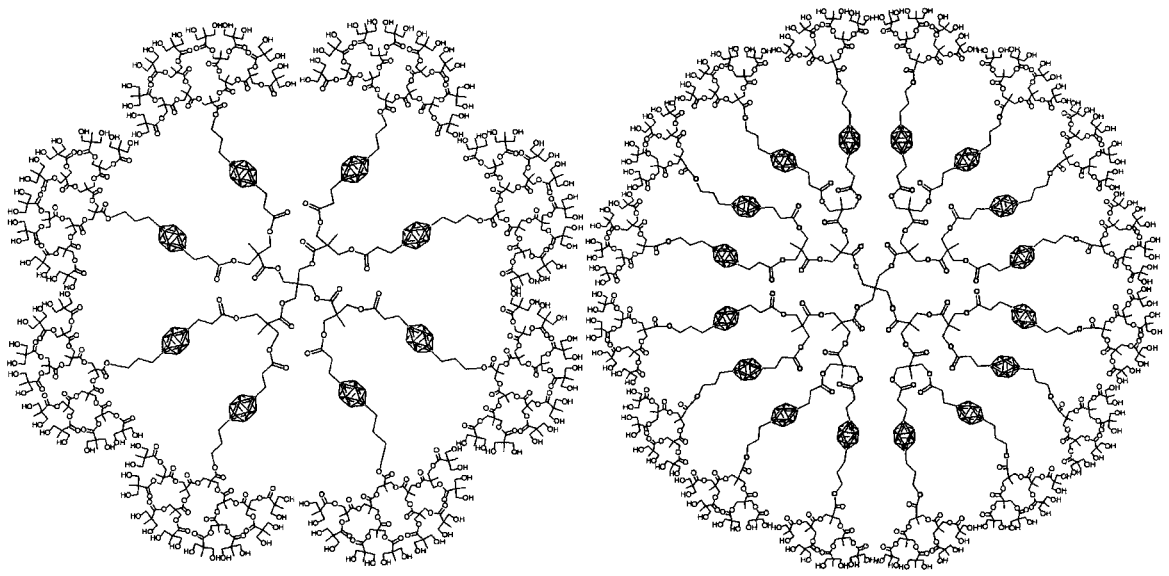

Figure 2.6. Structures of largest synthesized dendrimers containing 8 and 16 carborane cages.

2.2.2. Aqueous Solubility

Considering the potential therapeutic applications of carborane containing compounds, it was important to evaluate the aqueous solubility of each of these structures. Specifically, we were interested in determining the minimum number of peripheral alcohol groups required per carborane in order to impart water solubility at a level of 1 mg/mL or higher. Table 2.1 summarizes this data and clearly indicates that an alcohol:carborane ratio of 4:1 or lower is not sufficient for aqueous solubility. A ratio of 8:1 was also not sufficient for complete water solubility in the structures containing 4 and 8 carboranes, but did impart solubility to the fifth generation dendrimer containing 16 carboranes. Finally, an alcohol:carborane ratio of 16:1 allowed rapid dissolution of the

structures containing 4 and 8 carboranes to concentrations in excess of 5 mg/mL. It is expected that a cooperative effect between the hyrophilicity of the multiple hydroxyl groups and the overall globular shape of the dendrimers beyond generation 4 must dictate overall solubility.

Table 2.1. Aqueous solubility of carborane functionalized dendrimers.

	# of OH's per carborane			
# of carboranes	2	4	8	16
4	No	No	< 1 mg/mL[*†]	8 mg/mL
8	No	No	< 1 mg/mL[*†]	6 mg/mL
16	No	No	1 mg/mL[*]	-

[*] exhibits LCST

[†] completely soluble in 50/50 (v/v) MeOH/H_2O

Interestingly, during the course of these measurements, we found that heating the aqueous suspensions of 4-[G-3]-OH_{32} and 8-[G-4]-OH_{64} did not improve solubility. In fact, these molecules precipitated from solution at elevated temperatures, indicating that they exhibit a lower critical solution temperature (LCST). This phenomenon is explored in greater detail in Chapter 3.

2.2.3. Neutron Activation

To examine neutron activation of the dendrimer-encapsulated carborane cages, 10 mg/mL solutions of the hydroxy-terminated dendrimers 4-[G-3]-OH_{32}, 8-[G-4]-OH_{64}, and 16-[G-4]-OH_{64} in THF were placed in a thermal neutron beam at the Prompt Gamma Facility of the McMaster Nuclear Reactor. The energy profile of the emitted gamma radiation is given in Figure 2.7, clearly showing the characteristic gamma radiation signature at an energy of 480 keV, corresponding to boron neutron capture events. The small signal observed at 511 keV is due to gamma emission caused by annihilation of the positron by-product from the boron neutron capture event. Irradiation was conducted for a period of 6 h at a flux of 10^7 neutrons/cm^2·sec, during which no changes in signal intensity or energy were observed from the dendrimer samples. Additionally, NMR analysis of the dendrimer samples before and after neutron activation indicated no degradation during the course of these experiments. However, the detection of sample degradation due to neutron capture events at this neutron flux would not be expected, as the annihilation of only ~0.01% of the sample's ^{10}B atoms occurs during the 6 hour experiment.

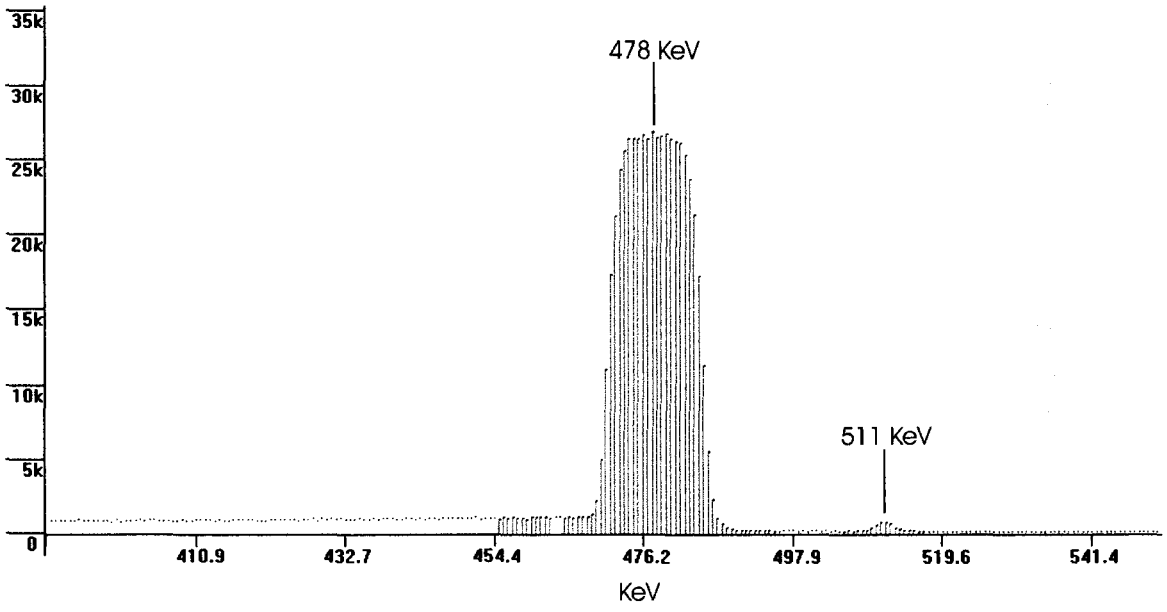

Figure 2.7. Gamma energy profile resulting from neutron capture events occurring within a 10 mg/mL solution of 16-[G-4]-OH_{64}.

2.3. Conclusion

We have shown that a bifunctional carborane derivative bearing an acid group and a benzyl ether protected alcohol serves as a highly effective synthon for the incorporation of carborane cages within an aliphatic polyester dendrimer. The insertion of 4, 8, or 16 carboranes was accomplished in high yield using a previously reported divergent synthesis. It was subsequently possible to further dendronize the macromolecular periphery to install a controllable number of hydroxyl functionalities that imparted aqueous solubility to the final structures. We found that a minimum of 8 alcohols was required to achieve water solubility. Additionally, it was found that all structures having an alcohol to carborane ratio of 8:1 exhibited a lower critical solution temperature, which

varied with the total number of carboranes in the structure. Neutron activation experiments indicated that neutron capture was occurring within the synthesized dendrimers. This family of dendrimers has proven to be extremely versatile, allowing complete control over the location and number of carborane moieties, as well as overall solubility. These structures should therefore serve as potential BNCT agents, and their applicability for this purpose will be investigated in the near future.

2.4. Experimental

2.4.1. Materials and Characterization

All chemicals were purchased from Sigma-Aldrich and used without any purification. NMR spectra were collected on Bruker DXR 500 MHz and Avance 600 MHz. ^{1}H spectra were recorded at 600 MHz, ^{11}B spectra were recorded at 190 MHz, and ^{13}C NMR spectra were recorded at 150 MHz. $CDCl_3$ and MeOD (D4) were used as solvents, and the non-deuterated solvent signals were used as internal standards for both the ^{1}H and ^{13}C spectra. In ^{1}H NMR spectra where aliphatic signals overlap with signals from the B-H protons in the carborane cage, an accurate integration could not be assigned. In these cases, theoretical integration values are provided in parentheses { } (see below). Tetrahydrofuran was distilled under nitrogen from Na / benzophenone prior to use. Dichloromethane (CH_2Cl_2) was distilled from CaH_2 under nitrogen prior to use. Exact masses of the dendritic molecules were determined by MALDI-TOF mass spectrometry using a Micromass TofSpec 2E spectrometer in positive ion mode using 2-(4-hydroxyphenyl-azo) benzoic acid (HABA) as the matrix. The MALDI-TOF

spectrometer was calibrated using four peptides, including Substance P (M/Z = 1348 Da), Angiotensinogen (M/Z = 1759 Da), Adrenocorticotropic hormone, fragments 18 - 39 (M/Z = 2466 Da), and Cytochrome C (M/Z = 12361 Da and 6181 Da for doubly charged species). Neutron capture studies were performed at the McMaster Nuclear Reactor in the Prompt Gamma facility. Samples were irradiated with a neutron flux of 10^7 neutron / $cm^2 \cdot sec$.

2.4.2. Synthesis

2.4.2.1. General Procedure for Dendrimer Growth

To a flame-dried round-bottom flask equipped with a magnetic stir bar (under argon atmosphere), the benzylidene protected anhydride, the hydroxyl-terminated dendrimer (generation 0 through 4), and 4-dimethylaminopyridine were all dissolved in a 3:2 ratio of CH_2Cl_2 and pyridine. After stirring at room temperature for over 12 h, approximately 2 mL of water was added and the reaction was stirred for an additional 18 h in order to quench the excess anhydride. The product was isolated by diluting the mixture with CH_2Cl_2 (150 mL) and extracting with 1 M $NaHSO_4$ (3 × 150 mL), saturated aqueous $NaCO_3$ (2 × 150 mL), and brine (150 mL). The organic layer was removed by rotary evaporation in vacuo. The product was then precipitated three times from a 10:1 hexanes:ethyl acetate mixture. Any residual solvent was removed in vacuo to yield white foam with typical yield of greater than 85%.

2.4.2.2. General Procedure for Deprotection by Hydrogenolysis

To a flame-dried round-bottom flask equipped with a magnetic stir bar, the benzyl or benzylidene protected dendrimer was dissolved in a 1:1 mixture of CH_2Cl_2:MeOH (total of 20 mL). Pd/C (10%) was added and the flask was evacuated and back-filled with hydrogen three times (H_2 pressure: 1 atm). After vigorous stirring for 24 h, the reaction mixture was filtered through a celite plug in a fritted glass funnel and the filtrate was evaporated to dryness on a rotary evaporator in vacuo. The remaining residue was composed of the desired product, which was isolated as white foam in quantitative yields.

2.4.2.3. General Procedure for Coupling of Carborane Acid to Dendrimer Periphery

To a flame-dried round-bottom flask (under argon atmosphere) equipped with a magnetic stir bar, 1.25 equivalents of the carborane acid per peripheral alcohol was added to the core (pentaerythritol) or the hyper-core (G-1 or G-2 hydroxy-terminated dendrimers), and a catalytic amount of 4-dimethylaminopyridine/p-toluene sulphonic acid salt (DPTS) were dissolved in a 3:2 ratio of CH_2Cl_2:pyridine. Subsequently, 1.3 equivalents of EDC per peripheral alcohol was added and the reaction was allowed to stir for 18 h at room temperature. Both the CH_2Cl_2 and pyridine were removed from the crude mixture by rotary evaporation in vacuo. The compounds were isolated by flash chromatography using various compositions of ethyl acetate and hexanes as eluent (*vide infra*). Yields were typically greater than 93%.

2.4.2.4. Synthesis of 1-(3-hydroxypropyl)-1,12-dicarbadodecaborane (2.5)

Para-carborane (300 mg, 2.08 mmol) was dissolved in 60 mL of tetrahydrofuran (THF) and placed in a flame-dried round-bottom flask equipped with a magnetic stir bar under an argon atmosphere. The reaction mixture was cooled to 0 °C and butyllithium (945 μL, 2.08 mmol, 1.0 eq) was added drop wise to the reaction mixture while stirring. After 1 h of stirring at 0°C, trimethylene oxide (135 μL, 2.08 mmol, 1.0 eq) was added and the reaction mixture was allowed to warm to room temperature. The mixture was stirred for an additional 2 h and was then quenched by addition of 20 mL of aqueous HCl (0.2 M). The reaction mixture was then poured into a separatory funnel containing 50 mL of CH_2Cl_2 and 50 mL of water. The organic layer was separated, dried over $MgSO_4$, and evaporated to yield a white glass: 0.211 g (50%). ^{1}H NMR (500 MHz, $CDCl_3$): δ = 1.43 (m, 2), 1.72* (m, {2}), 2.63* (s, {1}), 3.48 (t , 2, J = 6). ^{13}C NMR (125 MHz, $CDCl_3$): δ = 32.25, 35.32, 58.07, 61.85, 84.20. ^{11}B NMR (160 MHz, $CDCl_3$, proton-decoupled): δ = -14.29, -11.78.

2.4.2.5. Synthesis of 1-(3-*tert*-butyldiphenyl(propoxy)silyl)-1,12dicarbadodecaborane (2.6)

To a round-bottom flask equipped with a magnetic stir bar was added compound **2.5** (1.00 g, 4.94 mmol), imidazole (0.673 g, 9.89 mmol, 2.0 eq), and 60 mL of DMF. The solution was allowed to cool to 0°C and *tert*-butylchlorodiphenylsilane (2.04 g, 7.41 mmol, 1.5 eq) was added. The reaction mixture was stirred for 3 h and then quenched

with 20 mL of water. The mixture was added to a separatory funnel and extracted with ether (3 × 20 mL). The ether layers were collected and additionally washed with 2 M HCl (3 x 150 mL), 10% NaOH (3 x 150 mL), and brine (1 x 150 mL). The product was isolated by column chromatography (9:1 hexanes:ethyl acetate), yielding a white glass: 2.12 g (98%). ^{1}H NMR (500 MHz, $CDCl_3$): δ = 1.04 (s, 9), 1.43 (m, 2), 1.72* (m, {2}), 2.63* (s, {1}), 3.50 (t , 2, *J* = 6), 7.44 (m, 6), 7.62 (m, 4). ^{13}C NMR (125 MHz, $CDCl_3$): δ = 19.15, 26.81, 32.25, 35.51, 57.95, 62.76, 84.59, 127.63, 129.62, 133.72, 135.51. ^{11}B NMR (160 MHz, $CDCl_3$, proton-decoupled): δ = -14.29, -11.72.

2.4.2.6. Synthesis of 12-(3-*tert*-butyldiphenylsilyloxy)propyl-1,12 dicarbadodecaborane-1-carboxylic acid (2.7)

To a flame-dried round-bottom flask equipped with a magnetic stir bar was added compound **2.6** (0.199 g, 0.452 mmol) and 9 mL of THF. The solution was cooled to 0°C followed by addition of n-butyl lithium (0.224 mL, 0.477 mmol, 1.05 eq). The mixture was stirred for 1 h, cooled to –78 °C, and CO_2 was bubbled into the reaction. The formation of a white precipitate was observed after ca. 15-30 min. After 3 hrs of bubbling, the reaction was quenched with 30 mL of HCl (0.2 M). This was followed by the addition of 50 mL of H_2O and extraction of the resulting mixture using CH_2Cl_2 (2 × 50 mL). The organic phases were collected, dried (Na_2SO_4), filtered, and evaporated to dryness in vacuo to yield a white crystalline solid (184 mg, 84%). ^{1}H NMR (600 MHz, $CDCl_3$): δ = 1.05 (s, 9 H), 1.39 (m, 2 H), 1.76* (m, 2 H), 3.50 (t, *J* = 6, 2 H), 7.45 (m, 6),

7.63 (m, 4). ^{13}C NMR (150 MHz, $CDCl_3$): δ = 18.68, 26.33, 31.71, 34.53, 62.13, 73.00, 83.62, 127.21, 129.22, 133.12, 135.04, 167.05. ^{11}B NMR (190 MHz, $CDCl_3$, proton-decoupled): δ = -13.06, -12.31. Calc.: $[M]^+$ m/z = 484.7. Found ES-MS: $[M]^+$ = 484.5.

2.4.2.7. Synthesis of 1-(3-*tert*-butyldiphenyl(propoxy)silyl)-1-(3-hydroxypropyl)-1,12-dicarbadodeca-borane (2.9)

To a flame-dried round-bottom flask equipped with a magnetic stir bar, compound **2.6** (0.219 g, 0.498 mmol) and 100 mL of THF were added. The reaction vessel was cooled to 0 °C and 1.8 M n-butyl lithium (0.553 mL, 0.996 mmol, 2.0 eq) was slowly added. The mixture was allowed to warm to room temperature while stirring for 4 h. Subsequently, the reaction mixture was again cooled to 0°C and trimethylene oxide (48.6 μL, 0.747 mmol, 1.5 eq) was added. The reaction was then allowed to warm to room temperature, and was stirred overnight. The THF was then evaporated in vacuo and the residue was taken up in 100 mL of ether, poured into a separatory funnel and washed with 2 M HCl (2 x 100 mL). The organic layer was then dried ($MgSO_4$), filtered, and evaporated to dryness in vacuo The product was isolated by column chromatography, initially eluted using 100% CH_2Cl_2 to remove the unreacted staring material, followed by a mixture of 8:2 CH_2Cl_2:ethyl acetate to elute the product. This resulted in 0.150 g of a clear oil, (61% yield). ^1H NMR (500 MHz, $CDCl_3$): δ = 1.02 (s, 9), 1.41 (m, 4), 1.73* (m, {4}), 3.47 (t , 2, *J* = 6), 7.41(m, 6), 7.59 (m, 4) . ^{13}C NMR (125 MHz, $CDCl_3$): δ = 19.07, 26.60, 32.36, 34.10, 61.86, 62.72, 78.46, 78.98, 127.55, 129.53, 133.65, 135.43. ^{11}B

NMR (160 MHz, $CDCl_3$, proton-decoupled): δ = -11.97. Anal. Calc. C 57.79%, H 8.49%. Found: C 57.76%, H 8.55%.

2.4.2.8. Synthesis of 3-(12-(3-*tert*-butyldiphenylsilyloxy)propyl)-1,12-dicarba-dodecaboranyl-1-(3-propionic acid) (2.10)

To a flame-dried round-bottom flask equipped with a magnetic stir bar and back-filled with argon, compound **2.9** (0.450 g, 0.902 mmol) and 100 mL of CH_2Cl_2 were added. TEMPO (35.0 mg, 0.226 mmol, 0.25 eq) and iodobenzene diacetate (0.641 g, 1.99 mmol, 2.2 eq) were added to the solution and stirred at room temperature for 6 h. 100 μL of a 1:1 mixture of CH_3CN:water was added and the reaction was allowed to stir for an additional 24 h. The THF was evaporated in vacuo, and the residue was taken up in 5 mL of hexanes. This crude mixture was triturated for 10 minutes, after which white crystals began to precipitate. The white crystals were isolated by filtration and washed with cold hexanes. Trituration of the filtrate was repeated until precipitation of the white crystals ceased (~3 crops.) The product was isolated as a white solid 0.393 g (85 %). ^{1}H NMR (500 MHz, $CDCl_3$): δ = 1.00 (s, 9), 1.34 (m, 2), 1.72* (m, {2}), 1.96* (m, {2}), 2.23 (m, {2}), 3.45 (t, 2, J = 6), 7.36 (m, 6), 7.58 (m, 4). ^{13}C NMR (125 MHz, $CDCl_3$): δ = 19.15, 26.81, 31.95, 32.40, 33.22, 34.37, 62.76, 79.51, 127.64, 129.63, 133.73, 135.51, 176.34. ^{11}B NMR (160 MHz, $CDCl_3$, proton-decoupled): δ = -12.13. Calc.: $[M]^+$ m/z = 512.77. Found ES-MS: $[M + HCOOH]^+$ = 558.2. Anal. Calc. C 56.22%, H 7.86%. Found: C 56.37%, H 7.84%.

2.4.2.8. Synthesis of 2.11

The coupling was carried out as described above, specifically using **2.8** (0.042 g, 0.187 mmol), **2.10** (0.240 g, 0.468 mmol, 2.5 equiv.), EDC (0.108 g, 0.561 mmol, 3 equiv.) and a catalytic amount of DPTS (~25 mg) dissolved in 20 mL of CH_2Cl_2 for 18 h at room temperature. Flash chromatography was performed using 9:1 CH_2Cl_2:ethyl acetate as eluent. Yield: 0.183 g, white solid (81%). ^{1}H NMR (500 MHz, $CDCl_3$): δ = 1.01 (s, 18), 1.21 (s, 3), 1.37 (m, 4), 1.72* (m, {4}), 1.90* (m, {4}), 2.09* (m, {4}) 3.47 (t, 4, *J* = 6), 4.15 (m, 4), 7.36 (m, 15), 7.58 (m, 10). ^{13}C NMR (125 MHz, $CDCl_3$): δ = 17.78, 19.16, 26.82, 32.06, 32.41, 33.35, 34.38, 46.23, 62.77, 63.71, 65.61, 66.89, 79.51, 127.64, 128.17, 128.52, 128.62, 129.63, 133.73, 135.51, 171.04, 172.29. ^{11}B NMR (160 MHz, $CDCl_3$, proton-decoupled): δ = -12.15. Calc.: $[M]^+$ m/z = 1213.78. Found ES-MS: $[M + NH_4]^+$ = 1231.5.

2.4.2.10. Synthesis of 3-[G-0]-(OTBDPS)$_3$ (2.13)

The coupling was carried out as described above, specifically using **2.2** (0.027 g, 0.089 mmol), **2.10** (0.159 g, 0.310 mmol, 3.5 equiv.), EDC (0.68 g, 0.354 mmol, 4 equiv.) and a catalytic amount of DPTS (approx. 10 mg) dissolved in 2 mL of CH_2Cl_2 for 18 h at room temperature. Flash chromatography was performed using 100% CH_2Cl_2 as eluent. Yield: 0.148 g, white foam (93%). ^{1}H NMR (500 MHz, $CDCl_3$): δ = 1.02 (s, 27), 1.39 (m, 6), 1.72* (m, {6}), 2.10* (m, {6}), 2.43* (m, {6}) 3.48 (t, 6, *J* = 6), 6.93 (d, 6, *J* = 8.7), 7.04 (d, 6, *J* = 8.7), 7.39 (m, 20), 7.59 (m, 10). ^{13}C NMR (125 MHz, $CDCl_3$): δ =

19.15, 26.80, 30.79, 32.11, 32.41, 33.84, 34.37, 51.60, 62.74, 79.57, 120.72, 127.63, 129.62, 133.71, 135.50, 146.09, 148.70, 170.07, ^{11}B NMR (160 MHz, $CDCl_3$, proton-decoupled): δ = -11.95. Calc.: $[M]^+$ m/z = 1790.61. Found MALDI-TOF MS: $[M + Na]^+$ = 1821. Anal. Calc. C 61.71%, H 7.43%. Found: C 61.76%, H 7.47%.

2.4.2.11. Synthesis of 6-[G-1]-(OTBDPS)$_6$ (2.14)

The coupling was carried out as described above, specifically using **2.4** (0.017 g, 0.024 mmol), **2.10** (0.100 g, 0.195 mmol, 8 equiv.), EDC (0.047 g, 0.244 mmol, 10 equiv.) and a catalytic amount of DPTS (~15 mg) dissolved in 1 mL of CH_2Cl_2 and 0.67 mL of pyridine for 16 h at room temperature. Flash chromatography was performed using 100% CH_2Cl_2 as eluent. Yield: 0.074 g, white foam (84%). ^{1}H NMR (500 MHz, $CDCl_3$): δ = 1.01 (s, 56), 1.34 (s, 9), 1.35 (m, 12), 1.72* (m, {12}), 1.97* (m, {12}), 2.20* (m, {12}) 3.47 (t, 12, *J* = 6), 4.29 (q, 12, J = 1.8, 4.2) 6.96 (d, 6, *J* = 8.7), 7.11 (d, 6, *J* = 8.7), 7.36 (m, 40), 7.59 (m, 20). ^{13}C NMR (125 MHz, $CDCl_3$): δ = 17.85, 19.14, 26.81, 32.10, 32.40, 33.41, 34.37, 46.59, 51.73, 62.75, 65.39, 79.52, 120.66, 127.63, 129.61, 129.75, 133.70, 135.49, 146.33, 148.61, 171.03. ^{11}B NMR (160 MHz, $CDCl_3$, proton-decoupled): δ = -12.00. Calc.: $[M]^+$ m/z =3623.22. Found MALDI-TOF MS: $[M + K]^+$ = 3661. Anal. Calc. C 59.34%, H 7.51%. Found: C 59.51%, H 7.53%.

2.4.2.12. Synthesis of 12-[G-2]-(OTBDPS)$_{12}$ (2.15)

The coupling was carried out as described above, specifically using **2.12** (0.035 g, 0.026 mmol), **2.10** (0.200 g, 0.390 mmol, 15 equiv.), EDC (0.090 g, 0.470 mmol, 18 equiv.) and a catalytic amount of DPTS (~25 mg) dissolved in 1 mL of CH_2Cl_2 and 0.67 mL of pyridine for 18 h at room temperature. Flash chromatography was performed using 100% CH_2Cl_2 as eluent. Yield: 0.150 g, white foam (79%). ^{1}H NMR (500 MHz, $CDCl_3$): δ = 1.01 (s, 108), 1.21 (s, 18), 1.35 (m, 24), 1.38 (s, 9) 1.72* (m, {24}), 1.96* (m, {24}), 2.17* (m, {24}) 3.47 (t, 24, *J* = 6), 4.15 (q, 24, J = 1.8, 4.2), 4.35 (s, 12), 6.96 (d, 6, *J* = 8.7), 7.11 (d, 6, *J* = 8.7), 7.39 (m, 80), 7.59 (m, 40). ^{13}C NMR (125 MHz, $CDCl_3$): δ = 17.88, 19.14, 26.82, 32.07, 32.41, 33.34, 34.38, 46.31, 62.75, 65.21, 79.48, 120.66, 127.63, 129.61, 129.82, 133.70, 135.49, 170.98, 171.71. ^{11}B NMR (160 MHz, $CDCl_3$, proton-decoupled): δ = -11.99. Calc.: $[M]^+$ m/z = 7288.43. Found MALDI-TOF MS: $[M + K]^+$ = 7340.

2.4.2.13. Synthesis of 1,12-bis(3-hydroxypropyl)-1,12-dicarbadodecaborane (2.16)

To a flame-dried round-bottom flask equipped with a magnetic stir bar and back-filled with argon, p-carborane (2.00 g, 13.9 mmol) was added along with 150 mL of THF. The solution was cooled to 0°C and n-butyl lithium (12.9 mL, 27.7 mmol, 2.0 eq) was added. The reaction mixture was allowed to warm to room temperature and was stirred for 2 h. Trimethylene oxide (1.79 mL, 27.7 mmol, 2.0 eq) was then added via argon-filled syringe, and the reaction mixture was stirred for an additional 12 h at room temperature.

The THF was then evaporated in vacuo and the residue was taken up in 100 mL of CH_2Cl_2, poured into a separatory funnel and washed with 1 M HCl (3 x 100 mL). The organic layer was then dried ($MgSO_4$), filtered, and evaporated to dryness in vacuo. The crude product was crystallized from chloroform to yield 3.32 g of white needles (92%). ^{1}H NMR (500 MHz, MeOD): δ = 1.36 (m, 4), 1.72* (m. {4}), 3.35 (t , 4, *J* = 6). ^{13}C NMR (125 MHz, MeOD): δ = 33.64, 35.50, 61.84, 80.33. ^{11}B NMR (160 MHz, MeOD, proton-decoupled): δ = -11.99. Calc.: $[M]^+$ m/z = 260.4. Found ES-MS: $[M + NH_4]^+$ = 278.3.

2.4.2.14. Synthesis of 1-(3-(benzyloxy)propyl)-12-(3-hydroxypropyl)-1,12-dicarba-dodecaborane (2.17)

To a flame-dried round-bottom flask equipped with a magnetic stir bar and back-filled with argon, compound **2.16** (0.70 g, 2.69 mmol), NaH (0.25 g, 10.40 mmol, 3.9 eq), and 40 mL of THF were added. The mixture was cooled to 0 °C and stirred for 2 h. Tetra-butyl ammonium iodide (0.10 g, 0.27 mmol, 0.1 eq) and benzyl bromide (0.46 g, 2.69 mmol, 1.0 eq) were then added and the mixture was allowed to warm to room temperature and stirred for an additional 12 h. The THF was then evaporated in vacuo and the residue was taken up in 100 mL of ether, poured into a separatory funnel and washed with 1 M HCl (3 x 100 mL). The organic layer was then dried ($MgSO_4$), filtered, and evaporated to dryness in vacuo. The product was finally isolated by column chromatography using a 7:3 mixture of hexanes:ethyl acetate, yielding 0.448 g of white

solid (48%). ^{1}H NMR (500 MHz, $CDCl_3$): δ = 1.42 (m, 2), 1.46 (m,2), 1.72* (m, {4}), 3.29 (t, 2, J = 6), 3.46 (t , 2, *J* = 6), 4.41 (s, 2), 7.27 (m, 3), 7.33 (m, 2). ^{13}C NMR (125 MHz, $CDCl_3$): δ = 29.64, 32.45, 34.18, 34.55, 61.89, 69.20, 72.85, 78.68, 78.87, 127.59, 128.36, 138.25. ^{11}B NMR (160 MHz, $CDCl_3$, proton-decoupled): δ = -11.99. Calc.: $[M]^+$ m/z = 350.5. Found ES-MS: $[M + NH_4]^+$ = 368.5.

2.4.2.15. Synthesis of 12-(benzyloxy)propyl-1,12-dicarbadodecaboranyl-1-(3-propionic acid) (2.18)

To a flame-dried round-bottom flask equipped with a magnetic stir bar and back-filled with argon, compound **2.17** (0.20 g, 0.571 mmol) and 25 mL of CH_2Cl_2 were added. TEMPO (23.3 mg, 0.143 mmol, 0.25 eq) and iodobenzene diacetate (0.404 g, 1.26 mmol, 2.2 eq) were then added to the solution and allowed to stir at room temperature for 6 h. Subsequently, 100 μL of a 1:1 mixture of CH_3CN:water was added to the reaction and allowed to stir for a further 24 h. The THF was evaporated in vacuo, and the residue was taken up in 5 mL of hexanes. This mixture was triturated for 10 minutes, after which white crystals began to precipitate. The white crystals were isolated by filtration and washed with cold hexanes. The trituration of the filtrate was repeated until precipitation of the white crystals ceased (~3 crops.). The product was isolated as a white solid, yielding 0.190 g (91%). ^{1}H NMR (500 MHz, $CDCl_3$): δ = 1.46 (m, 2), 1.73* (m, {2}), 1.98* (m, {2}), 2.24* (m, {2}), 3.29 (t , 2, *J* = 6), 4.42 (s, 2) 7.28 (m, 3), 7.34 (m, 2). ^{13}C NMR (125 MHz, $CDCl_3$): δ = 29.62, 31.91, 33.21, 34.57, 69.12, 72.85, 78.72, 78.89,

127.59, 128.36, 138.20, 176.51. ^{11}B NMR (160 MHz, $CDCl_3$, proton-decoupled): δ = -12.01. Calc.: $[M]^+$ m/z = 364.49. Found ES-MS: $[M]^+$ = 364.5.

2.4.2.16. Synthesis of 0-[G-1]-$(O_2Bn)_4$

The generation growth was carried out as described above, specifically using pentaerythritol (0.053 g, 0.391 mmol), **2.1** (1.00 g, 2.35 mmol, 6 equiv.) and a catalytic amount of DMAP (~40 mg), all dissolved in 3 mL of CH_2Cl_2 and 2 mL of pyridine and stirred for 24 h at room temperature. Yield: 0.342 g, white foam (92%). ^1H NMR (600 MHz, $CDCl_3$): δ = 0.86 (s, 12), 3.58 (d, 8, J = 11.4), 4.31 (s,8), 4.59 (d, 8, J = 11.4), 5.3 (s, 8), 7.29 (m ,12), 7.41 (m, 8). ^{13}C NMR (150 MHz, $CDCl_3$): δ = 17.07, 42.16, 43.34, 61.08, 73.07, 101.22, 125.65, 127.64, 128.27, 137.29, 172.55. Calc.: $[M]^+$ m/z = 953.0. ES-MS: $[M + NH_4]^+$ = 971.4. Anal.: Calc. C 66.79%, H 6.35%. Found: C 66.67%, H 5.79%.

2.4.2.17. Synthesis of 0-[G-1]-OH_8 (2.19)

Deprotection of 0-[G-1]-$(O_2Bn)_4$ (0.300 g, 0.315 mmol) in 20 mL of (1:1) CH_2Cl_2:MeOH was carried out as above for 16 h at room temperature under H_2 atmosphere. Yield: 0.187 g, white foam (99%). ^1H NMR (600 MHz, MeOD): δ = 1.20 (s, 12), 3.62 (d, 8, J = 10.8), 3.72 (d, 8, J = 10.8), 4.26 (s, 8). ^{13}C NMR (150 MHz, MeOD):

δ = 15.38, 42.40, 47.53, 50.09, 64.06, 174.08. Calc.: $[M]^+$ m/z = 600.61. Found ES-MS: $[M + NH_4]^+$ = 618.3. Anal.: Calc. C 49.99%, H 7.38%. Found: C 38.20%, H 8.17%.

2.4.2.18. Synthesis of 0-[G-2]-$(O_2Bn)_8$

The generation growth was carried out as described above, specifically using **2.19** (0.120 g, 0.200 mmol), **2.1** (0.852 g, 2.00 mmol, 10 equiv.) and a catalytic amount of DMAP (~25 mg) all dissolved in 6 mL of CH_2Cl_2 and 4 mL of pyridine and stirred for 18 h at room temperature. Yield: 0.445 g, white foam (>99%). ^{1}H NMR (600 MHz, $CDCl_3$): δ = 0.90 (s, 24), 1.15 (s, 12), 3.50 (q, 16, *J* = 6.0, 12.0), 3.89 (s, 8) 4.33 (q, 16, *J* = 10.8, 29.4), 4.53 (q, 16, *J* = 1.8, 4.2), 5.35 (s, 8), 7.29 (m, 24), 7.39 (m, 16). ^{13}C NMR (150 MHz, $CDCl_3$): δ = 17.62, 17.66, 42.54, 46.96, 61.31, 64.89, 73.41, 73.45, 101.67, 126.20, 128.12, 128.85, 137.89, 171.76, 173.20. Calc.: $[M]^+$ m/z = 2234.38. Found MALDI-TOF MS: $[M + Na]^+$ = 2258. Anal.: Calc. C 65.04%, H 6.32%. Found: C 64.55%, H 6.54%.

2.4.2.19. Synthesis of 0-[G-2]-OH_{16} (2.20)

Deprotection of 0-[G-2]-$(O_2Bn)_8$ (0.363 g, 0.162 mmol) in 20 mL of (1:1) CH_2Cl_2:MeOH was carried out as above for 16 h at room temperature under H_2 atmosphere. Yield: 0.238 g, white foam (96%). ^{1}H NMR (600 MHz, MeOD): δ = 1.18 (s, 24), 1.35 (s, 12), 3.62 (d, 16, *J* = 10.8), 3.70 (q, 16, *J* = 2.4, 10.8) 4.30 (s, 8), 4.31 (d, 8, *J* = 11.4), 4.39 (d, 8, *J* = 11.4). ^{13}C NMR (150 MHz, MeOD): δ = 17.38, 18.31, 44.37,

48.11, 51.85, 63.69, 65.91, 66.14, 173.82, 176.00. Calc.: $[M]^+$ m/z = 1529.53. Found MALDI-TOF MS: $[M + Na]^+$ = 1553. Anal. Calc. C 51.04%, H 7.12%. Found: C 50.86%, H 7.37%.

2.4.2.20. Synthesis of 4-[G-0]-OBn_4 (2.21)

The coupling was carried out as described above, specifically using **2.18** (0.250 g, 0.686 mmol, 6 equiv.), pentaerythritol (0.016 g, 0.114 mmol, 1 equiv.), EDC (0.175 g, 0.915 mmol, 8 equiv.) and a catalytic amount of DPTS (~50 mg) dissolved in 3 mL of CH_2Cl_2 and 2 mL of pyridine for 24 h at room temperature. Flash chromatography was performed using 1:1 hexanes:ethyl acetate as eluent. Yield: 0.172 g, white foam (99%). ^1H NMR (600 MHz, $CDCl_3$): δ = 1.44 (m, 8), 1.71* (m, {8}), 1.93* (m, {8}), 2.15* (m, {8}) 3.28 (t, 8, *J* = 6), 3.97 (s, 8), 4.41 (s, 8), 7.27 (m, 12), 7.33 (m, 8). ^{13}C NMR (150 MHz, $CDCl_3$): δ = 29.63, 31.94, 33.28, 34.56, 41.71, 62.11, 69.11, 72.79, 79.33, 127.56, 127.85, 128.04, 128.35, 138.21, 170.98. ^{11}B NMR (190 MHz, $CDCl_3$, proton-decoupled): δ = -12.26. Calc.: $[M]^+$ m/z = 1522.05. Found MALDI-TOF MS: $[M + Na]^+$ = 1546. Anal. Calc. C 51.29%, H 7.69%. Found: C 50.06%, H 7.81%.

2.4.2.21. Synthesis of 4-[G-0]-OH_4

Deprotection of **2.21** (0.307 g, 0.202 mmol) in 20 mL of (1:1) CH_2Cl_2:MeOH was carried out as above for 16 h at room temperature under H_2 atmosphere. Yield: 0.210 g,

white foam (92%). ^{1}H NMR (600 MHz, $CDCl_3$): δ = 1.42 (m, 8), 1.71* (m, {8}), 1.93* (m, {8}), 2.15* (m, {8}) 3.46 (t, 8, *J* = 6), 3.99 (s, 8). ^{13}C NMR (150 MHz, $CDCl_3$): δ = 31.92, 32.40, 33.27, 34.16, 41.71, 61.82, 62.15, 79.18, 171.01. ^{11}B NMR (190 MHz, $CDCl_3$, proton-decoupled): δ = -12.26. Calc.: $[M]^+$ m/z = 1161.59. Found MALDI-TOF MS: $[M + Na]^+$ = 1178. Anal.: Calc. C 38.26%, H 7.98%. Found: C 38.46%, H 7.95%.

2.4.2.22. Synthesis of 4-[G-1]-(O_2Bn)$_4$.

The generation growth was carried out as described above with 4-[G-0]-OH_4 (0.150 g, 0.129 mmol), **2.1** (0.440 g, 1.03 mmol, 8 equiv.) and a catalytic amount of DMAP (~25 mg) all dissolved in 3 mL of CH_2Cl_2 and 2 mL of pyridine and stirred for 18 h at room temperature. Yield: 0.236 g, white foam (93%). ^{1}H NMR (600 MHz, $CDCl_3$): δ = 0.99 (s, 12), 1.53 (m, 8), 1.70* (m, {8}), 1.92* (m, {8}), 2.12* (m, {8}), 3.61 (d, 8, *J* = 11.4), 3.96 (s, 8), 4.03 (t, 8, *J* = 6), 4.58 (d, 8, *J* = 11.4), 5.43 (s, 4), 7.35 (m, 12) 7.42 (m, 8). ^{13}C NMR (150 MHz, $CDCl_3$): δ = 17.82, 28.61, 31.94, 33.26, 34.07, 41.75, 42.41, 62.08, 63.71, 73.50, 78.70, 101.78, 126.17, 128.20, 128.97, 137.74, 170.95, 173.75. ^{11}B NMR (190 MHz, $CDCl_3$, proton-decoupled): δ = -12.29. Calc.: $[M]^+$ m/z = 1978.45. Found MALDI-TOF MS: $[M + Na]^+$ = 2003. Anal.: Calc. C 51.60%, H 7.13%. Found: C 51.55%, H 7.36%.

2.4.2.23. Synthesis of 4-[G-1]-OH_8

Deprotection of 4-[G-1]-$(O_2Bn)_4$ (0.200 g, 0.101 mmol) in 20 mL of (1:1) CH_2Cl_2:MeOH was carried out as above for 16 h at room temperature under H_2 atmosphere. Yield: 0.153 g, white foam (93%). ^{1}H NMR (600 MHz, MeOD): δ = 1.14 (s, 12), 1.54 (m, 8), 1.79* (m, {8}), 2.01* (m, {8}), 2.23* (m, {8}), 3.59 (d, 8, *J* = 10.8), 3.66 (d, 8, *J* = 10.8), 3.97 (t, 8, *J* = 6), 4.05 (s, 8). ^{13}C NMR (150 MHz, MeOD): δ = 17.35, 29.83, 33.31, 34.32, 35.32, 43.28, 51.56, 63.42, 64.41, 65.85, 79.04, 80.37, 172.43, 176.43. ^{11}B NMR (190 MHz, MeOD, proton-decoupled): δ = -12.24. Calc.: $[M]^+$ m/z = 1626.02. Found MALDI-TOF MS: $[M + Na]^+$ = 1652. Anal. Calc. C 42.10%, H 7.69%. Found: C 42.41%, H 7.45%.

2.4.2.24. Synthesis of 4-[G-2]-$(O_2Bn)_8$

The generation growth was carried out as described above with 4-[G-1]-OH_8 (0.118 g, 0.074 mmol), **2.1** (0.504 g, 1.18 mmol, 16 equiv.) and a catalytic amount of DMAP (~25 mg) all dissolved in 3 mL of CH_2Cl_2 and 2 mL of pyridine and stirred for 18 h at room temperature. Yield: 0.236 g, white foam (88%). ^{1}H NMR (600 MHz, $CDCl_3$): δ = 0.95 (s, 24), 1.21 (s, 12), 1.35 (m, 8), 1.51 (m, 8), 1.92* (m, {8}), 2.14* (m, {8}), 3.61 (dd, 16, *J* = 1.2, 11.4), 3.74 (t, 8, *J* = 6), 3.96 (s, 8), 4.58 (q, 16, *J* = 11.4, 16.2), 4.57 (m, 16) 5.42 (s, 8), 7.32 (m, 24) 7.39 (m, 16). ^{13}C NMR (150 MHz, $CDCl_3$): δ = 17.69, 17.73, 28.21, 31.94, 33.27, 33.85, 42.56, 46.79, 62.02, 63.89, 65.41, 73.44, 73.50, 78.54, 101.68, 126.14, 128.09, 128.84, 137.78, 170.93, 172.42, 173.18. ^{11}B NMR (190 MHz, $CDCl_3$,

proton-decoupled): δ = -12.29. Calc.: $[M]^+$ m/z = 3259.80. Found MALDI-TOF MS: $[M + K]^+$ = 3315. Anal. Calc. C 56.37%, H 6.80%. Found: C 56.59%, H 6.82%.

2.4.2.24. Synthesis of 4-[G-2]-OH_{16}

Deprotection of 4-[G-2]-$(O_2Bn)_8$ (0.162 g, 0.050 mmol) in 20 mL of (1:1) CH_2Cl_2:MeOH was carried out as above for 16 h at room temperature under H_2 atmosphere. Yield: 0.120 g, white foam (94%). ^{1}H NMR (600 MHz, MeOD): δ = 1.16 (s, 24), 1.28 (s, 12), 1.57 (m, 8), 1.79* (m, {8}), 2.01* (m, {8}), 2.23* (m, {8}), 3.62 (m, 16), 3.69 (m, 16), 3.99 (t, 8, *J* = 6), 4.06 (s, 8),4.26 (m, 16). ^{13}C NMR (150 MHz, MeOD): δ = 15.46, 16.35, 27.79, 31.43, 32.43, 33.42, 41.48, 45.94, 49.88, 61.51, 63.37, 63.95, 64.45, 77.24, 78.29, 170.56, 172.38, 173.98. ^{11}B NMR (190 MHz, MeOD, proton-decoupled): δ = -12.23. $[M]^+$ m/z = 2554.94. Found MALDI-TOF MS: $[M + Na]^+$ = 2577. Anal.: Calc. C 45.60%, H 7.42%. Found: C 45.57%, H 7.60%.

2.4.2.25. Synthesis of 4-[G-3]-$(O_2Bn)_{16}$

The generation growth was carried out as described above with 4-[G-2]-OH_{16} (0.250 g, 0.098 mmol), **2.1** (1.36 g, 3.13 mmol, 32 equiv.) and a catalytic amount of DMAP (~25 mg) all dissolved in 6 mL of CH_2Cl_2 and 4 mL of pyridine. The reaction mixture was stirred for 18 h at room temperature. Yield: 0.558 g, white foam (98%). ^{1}H NMR (600 MHz, $CDCl_3$): δ = 0.93 (s, 48), 1.00 (s, 12), 1.22 (s, 24), 1.43 (m, 8), *1.62

(m, {8}), 1.95* (m, {8}), 2.17* (m, {8}), 3.61 (m, 32), 3.83 (t, 8, J = 6), 3.99 (s, 8), 4.03 (m, 16), 4.38 (m, 32), 4.59 (m, 32), 5.44 (s, 16), 7.33 (m, 48) 7.43 (m, 32). ^{13}C NMR (150 MHz, $CDCl_3$): δ = 16.73, 17.24, 27.80, 31.51, 32.84, 33.48, 42.10, 45.90, 46.42, 61.44, 63.57, 64.68, 65.31, 73.05, 78.08, 101.22, 125.71, 127.65, 128.38, 137.37, 170.47, 171.38, 172.72. ^{11}B NMR (190 MHz, $CDCl_3$, proton-decoupled): δ = -12.26. $[M]^+$ m/z = 5822.49. Found MALDI-TOF MS: $[M + Na]^+$ = 5840. Anal.: Calc. C 59.62%, H 6.58%. Found: C 59.76%, H 6.48%.

2.4.2.26. Synthesis of 4-[G-3]-OH_{32}

Deprotection of 4-[G-3]-$(O_2Bn)_{16}$ (0.500 g, 0.086 mmol) in 40 mL of (1:1) CH_2Cl_2:MeOH was carried out as above for 16 h at room temperature under H_2 atmosphere. Yield: 0.373 g, white foam (98%). ^{1}H NMR (600 MHz, MeOD): δ = 1.18 (s, 48), 1.29 (s, 12), 1.30 (s,24), 1.58 (m, 8), 1.79* (m, {8}), 2.00* (m, {8}), 2.23* (m, {8}), 3.62 (m, 32), 3.69 (m, 32), 4.01 (t, 8, J = 6), 4.05 (s, 8), 4.29 (m, 48). ^{13}C NMR (150 MHz, MeOD): δ = 15.48, 16.22, 16.44, 27.81, 28.54, 28.88, 31.43, 32.43, 33.36, 46.06, 49.90, 61.44, 63.58, 63.97, 64.28, 65.35, 77.25, 78.28, 170.57, 171.83, 174.02. ^{11}B NMR (190 MHz, MeOD, proton-decoupled): δ = -12.22. $[M]^+$ m/z = 4412.79. Found MALDI-TOF MS: $[M]^+$ = 4428. Anal.: Calc. C 48.18%, H 7.22%. Found: C 50.04%, H 7.74%.

2.4.2.27. Synthesis of 4-[G-4]-$(O_2Bn)_{32}$

The generation growth was carried out as described above with 4-[G-3]-OH_{32} (0.305 g, 0.069 mmol), **2.1** (1.88 g, 4.42 mmol, 64 equiv.) and a catalytic amount of DMAP (~50 mg) all dissolved in 6 mL of CH_2Cl_2 and 4 mL of pyridine and stirred for 18 h at room temperature. Yield: 0.660 g, white foam (87%). ^{1}H NMR (600 MHz, $CDCl_3$): δ = 0.94 (s, 96), 1.03 (s, 24), 1.11 (s, 12), 1.22 (s, 48), 1.45 (m, 8), *1.64 (m, {8}), 1.94* (m, {8}), 2.16* (m, {8}), 3.59 (m, 64), 3.84 (t, 8, *J* = 6), 3.97 (s, 8), 4.11 (m, 48), 4.38 (m, 64), 4.58 (m, 64), 5.42 (s, 32), 7.32 (m, 96) 7.43 (m, 64). ^{13}C NMR (150 MHz, $CDCl_3$): δ = 16.73, 16.81, 17.22, 27.84, 31.53, 32.84, 33.48, 42.08, 45.97, 46.04, 46.39, 63.70, 64.60, 64.95, 65.56, 72.96, 73.02, 101.19, 125.25, 127.65, 128.38, 137.42, 170.43, 170.91, 171.20, 171.39, 172.71. ^{11}B NMR (190 MHz, $CDCl_3$, proton-decoupled): δ = -12.25. $[M]^+$ m/z = 10947.89. Found MALDI-TOF MS: $[M]^+$ = 10957. Anal.: Calc. C 61.55%, H 6.44%. Found: C 61.46%, H 6.40%.

2.4.2.28. Synthesis of 4-[G-4]-OH_{64}

Deprotection of 4-[G-4]-$(O_2Bn)_{32}$ (0.523 g, 0.048 mmol) in 30 mL of (1:1) CH_2Cl_2:MeOH was carried out as above for 16 h at room temperature under H_2 atmosphere. Yield: 0.387 g, white foam (99%). ^{1}H NMR (600 MHz, MeOD): δ = 1.18 (s, 96), 1.33 (s, 84), 1.57 (m, 8), 1.83* (m, {8}), 2.00* (m, {8}), 2.23* (m, {8}), 3.63 (m, 64), 3.70 (m, 64), 4.03 (t, 8, *J* = 6), 4.05 (s, 8), 4.32 (m, 112). ^{13}C NMR (150 MHz, MeOD): δ = 15.53, 16.28, 16.49, 27.86, 31.34, 32.34, 33.34, 46.06, 46.19, 49.91, 63.64,

64.00, 64.30, 65.20, 65.62, 170.65, 171.38, 171.85, 171.89, 174.05. ^{11}B NMR (190 MHz, MeOD, proton-decoupled): δ = -12.21. $[M]^+$ m/z = 8128.47. Found MALDI-TOF MS: $[M]^+$ = 8141. Anal.: Calc. C 49.80%, H 7.09%. Found: C 50.00%, H 7.03%.

2.4.2.29. Synthesis of 8-[G-1]-OBn$_8$ (2.22)

The coupling was carried out as described above with **2.18** (0.500 g, 1.37 mmol, 11 equiv.), **2.19** (0.075 g, 0.125 mmol, 1 equiv.), EDC (0.400 g, 2.09 mmol, 15 equiv.) and a catalytic amount of DPTS (~70 mg) dissolved in 4.5 mL of CH_2Cl_2 and 3 mL of pyridine for 24 h at room temperature. Flash chromatography was performed using 75:25 hexanes:ethyl acetate as eluent. Yield: 0.391 g, white foam (93%). ^{1}H NMR (600 MHz, $CDCl_3$): δ = 1.23 (s, 12), 1.50 (m, 16), 1.75* (m, {16}), 2.00* (m, {16}), 2.22* (m, {16}), 3.32 (t, 16, J = 6), 4.06 (s, 8), 4.17 (m, 16), 4.45 (s, 16), 7.30 (m, 24), 7.37 (m, 16). ^{13}C NMR (150 MHz, $CDCl_3$): δ = 17.30, 29.20, 31.56, 32.81, 33.09, 34.13, 42.56, 45.92, 61.32, 64.57, 68.69, 72.38, 78.86, 127.12, 127.91, 137.79, 170.53, 171.14. ^{11}B NMR (190 MHz, $CDCl_3$, proton-decoupled): δ = -12.23. $[M]^+$ m/z = 3372.41. Found MALDI-TOF MS: $[M + Na]^+$ = 3395. Anal.: Calc. C 51.64%, H 7.53%. Found: C 51.74%, H 7.65%.

2.4.2.30. Synthesis of 8-[G-1]-OH$_8$

Deprotection of **2.22** (0.320 g, 0.095 mmol) in 30 mL of (1:1) CH_2Cl_2:MeOH was carried out as above for 16 h at room temperature under H_2 atmosphere. Yield: 0.251,

white foam (99%). ^{1}H NMR (600 MHz, MeOD): δ = 1.28 (s, 12), 1.42 (m, 16), 1.77* (m, {16}), 2.04* (m, {16}), 2.24* (m, {16}), 3.40 (t, 16, *J* = 6), 4.12 (s, 8), 4.23 (m, 16). ^{13}C NMR (150 MHz, MeOD): δ = 16.49, 31.51, 31.82, 32.51, 33.71, 42.83, 45.92, 59.98, 61.84, 64.84, 77.04, 78.97, 170.57, 171.43. ^{11}B NMR (190 MHz, MeOD, proton-decoupled): δ = -12.20. $[M]^+$ m/z = 2651.43 Found MALDI-TOF MS: $[M + Na]^+$ = 2674. Anal.: Calc. C 40.32%, H 7.76%. Found: C 40.43%, H 7.65%.

2.4.2.31. Synthesis of 8-[G-2]-$(O_2Bn)_8$

The generation growth was carried out as described above, specifically using 2-[G-1]-OH_8 (0.230 g, 0.087 mmol), **2.1** (0.600 g, 1.30 mmol, 16 equiv.) and a catalytic amount of DMAP (~25 mg) all dissolved in 6 mL of CH_2Cl_2 and 4 mL of pyridine and stirred for 18 h at room temperature. Yield: 0.329 g, white foam (88%). ^{1}H NMR (600 MHz, $CDCl_3$): δ = 1.02 (s, 24), 1.22 (s, 12), 1.55 (m, 16), *1.74 (m, {16}), *1.98 (m, {16}), *2.20 (m, {16}), 3.65 (d, 16, *J* = 11.4), 4.06 (m, 40), 4.62 (d, 16, *J* = 11.4), 5.46 (s, 8), 7.35 (m, 24), 7.45 (m, 16). ^{13}C NMR (150 MHz, $CDCl_3$): δ = 17.38, 18.83, 28.17, 31.56, 32.78, 33.63, 41.96, 45.90, 62.97, 63.27, 64.52, 71.87, 73.05, 78.58, 101.33, 125.67, 127.75, 128.52, 137.31, 170.50, 171.12, 173.29. ^{11}B NMR (190 MHz, $CDCl_3$, proton-decoupled): δ = -12.25. $[M]^+$ m/z = 4285.21. Found MALDI-TOF MS: $[M + Na]^+$ = 4308. Anal.: Calc. C 51.85%, H 7.06%. Found: C 51.66%, H 7.20%.

2.4.2.32. Synthesis of 8-[G-2]-OH_{16}

Deprotection of 8-[G-2]-$(O_2Bn)_8$ (0.329 g, 0.077 mmol) in 20 mL of (1:1) CH_2Cl_2:MeOH was carried out as above for 16 h at room temperature under H_2 atmosphere. Yield: 0.252, white foam (92%). ^{1}H NMR (600 MHz, MeOD): δ = 1.16 (s, 24), 1.29 (s, 12), 1.57 (m, 16), 1.81* (m, {16}), 2.04* (m, {16}), 2.27* (m, {16}), 3.65 (m, 32), 3.99 (t, 16, *J* = 6), 4.13 (s, 8), 4.23 (m, 16). ^{13}C NMR (150 MHz, MeOD): δ = 14.06, 15.09, 26.50, 30.03, 31.01, 32.01, 44.42, 48.17, 61.06, 62.49, 63.36, 75.69, 77.00, 169.05, 169.93, 173.06. ^{11}B NMR (190 MHz, MeOD, proton-decoupled): δ = -12.26. $[M]^+$ m/z = 3580.35. Found MALDI-TOF MS: $[M + Na]^+$ = 3597. Anal.: Calc. C 43.27%, H 7.54%. Found: C 45.66%, H 7.70%.

2.4.2.33. Synthesis of 8-[G-3]-$(O_2Bn)_{16}$

The generation growth was carried out as described above, specifically using 2-[G-2]-OH_{16} (0.200 g, 0.056 mmol), **2.1** (0.762 g, 1.79 mmol, 32 equiv.) and a catalytic amount of DMAP (~50 mg) all dissolved in 6 mL of CH_2Cl_2 and 4 mL of pyridine and stirred for 18 h at room temperature. Yield: 0.369 g, white foam (97%). ^{1}H NMR (600 MHz, $CDCl_3$): δ = 0.98 (s, 48), 1.22 (s, 12), 1.25 (s, 24), 1.40 (m, 16), 1.56 (m, 16), *1.97 (m, {16}), *2.20 (m, {16}), 3.64 (m, 32), 3.78 (t, 16, *J* = 6), 4.04 (s, 8), 4.16 (m, 16), 4.39 (m, 32), 4.61 (m, 32), 5.45 (s, 16), 7.35 (m, 48), 7.44 (m, 32). ^{13}C NMR (150 MHz, $CDCl_3$): δ = 17.28, 27.78, 31.56, 32.78, 33.42, 42.11, 45.91, 46.34, 63.46, 64.45, 64.94, 72.99, 73.05, 78.08, 101.224, 125.71, 127.65, 128.41, 137.35, 170.50, 171.13, 171.97,

172.74. ^{11}B NMR (190 MHz, $CDCl_3$, proton-decoupled): δ = -12.27. $[M]^+$ m/z = 6847.90. Found MALDI-TOF MS: $[M + Na]^+$ = 6862. Anal.: Calc. C 56.30%, H 6.77%. Found: C 56.51%, H 6.86%.

2.4.2.34. Synthesis of 8-[G-3]-OH_{32}

Deprotection of 8-[G-3]-$(O_2Bn)_{16}$ (0.321 g, 0.047 mmol) in 30 mL of (1:1) CH_2Cl_2:MeOH was carried out as above for 16 h at room temperature under H_2 atmosphere. Yield: 0.246, white foam (97%). ^{1}H NMR (600 MHz, MeOD): δ = 1.16 (s, 48), 1.28 (s, 12), 1.29 (s, 24), 1.59 (m, 16), 1.80* (m, {16}), 2.03* (m, {16}), 2.27* (m, {16}), 3.62 (m, 32), 3.68 (m, 32), 4.01 (t, 16, J = 6), 4.13 (s, 8), 4.27 (m, 48). ^{13}C NMR (150 MHz, MeOD): δ = 15.51, 16.41, 27.84, 31.51, 32.49, 33.46, 45.94, 49.88, 63.39, 63.96, 64.44, 64.89, 77.29, 78.36, 170.57, 171.48, 172.39, 173.99. ^{11}B NMR (190 MHz, MeOD, proton-decoupled): δ = -12.20. $[M]^+$ m/z = 5438.20. Found MALDI-TOF MS: $[M + Na]^+$ = 5453. Anal.: Calc. C 46.16%, H 7.34%. Found: C 46.03%, H 7.50%.

2.4.2.35. Synthesis of 8-[G-4]-$(O_2Bn)_{32}$

The generation growth was carried out as described above, specifically using 2-[G-3]-OH_{32} (0.200 g, 0.037 mmol), **2.1** (1.00 g, 2.35 mmol, 64 equiv.) and a catalytic amount of DMAP (~50 mg) all dissolved in 6 mL of CH_2Cl_2 and 4 mL of pyridine and stirred for 18 h at room temperature. Yield: 0.375 g, white foam (85%). ^{1}H NMR (600

MHz, $CDCl_3$): δ = 0.96 (s, 96), 1.00 (s, 24), 1.21 (s, 12), 1.23 (s, 48), 1.44 (m, 16), 1.63* (m, {16}), 1.97* (m, {16}), 2.19* (m, {16}), 3.641 (m, 64), 3.84 (t, 16, J = 6), 4.04 (m, 40), 4.15 (m, 16), 4.38 (m, 64), 4.59 (m, 64), 5.43 (s, 32), 7.34 (m, 96), 7.44 (m, 64). ^{13}C NMR (150 MHz, $CDCl_3$): δ = 16.75, 17.23, 27.81, 31.58, 32.78, 33.49, 42.10, 45.88, 46.42, 63.57, 64.29, 64.67, 65.22, 72.97, 73.04, 78.14, 101.21, 125.72, 127.65, 128.38, 137.39, 170.49, 171.38, 172.72. ^{11}B NMR (190 MHz, $CDCl_3$, proton-decoupled): δ = -12.25. $[M]^+$ m/z = 11973.30. Found MALDI-TOF MS: $[M + Na]^+$ = 11985. Anal.: Calc. C 59.49%, H 6.57%. Found: C 59.37%, H 6.56%.

2.4.2.36. Synthesis of 8-[G-4]-OH_{64}

Deprotection of 8-[G-4]-$(O_2Bn)_{32}$ (0.324 g, 0.027 mmol) in 30 mL of (1:1) CH_2Cl_2:MeOH was carried out as above for 16 h at room temperature under H_2 atmosphere. Yield: 0.247 g, white foam (99%). ^1H NMR (600 MHz, MeOD): δ = 1.18 (s, 96), 1.29 (s, 12), 1.30 (s, 24), 1.32 (s, 48), 1.59 (m, 16), 1.80* (m, {16}), 2.03* (m, {16}), 2.27* (m, {16}), 3.63 (m, 64), 3.70 (m, 64), 4.03 (m, 16), 4.12 (s, 8), 4.29 (m, 112). ^{13}C NMR (150 MHz, MeOD): δ = 15.53, 16.29, 16.50, 27.86, 28.55, 29.78, 30.35, 31.52, 32.50, 33.40, 35.08, 45.96, 46.07, 49.91, 63.62, 63.99, 64.29, 64.97, 65.33, 77.28, 78.36, 170.60, 171.62, 171.85, 174.04. ^{11}B NMR (190 MHz, MeOD, proton-decoupled): δ = -12.19. $[M]^+$ m/z = 9153.89. Found MALDI-TOF MS: $[M]^+$ = 9163. Anal.: Calc. C 48.42%, H 7.18%. Found: C 48.60%, H 7.26%.

2.4.2.37. Synthesis of 8-[G-5]-$(O_2Bn)_{64}$

The generation growth was carried out as described above, specifically using 2-[G-4]-OH_{64} (0.180 g, 0.020 mmol), **2.1** (1.07 g, 2.52 mmol, 128 equiv.) and a catalytic amount of DMAP (~50 mg) all dissolved in 6 mL of CH_2Cl_2 and 4 mL of pyridine and stirred for 18 h at room temperature. Yield: 0.364 g, white foam (83%). ^{1}H NMR (600 MHz, $CDCl_3$): δ = 0.93 (s, 192), 1.03 (s, 48), 1.11 (s, 24), 1.19 (s, 12), 1.22 (s, 96), 1.44 (m, 16), 1.63* (m, {16}), 1.95* (m, {16}), 2.17* (m, {16}), 3.58 (m, 128), 3.84 (m, 16), 4.06 (s, 64), 4.14 (m, 56), 4.38 (m, 128), 4.57 (m, 128), 5.41 (s, 64), 7.32 (m, 192), 7.42 (m, 128). ^{13}C NMR (150 MHz, $CDCl_3$): δ = 16.74, 16.85, 17.21, 27.84, 31.59, 32.78, 33.47, 42.08, 45.91, 46.03, 46.39, 64.59, 64.91, 65.36, 72.94, 73.00, 101.17, 125.74, 127.65, 128.38, 137.44, 170.92, 171.39, 172.72. ^{11}B NMR (190 MHz, $CDCl_3$, proton-decoupled): δ = -12.21. $[M]^+$ m/z = 22224.09. Found MALDI-TOF MS: $[M + Na]^+$ = 22223. Anal.: Calc. C 61.45%, H 6.44%. Found: C 61.64%, H 6.57%.

2.4.2.38. Synthesis of 8-[G-5]-OH_{128}

Deprotection of 8-[G-5]-$(O_2Bn)_{64}$ (0.314 g, 0.014 mmol) in 20 mL of (1:1) CH_2Cl_2:MeOH was carried out as above for 16 h at room temperature under H_2 atmosphere. Yield: 0.220 g, white foam (94%). ^{1}H NMR (600 MHz, MeOD): δ = 1.19 (s, 192), 1.22 (s, 12), 1.34 (bs, 168), 1.61 (m, 16), 1.83* (m, {16}), 2.02* (m, {16}), 2.27* (m, {16}), 3.64 (m, 128), 3.72 (m, 128), 4.04 (m, 16), 4.12 (s, 8), 4.30 (m, 240). ^{13}C NMR (150 MHz, MeOD): δ = 15.59, 16.34, 16.54, 24.21, 24.93, 27.84, 28.58, 31.55,

32.48, 32.68, 33.43, 46.07, 46.20, 49.91, 63.99, 64.02, 64.31, 65.20, 78.36, 170.61, 171.64, 171.91, 174.07. ^{11}B NMR (190 MHz, MeOD, proton-decoupled): δ = -12.18. $[M]^+$ m/z = 16585.26. Found MALDI-TOF MS: $[M]^+$ = Did Not Fly. Anal.: Calc. C 49.90%, H 7.07%. Found: C 50.15%, H 6.92%.

2.4.2.39. Synthesis of 16-[G-2]-OBn$_{16}$ (2.23)

The coupling was carried out as described above, specifically using **2.18** (0.656 g, 1.80 mmol, 20 equiv.), **2.20** (0.138 g, 0.090 mmol, 1 equiv.), EDC (0.520 g, 2.70 mmol, 30 equiv.) and a catalytic amount of DPTS (~100 mg) dissolved in 6 mL of CH_2Cl_2 and 4 mL of pyridine for 24 h at room temperature. Flash chromatography was performed using 7:3 hexanes:ethyl acetate as eluent. Yield: 0.592 g, white foam (93%). ^{1}H NMR (600 MHz, $CDCl_3$): δ = 1.20 (s, 24), 1.24 (s, 12), 1.50 (m, 32), 1.75* (m, {32}), 1.98* (m, {32}), 2.20* (m, {32}), 3.32 (t, 32, *J* = 6), 4.15 (m, 56), 4.44 (s, 32), 7.30 (m, 48), 7.37 (m, 32). ^{13}C NMR (150 MHz, $CDCl_3$): δ = 16.98, 17.39, 29.21, 31.60, 32.84, 34.13, 45.66, 46.24, 61.86, 64.29, 64.48, 68.70, 72.38, 78.85, 127.11, 127.91, 137.80, 170.51, 170.97, 171.16. ^{11}B NMR (190 MHz, $CDCl_3$, proton-decoupled): δ = -12.22. $[M]^+$ m/z = 7073.14. Found MALDI-TOF MS: $[M + Na]^+$ = 7094. Anal.: Calc. C 51.79%, H 7.47%. Found: C 51.69%, H 7.29%.

2.4.2.40. Synthesis of 16-[G-2]-OH_{16} (2.24)

Deprotection of **2.23** (0.455 g, 0.064 mmol) in 20 mL of (1:1) CH_2Cl_2:MeOH was carried out as above for 16 h at room temperature under H_2 atmosphere. Yield: 0.352 g, white foam (97%). ^{1}H NMR (600 MHz, MeOD): δ = 1.24 (s, 24), 1.28 (s, 12), 1.43 (m, 32), 1.83* (m, {32}), 2.02* (m, {32}), 2.27* (m, {32}), 3.40 (m, 32), 4,25 (m, 56). ^{13}C NMR (150 MHz, MeOD): δ = 16.51, 16.74, 31.57, 31.85, 32.61, 33.74, 45.72, 60.00, 64.79, 77.06, 78.99, 170.54, 171.39. ^{11}B NMR (190 MHz, MeOD, proton-decoupled): δ = -12.18. Anal.: Calc. C 41.16%, H 7.66%. Found: C 42.33%, H 8.16%.

2.4.2.41. Synthesis of 16-[G-3]-$(O_2Bn)_{16}$

The generation growth was carried out as described above, specifically using 16-[G-2]-OH_{16} (0.300 g, 0.053 mmol), **2.1** (0.727 g, 1.71 mmol, 32 equiv.) and a catalytic amount of DMAP (~50 mg), all dissolved in 6 mL of CH_2Cl_2 and 4 mL of pyridine and stirred for 18 h at room temperature. Yield: 0.430 g, white foam (91%). ^{1}H NMR (600 MHz, $CDCl_3$): δ = 1.02 (s, 48), 1.19 (s, 24), 1.22 (s, 12), 1.57 (m, 32), 1.75* (m, {32}), 1.98* (m, {32}), 2.20* (m, {32}), 3.64 (d, 32, J = 11.4), 4.15 (m, 88), 4.61 (d, 32, J = 11.4), 5.45 (s, 16), 7.35 (m, 48), 7.44 (m, 32). ^{13}C NMR (150 MHz, $CDCl_3$): δ = 16.97, 17.39, 28.18, 31.60, 32.81, 33.64, 41.96, 45.65, 46.21, 63.27, 64.43, 73.03, 78.25, 101.31, 125.74, 127.75, 128.52, 137.33, 170.47, 170.98, 171.15, 173.29. ^{11}B NMR (190 MHz, $CDCl_3$, proton-decoupled): δ = -12.24. $[M]^+$ m/z = 8898.73. Found MALDI-TOF MS: $[M + Na]^+$ = 8924. Anal.: Calc. C 51.96%, H 7.02%. Found: C 51.76%, H 7.27%.

2.4.2.42. Synthesis of 16-[G-3]-OH_{32}

Deprotection of 16-[G-3]-$(O_2Bn)_{16}$ (0.378 g, 0.042 mmol) in 30 mL of (1:1) CH_2Cl_2:MeOH was carried out as above for 16 h at room temperature under H_2 atmosphere. Yield: 0.309 g, white foam (97%). ^{1}H NMR (600 MHz, MeOD): δ = 1.15 (s, 48), 1.27 (s, 24), 1.32 (s, 12), 1.57 (m, 32), 1.82* (m, {32}), 2.03* (m, {32}), 2.29* (m, {32}), 3.65 (m, 64), 3.96 (m, 32), 4.28 (bm, 56). ^{13}C NMR (150 MHz, MeOD): δ = 15.58, 16.51, 16.74, 28.03, 31.57, 31.61, 33.52, 45.72, 49.66, 62.57, 63.99, 64.79, 77.06, 78.99, 170.52, 171.39, 174.56. ^{11}B NMR (190 MHz, MeOD, proton-decoupled): δ = -12.19. $[M]^+$ m/z = 7489.02. Found MALDI-TOF MS: $[M + Na]^+$ = 7519. Anal.: Calc. C 43.78%, H 7.48%. Found: C 43.91%, H 7.38%.

2.4.2.43. Synthesis of 16-[G-4]-$(O_2Bn)_{32}$

The generation growth was carried out as described above, specifically using 16-[G-3]-OH_{32} (0.218 g, 0.029 mmol), **2.1** (0.795 g, 1.86 mmol, 64 equiv.) and a catalytic amount of DMAP (~75 mg) all dissolved in 6 mL of CH_2Cl_2 and 4 mL of pyridine and stirred for 18 h at room temperature. Yield: 0.318 g, white foam (78%). ^{1}H NMR (600 MHz, $CDCl_3$): δ = 0.97 (s, 96), 1.20 (s, 24), 1.22 (s, 12), 1.24 (s, 48), 1.39 (m, 32), 1.57* (m, {32}), 1.96* (m, {32}), 2.19* (m, {32}), 3.63 (m, 64), 3.78 (m, 32), 4.13 (bm, 56), 4.38 (m, 64), 4.60 (m, 64), 5.45 (s, 32), 7.32 (m, 96), 7.43 (m, 64). ^{13}C NMR (150 MHz, $CDCl_3$): δ = 16.97, 17.28, 24.40, 27.79, 31.60, 32.80, 33.43, 42.11, 45.65, 46.33, 63.47, 64.37, 64.92, 72.98, 73.04, 78.11, 101.21, 125.71, 127.65, 128.41, 137.36, 170.46,

171.97, 172.74. ^{11}B NMR (190 MHz, $CDCl_3$, proton-decoupled): δ = -12.25. $[M]^+$ m/z = 14024.12. Found MALDI-TOF MS: $[M + K]^+$ = 14062. Anal.: Calc. C 56.27%, H 6.76%. Found: C 56.46%, H 6.86%.

2.4.2.44. Synthesis of 16-[G-4]-OH_{64}.

Deprotection of 16-[G-4]-$(O_2Bn)_{32}$ (0.249 g, 0.018 mmol) in 20 mL of (1:1) CH_2Cl_2:MeOH was carried out as above for 16 h at room temperature under H_2 atmosphere. Yield: 0.194 g, white foam (97%). ^{1}H NMR (600 MHz, MeOD): δ = 1.17 (s, 96), 1.30 (bs, 84), 1.59 (m, 32), 1.82* (m, {32}), 2.05* (m, {32}), 2.28* (m, {32}), 3.63 (m, 64), 3.70 (m, 64), 4.02 (bs, 32), 4.25 (bm, 120). ^{13}C NMR (150 MHz, MeOD): δ = 15.56, 16.49, 16.74, 27.88, 31.58, 32.61, 33.48, 45.94, 49.89, 63.42, 63.98, 64.43, 77.06, 78.99, 170.52, 172.40, 174.01. ^{11}B NMR (190 MHz, MeOD, proton-decoupled): δ = -12.17. $[M]^+$ m/z = 11204.71. Found MALDI-TOF MS: $[M + K]^+$ = 11250. Anal.: Calc. C 46.41%, H 7.30%. Found: C 46.60%, H 7.51%.

2.4.2.45. Synthesis of 16-[G-5]-$(O_2Bn)_{64}$

The generation growth was carried out as described above, specifically using 16-[G-4]-OH_{64} (0.130 g, 0.012 mmol), **2.1** (0.636 g, 1.49 mmol, 128 equiv.) and a catalytic amount of DMAP (~50 mg) all dissolved in 3 mL of CH_2Cl_2 and 2 mL of pyridine and stirred for 18 h at room temperature. Yield: 0.204 g, white foam (72%). ^{1}H NMR (600

MHz, $CDCl_3$): δ = 0.94 (s, 192), 0.99 (s, 36), 1.20 (bs, 144), 1.40 (m, 32), 1.62* (m, {32}), 1.96* (m, {32}), 2.17* (m, {32}), 3.59 (m, 128), 3.83 (bs, 32), 4.10 (bm, 120), 4.37 (m, 128), 4.58 (m, 128), 5.42 (s, 64), 7.32 (m, 192), 7.43 (m, 128). ^{13}C NMR (150 MHz, $CDCl_3$): δ = 16.76, 17.22, 24.43, 27.82, 31.62, 32.80, 33.50, 39.92, 42.10, 45.85, 46.41, 63.57, 64.23, 64.66, 65.12, 72.95, 73.02, 101.18, 125.73, 127.65, 128.38, 137.41, 170.42, 171.38, 172.73. ^{11}B NMR (190 MHz, $CDCl_3$, proton-decoupled): δ = -12.23. $[M]^+$ m/z = 24274.91. Found MALDI-TOF MS: $[M + K]^+$ = 24330. Anal.: Calc. C 59.42%, H 6.52%. Found: C 59.64%, H 6.57%.

2.4.2.46. Synthesis of 16-[G-5]-OH_{128}

Deprotection of 16-[G-5]-$(O_2Bn)_{64}$ (0.160 g, 6.59 μmol) in 20 mL of (1:1) CH_2Cl_2:MeOH was carried out as above for 16 h at room temperature under H_2 atmosphere. Yield: 0.110 g, white foam (90%). ^1H NMR (600 MHz, MeOD): δ = 1.17 (s, 192), 1.23 (s, 12), 1.27 (s, 24), 1.32 (bs, 144), 1.61 (m, 32), 1.83* (m, {32}), 2.04* (m, {32}), 2.28* (m, {32}), 3.64 (m, 128), 3.70 (m, 128), 4.03 (bs, 32), 4.25 (bm, 248). ^{13}C NMR (150 MHz, MeOD): δ = 15.58, 16.49, 16.56, 16.74, 24.24, 24.99, 27.88, 31.58, 32.61, 32.73, 33.48, 46.07, 49.91, 63.42, 64.01, 64.30, 65.57, 77.06, 78.99, 170.52, 171.88, 174.05. ^{11}B NMR (190 MHz, MeOD, proton-decoupled): δ = -12.18. Anal.: Calc. C 48.53%, H 7.16%. Found: C 48.59%, H 7.25%.

* Signal overlaps with signals from the B-H protons in the carborane cage. An accurate integration cannot be assigned. Theoretical integration is given in parentheses { }.

2.5. References

(1) Hawthorne, M. F. *Angewandte Chemie-International Edition* **1993**, *32*, 950-984.
(2) Soloway, A. H.; Tjarks, W.; Barnum, B. A.; Rong, F. G.; Barth, R. F.; Codogni, I. M.; Wilson, J. G. *Chemical Reviews* **1998**, *98*, 1515-1562.
(3) Taylor, H. J.; Goldhaber, M. *Nature* **1935**, *135*, 341.
(4) Locher, G. L. *Am. J. Roentgenol. Radium Ther.* **1936**, *36*, 1-13.
(5) Hawthorne, M. F.; Lee, M. W. *Journal of Neuro-Oncology* **2003**, *62*, 33-45.
(6) Valliant, J. F.; Guenther, K. J.; King, A. S.; Morel, P.; Schaffer, P.; Sogbein, O. O.; Stephenson, K. A. *Coordination Chemistry Reviews* **2002**, *232*, 173-230.
(7) Alam, F.; Soloway, A. H.; Mcguire, J. E.; Barth, R. F.; Carey, W. E.; Adams, D. *Journal of Medicinal Chemistry* **1985**, *28*, 522-525.
(8) Nakanishi, A.; Guan, L. F.; Kane, R. R.; Kasamatsu, H.; Hawthorne, M. F. *Proceedings of the National Academy of Sciences of the United States of America* **1999**, *96*, 238-241.
(9) Feakes, D. A.; Shelly, K.; Hawthorne, M. F. *Proceedings of the National Academy of Sciences of the United States of America* **1995**, *92*, 1367-1370.
(10) Ringsdorf, H. *Journal of Polymer Science Part C-Polymer Symposium* **1975**, 135-153.
(11) Bader, H.; Ringsdorf, H.; Schmidt, B. *Angewandte Makromolekulare Chemie* **1984**, *123*, 457-485.
(12) Kopecek, J. *Polym. Med.* **1977**, *7*, 191-221.
(13) Kopecek, J.; Kopeckova, P.; Minko, T.; Lu, Z. R. *European Journal of Pharmaceutics and Biopharmaceutics* **2000**, *50*, 61-81.
(14) Duncan, R. *Nature Reviews Drug Discovery* **2003**, *2*, 347-360.
(15) Duncan, R. *Anti-Cancer Drugs* **1992**, *3*, 175-210.
(16) Maeda, H.; Seymour, L. W.; Miyamoto, Y. *Bioconjugate Chemistry* **1992**, *3*, 351-362.
(17) Gillies, E. R.; Frechet, J. M. J. *Journal of the American Chemical Society* **2002**, *124*, 14137-14146.
(18) Matsumura, Y.; Maeda, H. *Cancer Research* **1986**, *46*, 6387-6392.
(19) Maeda, H.; Wu, J.; Sawa, T.; Matsumura, Y.; Hori, K. *Journal of Controlled Release* **2000**, *65*, 271-284.
(20) Seymour, L. W. *Critical Reviews in Therapeutic Drug Carrier Systems* **1992**, *9*, 135-187.
(21) Frechet, J. M. J. *Science* **1994**, *263*, 1710-1715.
(22) Esfand, R.; Tomalia, D. A. *Drug Discovery Today* **2001**, *6*, 427-436.
(23) Tomalia, D. A.; Naylor, A. M.; Goddard, W. A. *Angewandte Chemie-International Edition* **1990**, *29*, 138-175.
(24) Frechet, J. M. J.; Tomalia, D. A. *Dendrimers and Other Dendritic Polymers*; John Wiley & Sons, Ltd.: West Sussex, 2001.
(25) Newkome, G. R.; Moorefield, C. N.; Vogtle, F. *Dendritic Macromolecules: Concepts, Synthesis, Perspectives*; VCH: Weinheim, Germany, 1996.

(26) Ihre, H. R.; Padilla De Jesus, O. L.; Szoka, F. C. J.; Frechet, J. M. J. *Bioconjugate Chemistry* **2002**, *13*, 443-452.
(27) Nemoto, H.; Cai, J. P.; Yamamoto, Y. *Journal of the Chemical Society, Chemical Communications* **1994**, 577-578.
(28) Nemoto, H.; Wilson, J. G.; Nakamura, H.; Yamamoto, Y. *Journal of Organic Chemistry* **1995**, *60*, 1478-1478.
(29) Barth, R. F.; Adams, D. M.; Soloway, A. H.; Alam, F.; Darby, M. V. *Bioconjugate Chemistry* **1994**, *5*, 58-66.
(30) Yao, H. J.; Grimes, R. N.; Corsini, M.; Zanello, P. *Organometallics* **2003**, *22*, 4381-4383.
(31) Nunez, R.; Gonzalez, A.; Vinas, C.; Teixidor, F.; Sillanpaa, R.; Kivekas, R. *Organic Letters* **2005**, *7*, 231-233.
(32) Qualmann, B.; Kessels, M. M.; Musiol, H. J.; Sierralta, W. D.; Jungblut, P. W.; Moroder, L. *Angewandte Chemie-International Edition* **1996**, *35*, 909-911.
(33) Armspach, D.; Cattalini, M.; Constable, E. C.; Housecroft, C. E.; Phillips, D. *Chemical Communications* **1996**, 1823-1824.
(34) Thomas, J.; Hawthorne, M. F. *Chemical Communications* **2001**, 1884-1885.
(35) Malik, N.; Wiwattanapatapee, R.; Klopsch, R.; Lorenz, K.; Frey, H.; Weener, J. W.; Meijer, E. W.; Paulus, W.; Duncan, R. *Journal of Controlled Release* **2000**, *68*, 299-302.
(36) Newkome, G. R.; Moorefield, C. N.; Keith, J. M.; Baker, G. R.; Escamilla, G. H. *Angewandte Chemie-International Edition* **1994**, *33*, 666-668.
(37) Ihre, H.; Padilla De Jesus, O. L.; Fréchet, J. M. J. *Journal of the American Chemical Society* **2001**, *123*, 5908-5917.
(38) Ihre, H.; Hult, A.; Soderlind, E. *Journal of the American Chemical Society* **1996**, *118*, 6388-6395.
(39) Ihre, H.; Hult, A.; Frechet, J. M. J.; Gitsov, I. *Macromolecules* **1998**, *31*, 4061-4068.
(40) De Jesus, O. L. P.; Ihre, H. R.; Gagne, L.; Frechet, J. M. J.; Szoka, F. C. *Bioconjugate Chemistry* **2002**, *13*, 453-461.
(41) Leites, L. A. *Chemical Reviews* **1992**, *92*, 279-323.
(42) Herzog, A.; Knobler, C. B.; Hawthorne, M. F.; Maderna, A.; Siebert, W. *Journal of Organic Chemistry* **1999**, *64*, 1045-1048.
(43) deNooy, A. E. J.; Besemer, A. C.; vanBekkum, H. *Synthesis-Stuttgart* **1996**, 1153-1174.
(44) Greene, T. W.; Wuts, P. G. W. *Protective Groups in Organic Synthesis*, 3rd ed.; Wiley-Interscience, 1999.
(45) Moore, J. S.; Stupp, S. I. *Macromolecules* **1990**, *23*, 65-70.

Chapter 3 - Thermally Induced Phase Transition of Carborane-Functionalized Aliphatic Polyester Dendrimers in Aqueous Media

Abstract

Three recently reported aliphatic polyester dendrimers of generation 3, 4, and 5, having 4, 8, and 16 carborane cages within their interior, respectively, were found to exhibit a thermally-induced, reversible precipitation in aqueous solution. The cloud-point temperatures for these molecules were observed between 40 and 80°C, depending on the dendrimer generation. The three dendrimers investigated have a hydroxyl to carborane ratio of 8:1, which provides the ideal balance between hydrophobic interior and hydrophilic exterior to enable the thermally-induced phase transition to occur. It was found that repeated heat/cool cycles resulted in a decreasing cloud point temperature and increased dendrimer solubility. Additionally, the effect of pH on the cloud point was investigated, indicating no significant changes as long as the dendrimers remained stable. Size exclusion chromatography indicated that dendrimer degradation was occurring at pH above 7.0. This chapter has been reproduced in part with permission from *Langmuir* **2006**, 5251-5255. Copyright 2006 American Chemical Society.

3.1. Introduction

Thermally induced polymer phase transitions have been heavily investigated since the discovery of the lower critical solution temperature (LCST) of poly(N-isopropyl acrylamide) in aqueous solution.[1-6] Above the LCST, the hydration sphere responsible for polymer solubility becomes entropically unfavourable and dissociates. At this point, polymer-polymer interactions become more thermodynamically favourable than polymer-solvent interactions, allowing polymer chains to aggregate and precipitate.[7, 8] Such thermally induced phase transitions have been observed for a number of other water-soluble polymers, including poly(ethylene glycol),[9, 10] poly(hydroxypropyl acrylate),[11] poly(hydroxyethyl methacrylate),[12] and several others.[13] Each of these polymers exhibits an intrinsic balance between hydrophilic and hydrophobic structural components,[14] enabling large changes in enthalpy and entropy of solution as temperature is varied. Investigation of thermally responsive polymers has focused primarily on linear polymer architectures. However, Kono and co-workers have recently reported the first examples of dendritic structures exhibiting phase transitions similar to their linear counterparts.[15] This was accomplished using poly(amidoamine) (PAMAM) and poly(propyleneimine) (PPI) dendrimers modified at their periphery with isobutyramide groups. It was observed that LCST values decreased with an increase in dendrimer generation, an increase in solution concentration, as well as with an increase in pH.[15] In addition, Thayumanavan and co-workers have prepared thermally responsive dendritic micelles, where generation 1 to 3 dendrons decorated with pentaethylene glycol and n-

decyl chains at each monomer unit were found to aggregate in aqueous solution and precipitate at elevated temperatures.[16]

Recently, we reported[17] the synthesis and properties of a family of aliphatic polyester dendrimers[18, 19] that are internally functionalized with carborane cages and have peripheral hydroxyl groups. Not surprisingly, we found that aqueous solubility of the dendrimers was enhanced when the ratio of peripheral hydroxyl groups to internal hydrophobic carboranes was increased. Regardless of the position of the carborane layer, the dendrimers began to exhibit aqueous solubility at a hydroxyl:carborane ratio of 8:1. Three such dendrimers were prepared, having 4, 8, and 16 carboranes within generation 3, 4, and 5 dendrimers, respectively (Figure 3.1). Interestingly, upon heating the aqueous solutions of any one of these three structures, a reversible precipitation (or cloud point) was observed at temperatures between 40 and 80°C, depending on the dendrimer generation. Considering the extreme hyrophobicity of the para-carborane moieties introduced within these otherwise hydrophilic dendrimers, it is likely that a hydrophobic/hydrophilic balance is achieved that is similar to what exists in the thermally responsive linear polymers, as well as the recently reported dendrimer examples. However, in contrast to Kono's and Thayumanavan's dendrimer examples, where either a hydrophilic dendrimer structure was modified with hydrophobic isobutyramide groups on its periphery[15] or the entire dendron was decorated with both hydrophobic n-decyl and hydrophilic pentaethylene glycol groups,[16] our mostly hydrophilic dendrimer structures are modified with hydrophobic groups only on their interior.[17] This previously unobserved thermal solubility transition within internally modified dendrimers prompted

us to investigate these molecules in more detail. Here, we present a series of cloud point measurements for dendrimers 4-[G-3]-OH_{32} (section 2.4.2.26), 8-[G-4]-OH_{64} (section 2.4.2.36), and 16-[G-5]-OH_{128} (section 2.4.2.46), specifically focusing on the effect of dendrimer generation, repeated heat-cool cycles, and pH on their thermal transitions in aqueous solution.

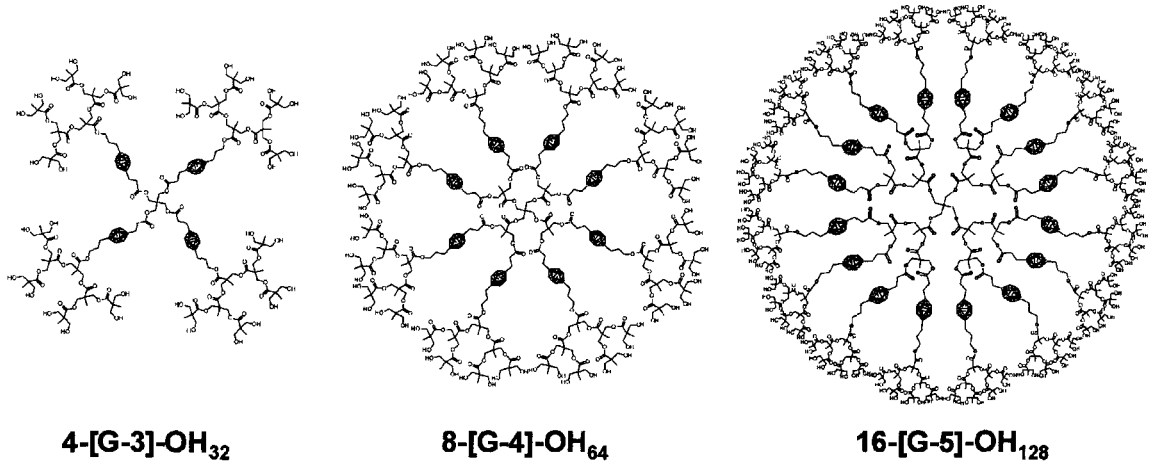

Figure 3.1. Structures of three carborane containing aliphatic poly(ester) dendrimers that exhibit a reversible thermally-induced precipitation.

3.2. Results and Discussion

The three dendrimers investigated have a common hydroxyl to carborane ratio of 8:1, due to the presence of third-generation (G-3) dendrons attached to each carborane. It was found that decreasing this ratio produced water-insoluble dendrimers, while increasing it resulted in no observable cloud point in water. Thus, the 8:1 ratio in each dendrimer provides the right balance of hydrophobic interior and hydrophilic exterior to

enable the thermally-induced phase transitions. It should be noted that aliphatic polyester dendrimers not functionalized with carborane cages are fully water soluble and exhibit no cloud point.[20]

We initially investigated the effect of dendrimer generation on the cloud point. These studies were performed by heating aqueous dendrimer solutions from 30°C to 90°C at a rate of 0.5°C per minute, while recording % transmittance measurements in 0.5°C increments at 500 nm. The onset of turbidity was measured at the temperature where a 1% decrease in transmittance was observed. Both Kono[15] and Thayumanavan[16] reported that cloud point temperature decreased with increasing generation, indicating reduced aqueous solubility. In the case of isobutyramide-functionalized PAMAM and PPI dendrimers, this was likely due to a higher density of hydrophobic peripheral groups as the dendrimers increase in size and become more globular in shape.[15] Similarly, in our dendrimer series, size and shape effects also seemingly control the cloud point temperature, but the overall trend is somewhat different. It was found that the lowest generation (4-[G-3]-OH_{32}) dendrimer, bearing four carborane cages, exhibits the lowest cloud point temperature of approximately 52 ± 1°C, indicating that this structure is least soluble of the three (Figure 3.2). Since it is known that dendrimers do not adopt a globular shape until approximately the 4th generation,[21] this dendrimer should exhibit a somewhat flattened, open structure that exposes the interior carboranes, allowing them to greatly impact and limit the molecule's solubility in water through intermolecular hydrophobic interactions. In contrast, the 8-[G-4]-OH_{64} dendrimer was found to exhibit the highest cloud point temperature of approximately 84 ± 2°C. Considering that this

structure can be expected to adopt a globular shape in solution, it is reasonable that the interior carboranes are effectively masked from the surrounding aqueous environment. This site-isolation of interior carboranes effectively suppresses intermolecular hydrophobic interactions at low temperatures, thereby raising the observed cloud point. Surprisingly, in the case of the 16-[G-5]-OH_{128} dendrimer, the cloud point temperature was found at a lower temperature than the G-4 structure, approximately 66 ± 1°C. Although this G-5 dendrimer is also expected to exhibit a globular shape in solution, the 16 carborane cages are located one generation further from the core, relative to the G-4 structure, enabling greater mobility. Here, steric crowding of the interior carboranes may result in some cages being pushed closer to the dendrimer surface, where they become more exposed to the aqueous environment. Such carborane exposure may cause the decreased cloud point for this structure.

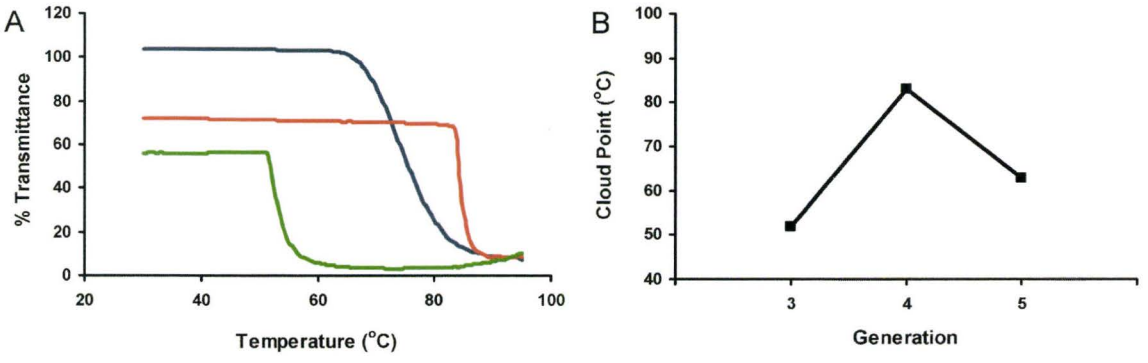

Figure 3.2. A) Initial cloud points of 4-[G-3]-OH_{32} (green), 8-[G-4]-OH_{64} (red), and 16-[G-5]-OH_{128} (blue). B) The influence of dendrimer generation on cloud point.

Upon further investigation of these thermal transitions of each dendrimer, it was found that repeated heat-cool cycles did not result in reproducible cloud-point curves (Figure 3.3). Instead, the turbidity onset temperature decreased slightly over the first four heat-cool cycles, before reaching an equilibrium temperature at which further temperature cycling resulted in no real change in the cloud point temperature. Figure 3.3C depicts this data for the G-5 dendrimer, where the cloud point decreased from an initial value of 66 ± 1°C to a final value of 59 ± 1°C after six iterations. Similar behaviour was observed for the G-3 and G-4 dendrimers, where six repeated heat-cool cycles decreased the turbidity onset temperature by 9.0°C and 8.5°C, respectively (Figure 3.4A).

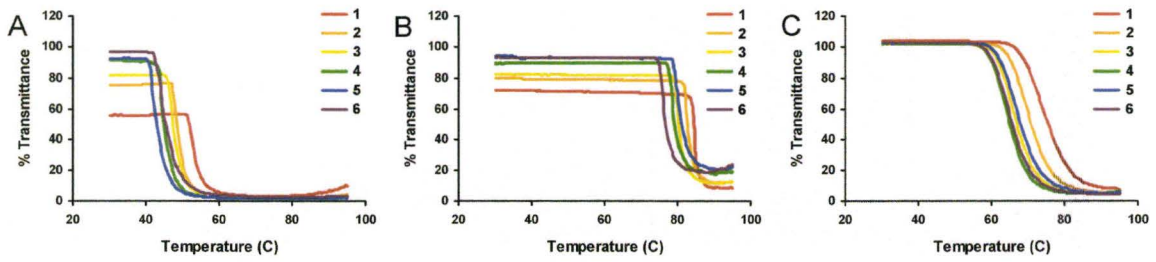

Figure 3.3. Turbidity results from six heating/cooling iterations of 4-[G-3]-OH_{32} (A), 8-[G-4]-OH_{64} (B) and 16-[G-5]-OH_{128} (C).

Surprisingly, it was also found that solubility of G-3 and G-4 dendrimers increased with repeated heat-cool cycles, likely due to the gradual break-up of large insoluble aggregates suspended in the solvent. As can be observed in Figure 3.3A and 3.3B, the initial dendrimer-water mixtures at a concentration of 1 mg/mL were slightly

heterogeneous, resulting in light scattering and a transmittance well below 100%. However, after four heat-cool iterations, the mixtures consistently became homogeneous and transparent, with transmittances of nearly 100% (Figure 3.4B). We initially postulated that this behaviour may be due to dendrimer degradation over the course of repeated heat-cool cycles. However, GPC analysis indicated no appreciable differences in the dendrimer samples before and after the temperature cycling. In fact, deliberate degradation of these structures under basic conditions (vide infra) resulted in precipitation of dendrimer fragments and a complete loss of the thermal transition behaviour. It therefore seems that repeated temperature cycling breaks up large aggregates into smaller, more soluble aggregates, but these smaller aggregates undergo the thermal solubility transition at lower temperature.

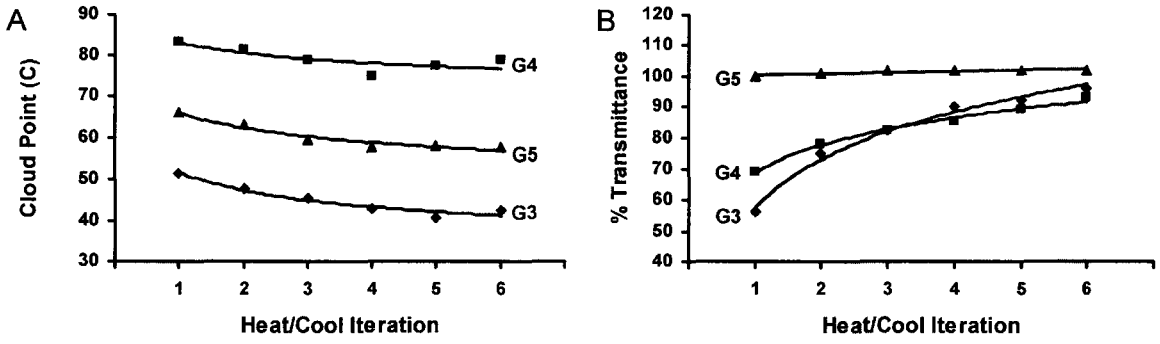

Figure 3.4. The effect of heat/cool iterations on cloud point (A) and on % transmittance (B).

Large aggregates breaking into smaller individual particles was confirmed using dynamic light scattering (DLS). Each dendrimer sample was diluted in water to

nanomolar concentration and the hydrodynamic radii were measured before and after each heat / cool iteration. Figure 3.5A, indicates that prior to heating a large population was observed on the order of 100 nm and a small population on the order of 1000 nm. After four heat/cool iterations (Figure 3.5B) smaller populations were observed for particle diameters of 1 nm and 10 nm. The smaller diameter populations made up 26% (1 nm) and 14% (10 nm) of the total intensity. Since the larger particles scatter more light (Mie scattering) the actual composition of the solution would significantly favour the smaller particles. Similar results were observed for 4-[G-3]-OH_{32} and 8-[G-4]-OH_{64}, however, a greater number of heat/cool iterations were required due to the initial insolubility of these compounds.

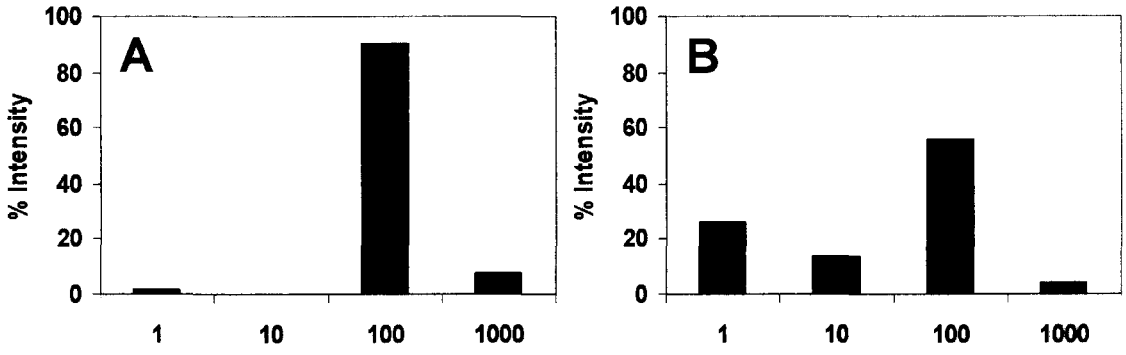

Figure 3.5. Dynamic light scattering of 16-[G-5]-OH_{128} before heating (A) and after four heat/cool iterations (B).

To determine the effect of pH on the thermal transitions of the three dendrimers, four buffered solutions were prepared using acetic acid (pH = 5.0), NaH_2PO_4 (pH = 6.2 and pH = 7.5) and ethanolamine (pH = 10.1). Each buffered solution was prepared with

an ionic strength of 0.15 M and was targeted to a pH of 5.0, 6.2, 7.4, and 9.0 at 60°C, based on their intrinsic temperature coefficients.[22] It was found that, under mildly acidic conditions (pH = 5.0 and 6.2), cloud point results from six heat/cool iterations for all three dendrimer generations exhibited little to no difference from the same experiment at neutral pH. However, at pH = 7.4, cloud point temperatures did not stabilize after six heat-cool iterations, but rather continued to decrease. In the case of dendrimer 8-[G-4]-OH_{64}, significant precipitation was observed at the end of this process, indicating dendrimer degradation. At a pH of 9.0, the cloud point completely disappeared after two heat-cool iterations in all three dendrimers (Figure 3.6B). A significant amount of precipitation was observed, indicating that the dendrimer structures were degrading to smaller, insoluble fragments. GPC analysis confirmed the degradation of these dendrimers at high pH. As seen in Figure 3.7, each sample was relatively stable at pH 5.0 and 6.2. However, an onset of dendrimer degradation was observed at pH 7.4, and the samples subjected to a pH of 9 showed extensive degradation. Surprisingly, GPC analysis showed a clean progression to lower molecular weight, with samples maintaining their low polydispersity and the general shape of the original chromatogram. This indicates that degradation may be occurring at a particularly labile ester linkage (i.e., at the carborane spacer) in a stepwise manner. Small peaks at double and triple the molecular weight were also found in the chromatograms, consistent with previous observations.[19, 23, 24] Corresponding signals at higher than expected molecular weights were not observed by MALDI-TOF mass spectrometry, possibly indicating that non-covalent aggregation of these structures is occurring in solution.

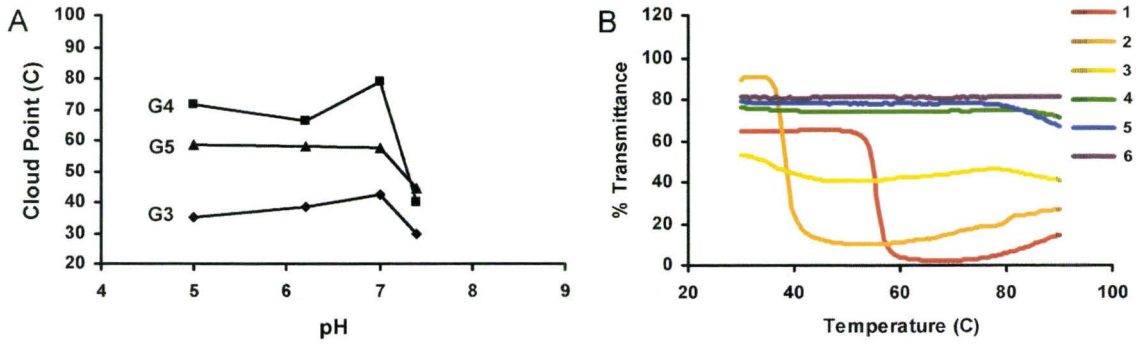

Figure 3.6. A) Cloud point temperatures after six heat/cool iterations at different pH. B) Turbidity traces from six heat/cool iterations of 16-[G-5]-OH_{128} in an aqueous solution buffered at pH = 9.

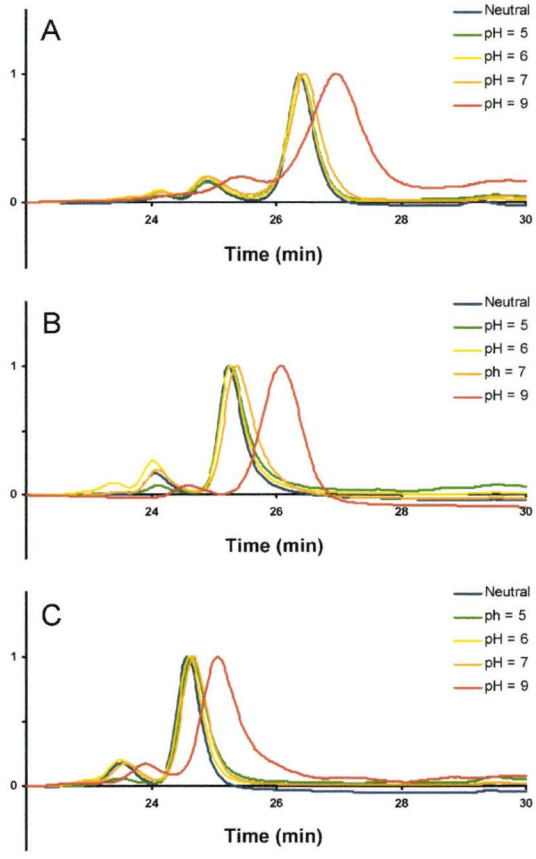

Figure 3.7. Size exclusion chromatograms of dendrimer 4-[G-3]-OH_{32} (A), 8-[G-4]-OH_{64} (B), and 16-[G-5]-OH_{128} (C) after 2 heating/cooling iterations at various pH.

3.3. Conclusion

Three Dendrimers, 4-[G-3]-OH_{32}, 8-[G-4]-OH_{64}, and 16-[G-5]-OH_{128}, were found to exhibit a reversible precipitation at elevated temperatures in aqueous solution. Each of these structures contains a ratio of peripheral hydroxyl groups to internal carboranes of 8:1, providing the necessary balance of hydrophobicity and hydrophilicity for the thermal transition to occur. Structures with a lower ratio exhibited no aqueous solubility and ones with a higher ratio remained soluble at all temperatures. The initial cloud point temperatures were measured to be 52 ± 1°C, 84 ± 2°C, and 66 ± 1°C for 4-[G-3]-OH_{32}, 8-[G-4]-OH_{64}, and 16-[G-5]-OH_{128}, respectively. The cloud point temperatures varied as a function of dendrimer generation, as well as the number of heating/cooling cycles that were carried out. It was found to decrease with consecutive temperature cycling, while dendrimer solubility was found to increase (for 4-[G-3]-OH_{32} and 8-[G-4]-OH_{64}). Under mildly acidic conditions, dendrimer cloud points were unaffected by pH. However, under basic conditions, the dendrimers were found to degrade, causing a disappearance of the thermal transition and precipitation of smaller dendrimer fragments.

3.4. Experimental

Cloud point determinations were made from turbidity measurements performed on a Varian 300 spectrophotometer equipped with a multisample holder and a recirculating water bath temperature controller. Solution temperatures were recorded using probes inserted directly into the sample solutions. Each sample was ramped from 30°C to 90°C at 0.5°C per minute. Cloud point values were designated as the point

where the percent transmittance decreased by 1%, and average values from three separate experiments were used.

Four buffered solutions were prepared at 22°C using acetic acid (pH = 5.0), NaH_2PO_4 (pH = 6.2 and pH = 7.5) and ethanolamine (pH = 10.1) using a VWR SB20 pH meter equipped with a VWR sympHony Ag electrode. Each buffered solution was prepared with an ionic strength of 0.15 M and was targeted to a pH of 5.0, 6.2, 7.4, and 9.0 at 60°C, based on their intrinsic temperature coefficients.

3.5. References

(1) Heskins, M.; Guillet, J. E. *Journal of Macromolecular Science - Chemistry* **1968**, *A2*, 1441-1455.
(2) Schild, H. G.; Tirrell, D. A. *Journal of Physical Chemistry* **1990**, *94*, 4352-4356.
(3) Idziak, I.; Avoce, D.; Lessard, D.; Gravel, D.; Zhu, X. X. *Macromolecules* **1999**, *32*, 1260-1263.
(4) Plate, N. A.; Lebedeva, T. L.; Valuev, L. I. *Polymer Journal* **1999**, *31*, 21-27.
(5) Liu, H. Y.; Zhu, X. X. *Polymer* **1999**, *40*, 6985-6990.
(6) Xia, Y.; Yin, X. C.; Burke, N. A. D.; Stover, H. D. H. *Macromolecules* **2005**, *38*, 5937-5943.
(7) Finch, C. A. *Chemistry and Technology of Water Soluble Polymers*; Plenum Press: New York, 1983.
(8) Schild, H. G. *Progress in Polymer Science* **1992**, *17*, 163-249.
(9) Nozary, S.; Modarress, H.; Eliassi, A. *Journal of Applied Polymer Science* **2003**, *89*, 1983-1990.
(10) Ataman, M. *Colloid and Polymer Science* **1987**, *265*, 19-25.
(11) Safrany, A. *Radiation Physics and Chemistry* **1999**, *55*, 121-126.
(12) Reyntjens, W.; Jonckheere, L.; Goethals, E.; Du Prez, F. *Macromolecular Symposia* **2001**, *164*, 293-300.
(13) Eeckman, F.; Moes, A. J.; Amighi, K. *International Journal of Pharmaceutics* **2002**, *241*, 113-125.
(14) Kubota, K.; Fujishige, S.; Ando, I. *Journal of Physical Chemistry* **1990**, *94*, 5154-5158.
(15) Haba, Y.; Harada, A.; Takagishi, T.; Kono, K. *Journal of the American Chemical Society* **2004**, *126*, 12760-12761.
(16) Aathimanikandan, S. V.; Savariar, E. N.; Thayumanavan, S. *JACS* **2005**, *127*, 14922-14929.
(17) Parrott, M. C.; Marchington, E. B.; Valliant, J. F.; Adronov, A. *JACS* **2005**, *127*, 12081-12089.
(18) Ihre, H.; Hult, A.; Soderlind, E. *Journal of the American Chemical Society* **1996**, *118*, 6388-6395.
(19) Ihre, H.; Padilla De Jesus, O. L.; Fréchet, J. M. J. *JACS* **2001**, *123*, 5908-5917.
(20) De Jesus, O. L. P.; Ihre, H. R.; Gagne, L.; Frechet, J. M. J.; Szoka, F. C. *Bioconjugate Chemistry* **2002**, *13*, 453-461.
(21) Frechet, J. M. J. *Science* **1994**, *263*, 1710-1715.
(22) Beynon, R. J.; Easterby, J. S. *Buffer Solutions: The Basics*; Oxford University Press: Oxford, 1996.
(23) Ihre, H. R.; Padilla De Jesus, O. L.; Szoka, F. C. J.; Frechet, J. M. J. *Bioconjugate Chemistry* **2002**, *13*, 443-452.
(24) Malkoch, M.; Claesson, H.; Lowenhielm, P.; Malmstrom, E.; Hult, A. *Journal of Polymer Science: Part A: Polymer Chemistry* **2004**, *42*, 1758-1767.

Chapter 4 - Synthesis and Core Functionalization of Aliphatic Polyester Dendrons

Abstract

The divergent synthesis and core modification of a series of aliphatic polyester dendrons using 2,2-bis(hydroxymethyl)propionic acid (bis-MPA) was accomplished. The synthesis utilizes a novel orthogonal protecting group strategy consisting of p-toluene sulfonyl ethyl (TSe) ester as an easily removable protecting group at the core of the dendron, and benzylidene protecting groups on the surface. The facile removal of the core TSe ester was accomplished with the non-nucleophilic base 1,8-diazabicyclo[5.4.0]undec-7-ene (DBU), while the surface benzylidene protecting groups were quantitatively removed via hydrogenolysis. This synthesis provided dendrons from generation 1 through 8 in high yield and purity. The dendrons from generation 5 through 8 were used to investigate the attachment of various nucleophiles at the core of each macromolecule. Using amidation chemistry, a bis-pyridyl ligand and a rheniated bis-pyridyl ligand were introduced at the dendron core. These materials provide the necessary precursors for labeling with radioactive technetium-99m. This chapter has been reproduced in part with permission from *Journal of the American Chemical Society* **2008**, ja-2008-078175. Copyright 2006 American Chemical Society.

4.1. Introduction

Over the past two decades, the use of synthetic macromolecules as drug-delivery agents has gained increasing momentum.[1-4] Polymer-based drug delivery agents exhibit improved solubility and increased vascular circulation time due to a decreased rate of renal filtration, a process that is abated by increasing the molecular size of the delivery system.[5, 6] This prolonged circulation time enables macromolecular drug delivery systems to passively target tumor tissues as a result of increased permeability of tumor vasculature to macromolecules and the limited lymphatic drainage away from a tumour.[7] Combined, these two factors allow the selective accumulation of macromolecules in tumor tissue, a phenomenon known as the enhanced permeation and retention (EPR) effect.[8-10]

Within the area of polymer therapeutics, dendritic macromolecules exhibit several distinct advantages over their linear counterparts. These include their precisely controlled architecture, monodispersity, and the ability to incorporate specific functional groups at the periphery, the interior, or the core of the molecule.[11-15] Dendrimers can therefore serve as highly versatile drug delivery vehicles, allowing for control over solubility, molecular weight, multiplicity of therapeutic agents, and potentially the incorporation of active targeting moieties.[7, 16]

Recently, Hult[17, 18] and Fréchet[19] developed an efficient synthesis of aliphatic polyester dendrimers based on 2,2-bis(hydroxymethyl)propanoic acid (bis-MPA). The resulting poly(2,2-bis(hydroxymethyl)-propanoic acid) (PMPA) dendrimer structures

were found to be promising as drug delivery agents, as they are biocompatible, non-immunogenic, non-toxic, water soluble, and well-tolerated *in vivo*.[16, 20]

Herein, we detail the synthesis, characterization and core modification of PMPA dendrons for subsequent radiolabeling with technetium-99m (^{99m}Tc), and *in vivo* biodistribution (Chapter 5). To accomplish this, an orthogonal protecting group that can be dendronized in a divergent manner was utilized to produce core-protected, high-generation, biocompatible PMPA dendrimers. This protecting group can be selectively cleaved in high yield at any generation to liberate a single, accessible carboxylic acid group. Amidation of the deprotected core with an amine-functionalized bis-pyridyl ligand allowed the introduction of an extremely efficient single-site chelator for the widely used radionuclide ^{99m}Tc.[21-23] It was hypothesized that a single, strongly-binding ligand for the radionuclide would have to be placed at the core of a high-generation dendrimer. This would ensure that radiolabeling occurs in a well-defined, site-specific manner, and at only a single point within the dendrimer framework. Furthermore, by introducing the radionuclide at the site-isolated core of the dendrimer, the overall size, shape, polarity, and mode of interaction of the dendrimer periphery with its external environment should not be appreciably affected.

This work represents early stages in the development of a dendrimer family that can house a therapeutic payload, be targeted to specific disease sites through peripheral modification, and can be monitored in real time upon injection into, perfusion through, and elimination from living patients.

4.2. Results and Discussion

4.2.1. General Synthesis

To produce PMPA dendrons in which the core could be modified at a later stage, it was necessary to first identify a protecting group for the carboxylic acid functionality that is stable to the dendrimer synthesis chemistry and could be efficiently removed under orthogonal conditions. After surveying a number of possibilities, we settled on the toluene sulfonyl ethyl (TSe) ester as a viable candidate because of its stability toward dendron growth/deprotection conditions and its facile cleavage using the non-nucleophilic base 1,8-diazabicyclo[5.4.0]undec-7-ene (DBU). The synthesis of our desired dendrons was therefore accomplished by initially reacting para-toluene sulfonyl ethanol (**4.1**) with the benzylidene protected anhydride of bis-MPA and 4-dimethylaminopyridine (DMAP). The excess anhydride was quenched with water, and the first-generation (G1) TSe-protected dendron (**4.2**) was obtained in 96% isolated yield after a simple extraction (Scheme 4.1). For the subsequent dendrimer growth reactions, it was found that using a 3:2 mixture of CH_2Cl_2 and pyridine, and a two-fold excess of the bis-MPA anhydride relative to each alcohol functionality constituted optimal conditions for all generations. The benzylidene protecting group of **4.2** was quantitatively removed by hydrogenolysis using a catalytic amount of 20% (w/w) $Pd(OH)_2/C$ and H_2 (1 atm) to produce the diol **4.3**. Subsequent iterations of these steps (Scheme 4.1) allowed the production of a series of hydroxyl-terminated dendrons, from G1 to G8, with isolated yields in excess of 90% up to the eighth generation. For simplicity, each dendron will be named according to the core functionality (TSe, COOH, etc.), the dendron generation

(Gx), and the peripheral groups (O_2Bn or OH). Therefore, the fifth-generation dendron (**4.11**) in Scheme 4.1 is referred to as TSe-G5-$(OH)_{32}$ and contains one core TSe moiety and 32 peripheral hydroxyls. Each of these dendron structures was fully characterized by ^1H and ^{13}C NMR, as well as MALDI-TOF mass spectrometry. The MALDI-TOF mass spectra of TSe-G5-$(OH)_{32}$ (3798 Da), TSe-G6-$(OH)_{64}$ (7,511 Da), TSe-G7-$(OH)_{128}$ (14,938 Da), and TSe-G8-$(OH)_{256}$ (29,792 Da), are depicted in Figure 4.1, showing observed signals that correspond to the sodium adducts of each of the dendrons.

Scheme 4.1. The synthesis of high molecular weight dendrons based on toluene sulfonyl ethanol and bis-MPA.

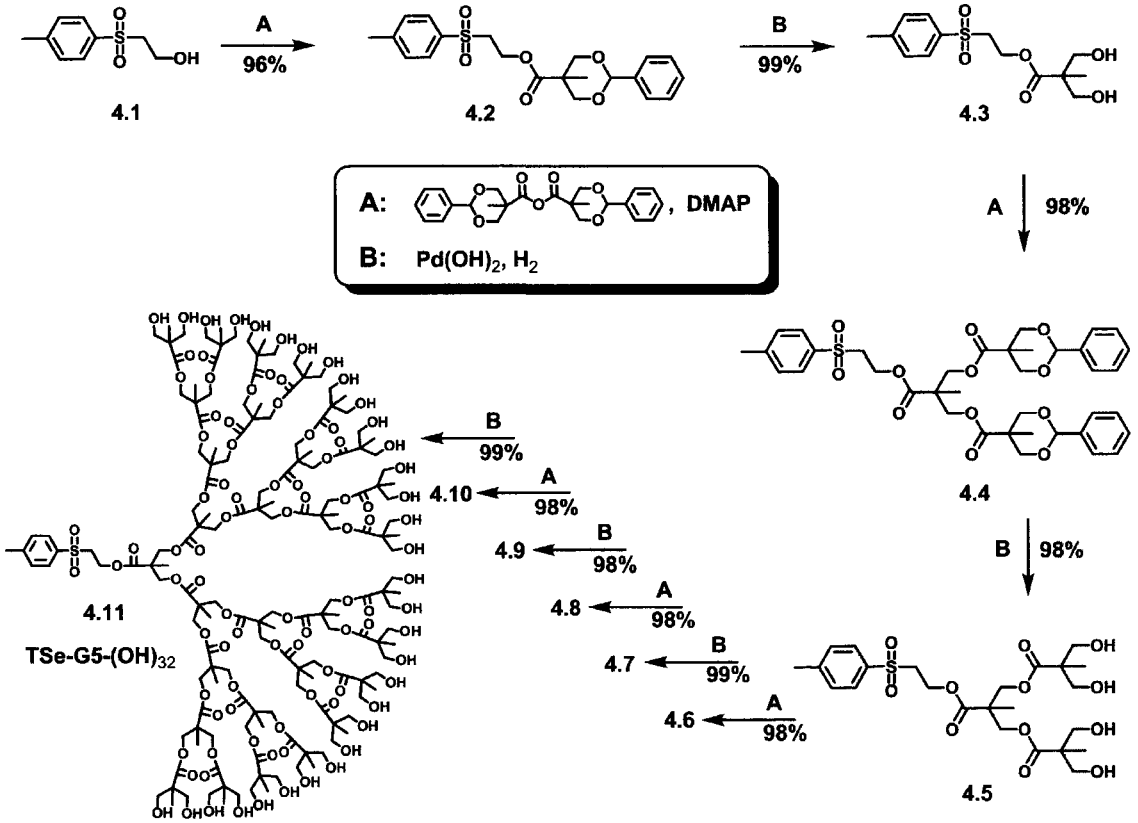

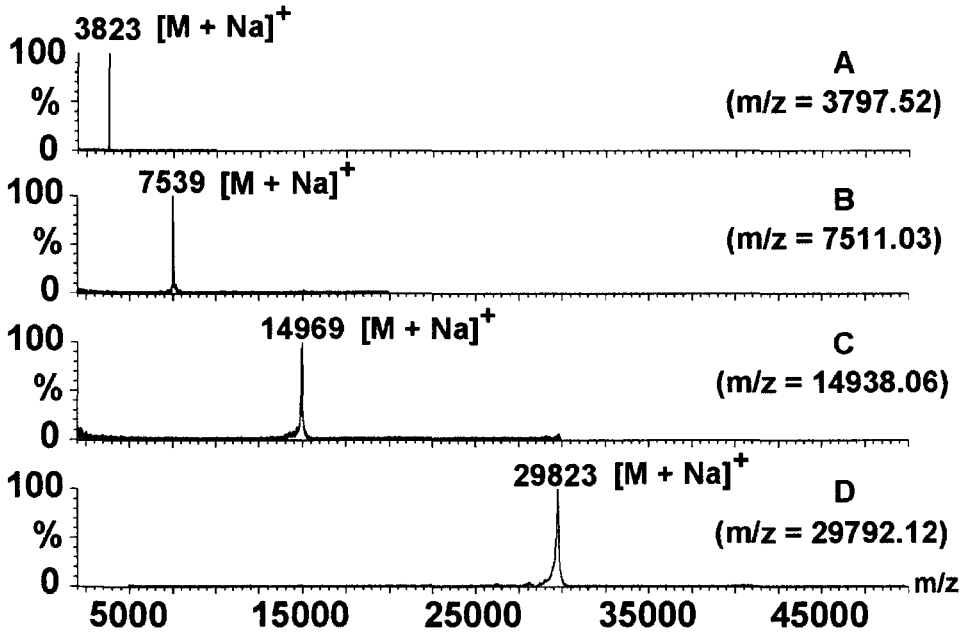

Figure 4.1. MALDI-TOF MS spectra of compounds TSe-G5-$(OH)_{32}$ (A), TSe-G6-$(OH)_{64}$ (B), TSe-G7-$(OH)_{128}$ (C), and TSe-G8-$(OH)_{256}$ (D).

The fourth to eighth generation fully protected dendrons were also characterized by size exclusion chromatography, coupled with viscometry and light-scattering data (using a Viscotek Triple Detector Array-301 system). The combination of a mass detector (refractive index) with a viscometer and light scattering detector enables the characterization of polymers having diverse compositions and architectures, without the inaccuracies that plague typical SEC systems calibrated with specific polymer standards. The molecular weight data measured with the triple detector array is given in Table 4.1, and is consistent with the expected doubling on going from one generation to the next. Narrow polydispersities were observed at each generation, in reasonable agreement with the MALDI-TOF data that indicates pure compounds of exact molecular weight.

Although the R_h values steadily increased with generation, they were all well below 3 nm, even for the relatively high-generation dendrimers.

Table 4.1. Molecular weight and hydrodynamic radius data for the G4 to G8 fully protected dendrons.

Compound	Theoretical Mol. Weight	SEC (TDA)		MALDI Mol. Weight*	R_h (nm)
		Mn	PDI		
TSe-G4-$(O_2Bn)_8$	2,645	2,860	1.003	2,668	1.15
TSe-G5-$(O_2Bn)_{16}$	5,206	6,480	1.004	5,232	1.42
TSe-G6-$(O_2Bn)_{32}$	10,328	10,900	1.047	10,354	1.82
TSe-G7-$(O_2Bn)_{64}$	20,572	23,460	1.031	20,605	2.27
TSe-G8-$(O_2Bn)_{128}$	41,060	47,570	1.019	41,074	2.80

* All MALDI signals correspond to the Na-adduct of the molecular ion.

Removal of the TSe protecting group was performed on G5 through G8 by reacting each dendron with an excess of DBU in dichloromethane (DCM). Thin layer chromatography (TLC) of this reaction with the G5 dendron indicated complete disappearance of starting materials within 1 h, however, the reaction was allowed to continue for an additional 12 h to ensure quantitative removal of the TSe group. The resulting dendrons were washed with $NaHSO_4$ (1 M) to remove the excess DBU, and precipitated three times in 9:1 hexanes:ethyl acetate. Deprotection of the internal TSe

ester was confirmed by ^{1}H NMR spectroscopy, where a complete disappearance of the aromatic signals at 7.8 ppm (2H) as well as the aliphatic proton signal at 2.5 ppm (3H) and 3.3 ppm (2 H) was observed for each generation (see example spectra for the G5 dendron in Figure 4.2). In addition, the MALDI mass spectrum for COOH-G5-$(O_2Bn)_{16}$ shows the removal of the TSe moiety, with a mass decrease of the expected 185 Da from the original mass of TSe-G5-$(O_2Bn)_{16}$ (Figure 4.3). Identical mass decreases were observed for the higher generation dendrons.

The benzylidene protecting groups of COOH-G5-$(O_2Bn)_{16}$ were quantitatively removed using the aforementioned hydrogenolysis conditions to produce the COOH-G5-$(OH)_{32}$ dendron with one internal carboxylic acid and 32 peripheral alcohols. The ^{1}H NMR spectrum of COOH-G5-$(OH)_{32}$, depicted in Figure 4.2, confirms the deprotection of the benzylidene groups by the complete disappearance of aromatic signals at 7.2-7.4 ppm as well as the disappearance of the acetal proton on each benzylidene at 5.5 ppm (16 H). Note that the ^{1}H NMR of the fully deprotected dendron, COOH-G5-$(OH)_{32}$, was recorded in deuterated methanol (as opposed to $CDCl_3$), which accounts for the observed shifts in all signals, as well as the appearance of extra signals at 3.31 and 4.87 ppm, due to the presence of methanol and water, respectively. Additionally, the MALDI-MS data shows the complete conversion of COOH-G5-$(O_2Bn)_{16}$ to COOH-G5-$(OH)_{32}$ by the decrease in observed mass from 5052 Da to 3641 Da (Figure 4.3). Identical deprotection chemistry procedures were successfully applied to the higher generation dendrons with no significant decrease in yields.

Scheme 4.2. Double deprotection of TSe-G5-$(O_2Bn)_{16}$.

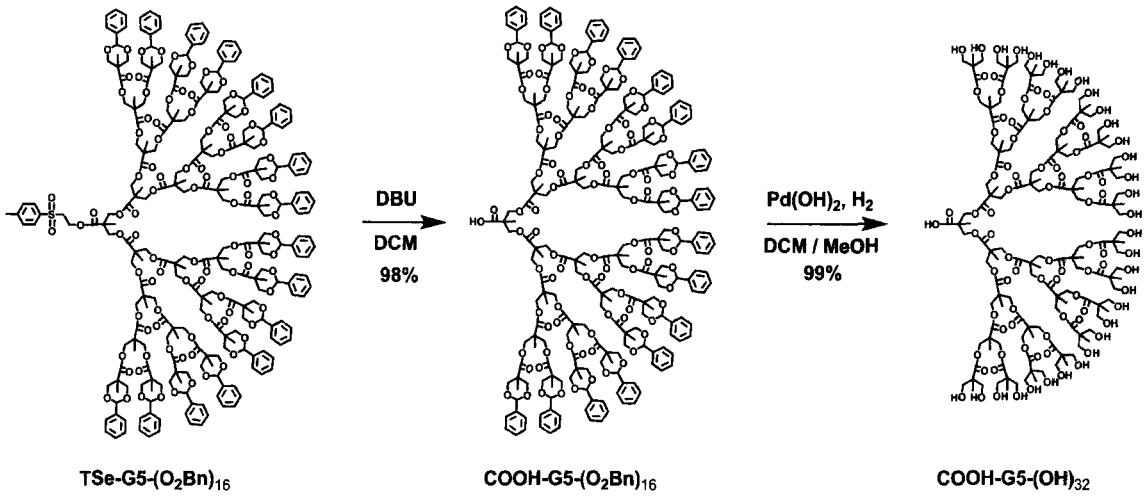

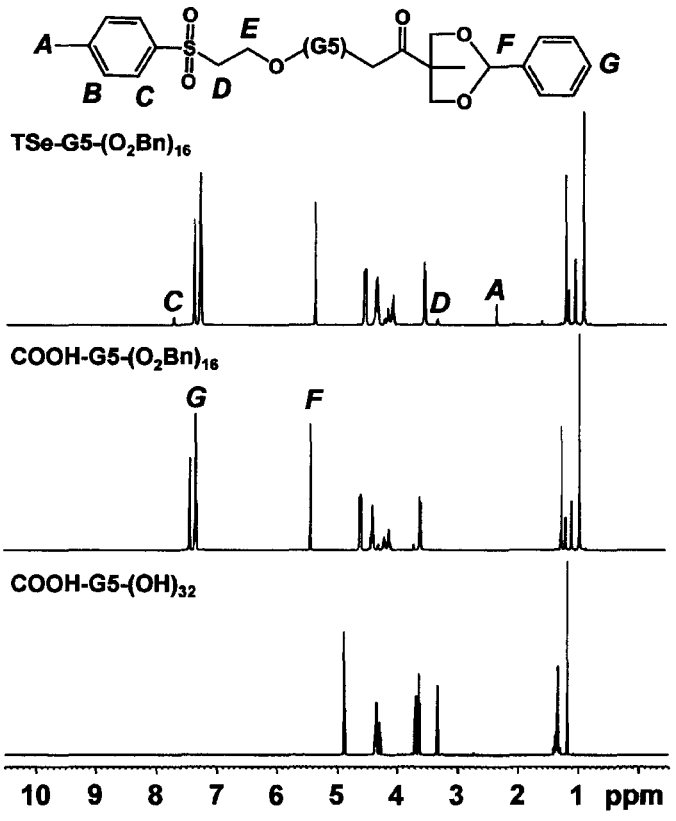

Figure 4.2. ^1H NMR spectra of TSe-G5-(O2Bn)$_{16}$ (in $CDCl_3$), COOH-G5-$(O_2Bn)_{16}$ (in $CDCl_3$), and COOH-G5-$(OH)_{32}$ (in CD_3OD).

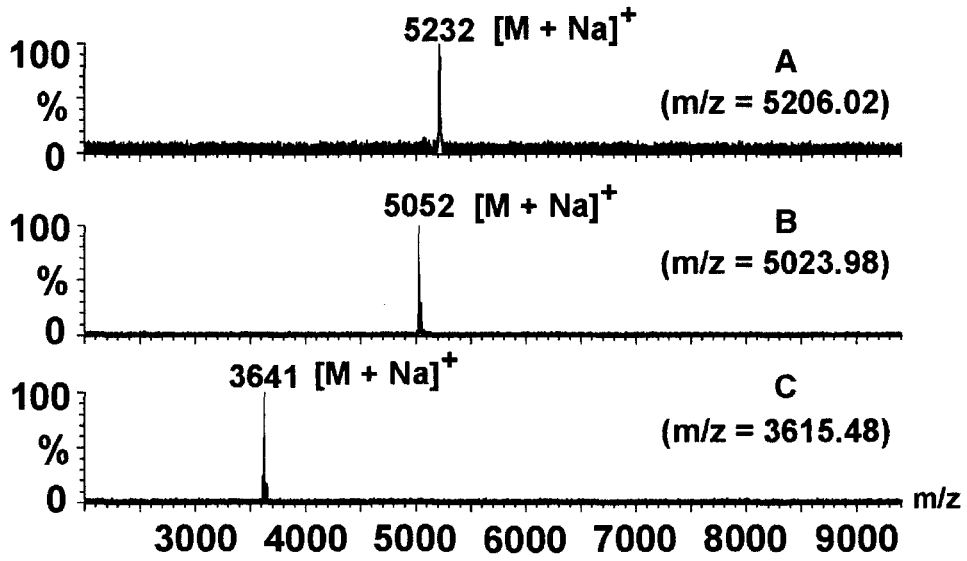

Figure 4.3. MALDI-TOF spectra of TSe-G5-$(O_2Bn)_{16}$ (A), COOH-G5-$(O_2Bn)_{16}$ (B), and COOH-G5-$(OH)_{32}$ (C).

4.2.2. Synthesis of a Bifunctional bis-Pyridyl Ligand for ^{99m}Tc

Having achieved the preparation of high-generation dendrons with a reactive acid functionality at the core, it became possible to introduce the required ligand for ^{99m}Tc. As stated above, placement of the ligand at the dendrimer core was considered critical to minimizing the impact of radionuclide introduction on the interactions of the macromolecule with its biological environment. Additionally, it was important for the linkage between the ligand and the dendron to be robust under physiological conditions, so as to ensure that the radionuclide could not be cleaved from the dendron during the radioimaging experiments. An amide linkage to the acid core was therefore preferable to the more labile ester linkage.

Having identified these requirements, we chose to prepare the bifunctional compound **4.13** (Scheme 4.3), bearing a free amine at one end and a bis-pyridyl metal chelating moiety at the other. The free primary amine of **4.13** could be coupled to the internal carboxylic acid of our aliphatic polyester dendrons at any generation, and the bis-pyridyl metal chelator could house the ^{99m}Tc radiotracer, as well as other homologous metal ions, such as rhenium.

The preparation of the bifunctional ligand was achieved by reductive amination of 2-pyridylcarboxaldehyde with commercially available t-butyl N-(6-aminohexyl)-carbamate hydrochloride in a mixture of acetic acid and dry dichloromethane. Upon mixing these components and stirring for 30 min, excess sodium triacetoxy borohydride was added and stirred for an additional 3 h to produce the t-BOC protected bis-pyridyl ligand **4.12** (Scheme 4.3). The t-BOC moiety was removed by treatment with trifluoroacetic acid (TFA), and ligand **4.13** was extensively purified by preparative HPLC to ensure a high degree of purity for subsequent coupling and metalation steps. Standard column chromatography proved inadequate for purifying this highly polar ligand to the extent required for radiotracer development.

In order to test conditions for the metalation chemistry with the bifunctional ligand **4.13**, and to produce a non-radioactive analog of the desired ^{99m}Tc complex as an HPLC standard, ligand **4.13** was reacted with $[Re(CO)_3(H_2O)_3]^+$ in methanol under microwave irradiation for 11 minutes at 110°C, followed by workup and purification by preparative HPLC to produce the Re complex **4.14**. The ^{1}H NMR spectra of compounds **4.13** and **4.14** are depicted in Figure 4.4. These spectra clearly indicate that successful

metalation had occurred, as can be seen from the disappearance of the proton signal at 3.82 ppm (4H) and appearance of two new signals at 4.41 ppm (2H) and 5.83 ppm (2H). These new signals appear as a result of the 8-membered ring structure that is formed upon Re chelation, forcing the pyridyl methylene protons to occupy either axial or equatorial positions, leading to two distinct signals. In addition, a dramatic shift of the signal at 2.65 ppm to 3.73 ppm, as well as smaller downfield shifts of the aromatic pyridyl protons (7.24, 7.85, and 8.68 ppm) indicated that the electronic environment around the pyridine rings and the tertiary amine had also changed.

Scheme 4.3. Synthesis of bis-pyridyl ligand 4.13 and rheniated bis-pyridyl ligand 4.14.

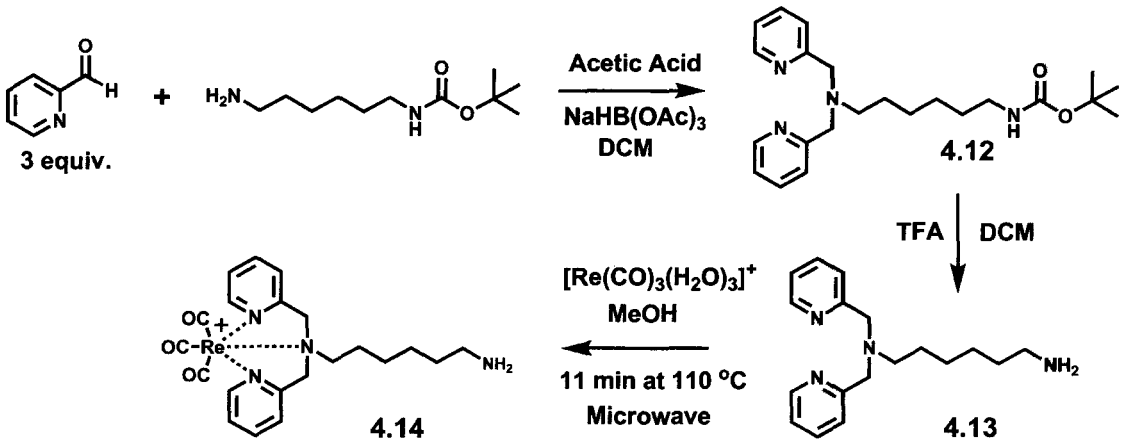

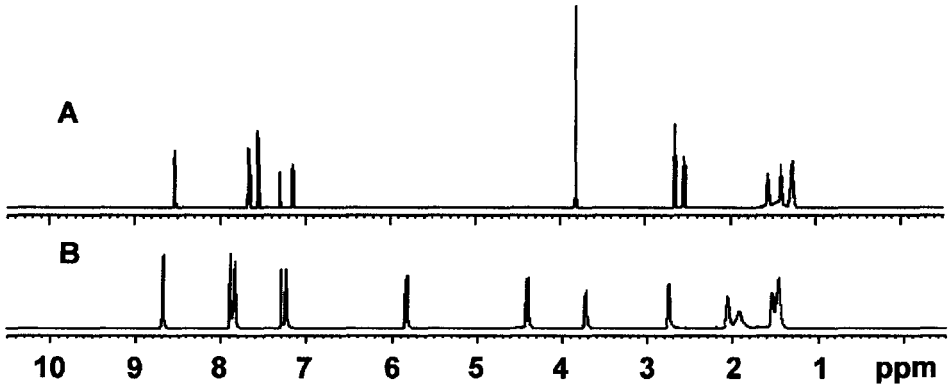

Figure 4.4. ^{1}H NMR of bis-pyridyl ligand 4.13 (A) and rheniated bis-pyridyl ligand 4.14 (B) in $CDCl_3$.

4.2.3. Amidation with the Dendron Core

At this point, the coupling chemistry between the bifunctional ligand (**4.13**) and the dendron core was investigated. Amidation of **4.13** with COOH-G5-$(O_2Bn)_{16}$ to yield the fifth-generation ligand-functionalized dendrimer proceeded smoothly using o-benzotriazole-N,N,N',N'-tetramethyluroniumhexafluoroalphosphate (HBTU) and 1-hyroxybenzotriazole (HOBT) as the coupling agents in minimal amounts of DCM. However, subsequent hydrogenolysis to produce the hydroxyl-terminated, ligand-functionalized dendrimer proved problematic. ^{1}H NMR analysis of the product mixture indicated the partial disappearance of aromatic protons, suggesting that the two pyridyl functionalities of ligand **4.13** are labile under the hydrogenolysis conditions. Considering the difficulty of chromatographically separating high generation dendrimers that only differ at their core, it was deemed futile to attempt purification of the resulting reaction mixture. Instead, the benzylidene protecting groups were first removed to produce the

fully deprotected dendrons, and then the core amidation with ligand **4.13** was performed as the final step in dendrimer synthesis. It was found that amidation proceeded smoothly for COOH-G5-$(OH)_{32}$, COOH-G6-$(OH)_{64}$ and COOH-G7-$(OH)_{128}$ dendrons using HBTU/HOBT as the coupling agents in minimal amounts of dimethylformamide (DMF).[24] Surprisingly, even though a large number of peripheral alcohol functionalities are present within the fully deprotected dendrons, each of which can potentially esterify the dendron core under the coupling conditions, no evidence for intramolecular esterification was observed. The primary amine of compound **4.13** must be sufficiently more nucleophilic that it preferentially reacts with the core acid functionality of the dendrons. Upon purification by preparative gel permeation chromatography (GPC) using MeOH as the mobile phase, the pure dendrimer products were isolated in typical yields of 60-75%. Unfortunately, all attempts to couple ligand **4.13** to the eighth generation dendron, COOH-G8-$(OH)_{256}$, resulted in no detectable conversion to the amide product. The poor reactivity at the G8 stage was attributed to extreme steric hindrance around the core acid functionality caused by the crowded dendrimer periphery.

The coupling of bis-pyridyl ligand **4.13** to the fully deprotected G5, G6, and G7 dendrons was followed by ^{1}H NMR spectroscopy and MALDI-TOF mass spectometry. Looking at COOH-G5-$(OH)_{32}$ as an example (Figures 4.5 and 4.6), successful coupling was evident from the appearance of aromatic signals at 7.33 (2H), 7.66 (2H), 7.85 (2H), and 8.48 (2H) ppm as well as aliphatic proton signals at 1.53 (2H), 1.62 (2H), 3.25 (2H), 3.76 (2H), and 3.87 (4H) ppm (Figure 4.5B). In addition, a small amide signal at 7.70 ppm can be seen adjacent to the aromatic signal at 7.66 ppm. It should be noted that not

all aliphatic peaks were resolved, possibly due to peak broadening as a result of the ligand being coupled to a macromolecular structure with slower relaxation times. The MALDI-TOF mass spectrum for BisPy-G5-$(OH)_{32}$ also confirmed the addition of ligand **4.13**, with a mass increase of 280 Da from the original observed mass (Figure 4.6). Similar spectral changes were also observed with the G6 and G7 dendrons (Figure 4.7 and Figure 4.8).

As mentioned above, the preparation of a non-radioactive analog, or standard, for each of the dendrimer structures to be radiolabeled is important for HPLC analysis of the radioactive products, as retention times of metalated species typically differ from those of unmetalated species. Rhenium is typically used as a non-radioactive standard of ^{99m}Tc due to its virtually identical atomic radius and similar reactivity.[25] Preparation of the non-radioactive Re standards was accomplished by coupling the rheniated ligand **4.14** using the same chemistry that was demonstrated to work for the unmetalated ligand, producing the desired dendrimers in yields ranging from 55% to 65%. This coupling chemistry was also confirmed by ^1H NMR spectroscopy where, in the case of G5, the appearance of the aromatic signals at 7.39 (2H), 7.61 (2H), 7.96 (2H), and 8.89 (2H) ppm, as well as the aliphatic proton signals at 1.55 (4H), 1.69 (2H), 3.25 (2H), and 3.76 (2H) ppm was observed (Figure 4.5C). Again, a small amide signal was observed at 7.73 ppm, signifying the formation of the coupled product. Further evidence for the successful preparation of the Re standards came from MALDI-TOF MS, which showed the expected increase of 528 Da as a result of introducing the rheniated ligand **4.14**. The MALDI spectrum for the fifth generation dendrimer, ReBisPy-G5-$(OH)_{32}$, is shown in

Figure 4.6C. Similar spectral changes were also observed with the G6 dendron (Figure 4.7).

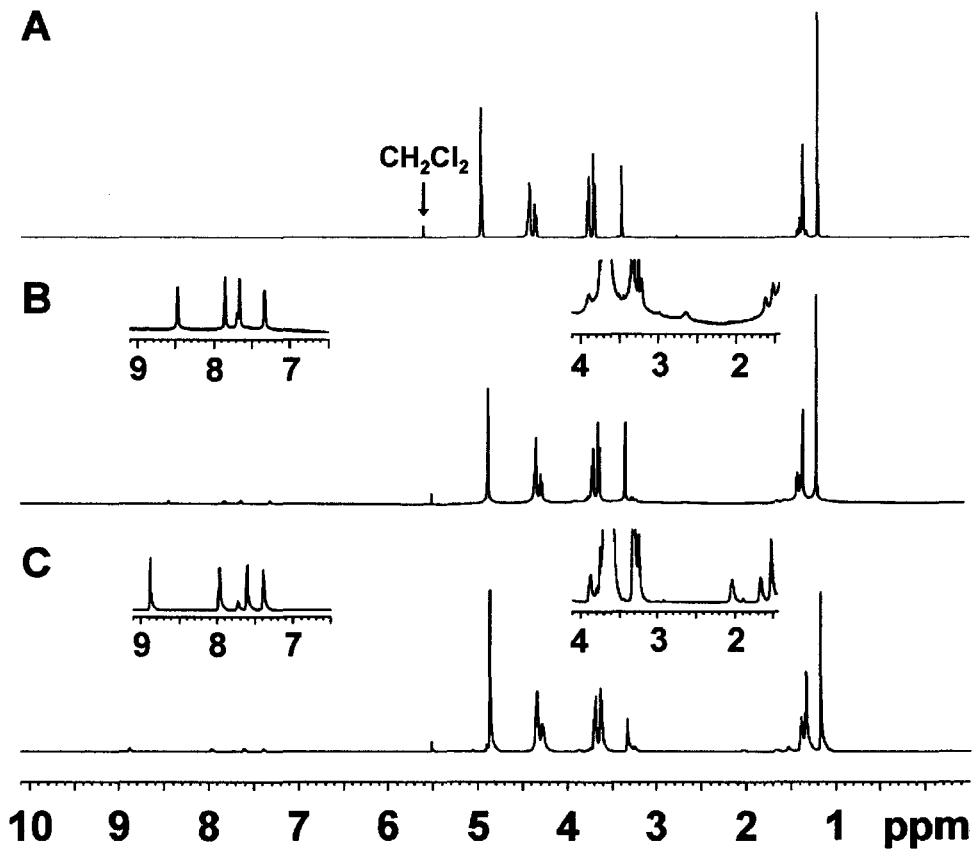

Figure 4.5. ^{1}H NMR spectra of COOH-G5-$(OH)_{32}$ (A), BisPy-G5-$(OH)_{32}$ (B), and $[ReBisPy\text{-}G5\text{-}(OH)_{32}]^+$ (C) in CD_3OD. Insets show the aromatic signals of the corresponding spectra in the range of 1.5 to 4.0 and 6.5 to 9.0 ppm.

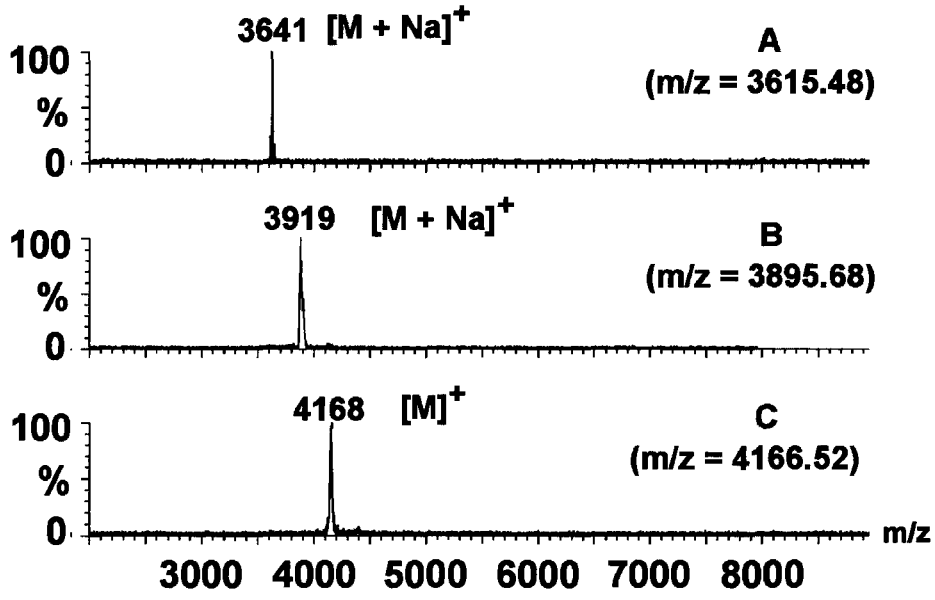

Figure 4.6. MALDI-TOF MS spectra of COOH-G5-$(OH)_{32}$ (A), BisPy-G5-$(OH)_{32}$ (B), and $[ReBisPy\text{-}G5\text{-}(OH)_{32}]^+$ (C).

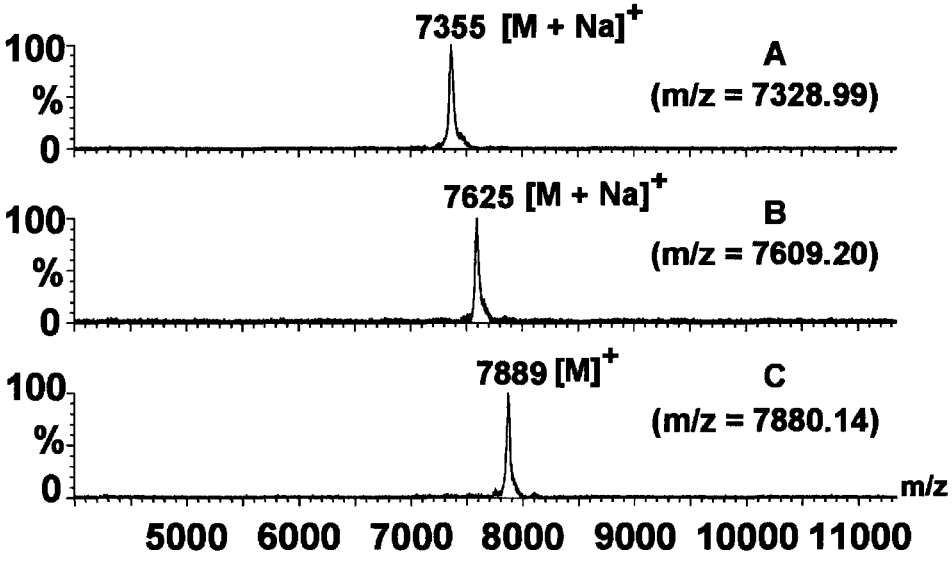

Figure 4.7. MALDI-TOF MS spectra of COOH-G6-$(OH)_{64}$, BisPy-G6-$(OH)_{64}$, and $[ReBisPy\text{-}G6\text{-}(OH)_{64}]^+$.

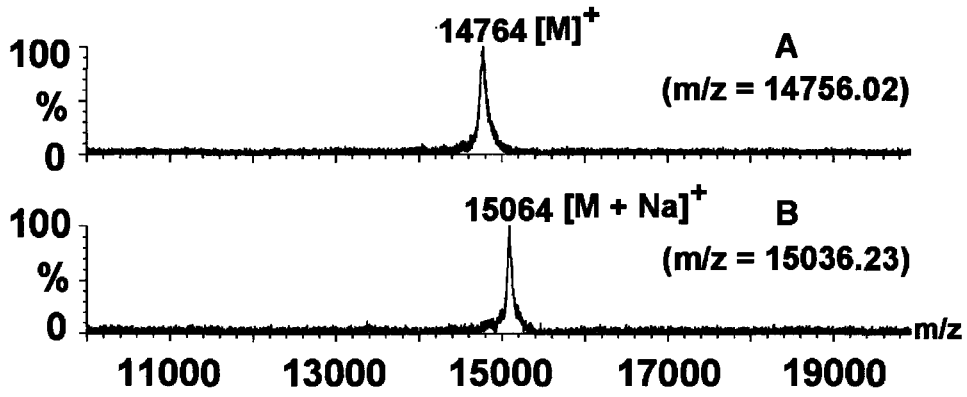

Figure 4.8. MALDI-TOF MS spectra of COOH-G7-$(OH)_{128}$, and BisPy-G7-$(OH)_{128}$.

4.3. Conclusion

The preparation of high-generation PMPA dendrons can be accomplished using toluene sulfonyl ethyl (TSe) ester as an easily removable core protecting group. Removal of the TSe moiety can be accomplished in high yield in dendrons of generation 1 through 8, and cleanly provides dendrons that can be modified at their core carboxylic acid functionality via amidation chemistry. Introduction of a bis-pyridyl ligand allowed the formation of high generation dendrimers that are capable of chelating various isotopes of Tc and Re. These materials provide the necessary precursors for labeling with radioactive technetium-99m.

4.4. Experimental

4.4.1. General Procedures

All chemicals were purchased from Sigma-Aldrich and used without any purification. NMR spectra were collected on Bruker Avance 600 MHz. ^{1}H spectra were recorded at 600 MHz and ^{13}C NMR spectra were recorded at 150 MHz. $CDCl_3$ and CD_3OD were used as solvents, and the non-deuterated solvent signals were used as internal standards for both the ^{1}H and ^{13}C spectra. Dichloromethane (CH_2Cl_2) was distilled from CaH_2 under nitrogen prior to use. Exact masses were determined by Micromass Quattro Ultima (low resolution ESI), Micromass Q-TOF Global Ultima (high resolution) and Micromass TofSpec 2E spectrometer (MALDI-TOF). MALDI-TOF was performed in positive ion mode using 2-(4-hydroxyphenyl-azo) benzoic acid (HABA) as the matrix. The MALDI-TOF spectrometer was calibrated using four peptides, including Substance P (M/Z = 1348 Da), Angiotensinogen (M/Z = 1759 Da), Adrenocorticotropic hormone, fragments 18 - 39 (M/Z = 2466 Da), and Cytochrome C (M/Z = 12361 Da and 6181 Da for doubly charged species). Analytical HPLC was performed using a Varian Pro Star model 330 PDA detector, model 230 solvent delivery system, a Bio-Rad IN/US γ-detector and a Varian C-18 nucleosil column. The mobile phase consisted of mixtures of H_2O with 0.1% TFA (solvent A) and acetonitrile with 0.1% TFA (solvent B). The elution protocol consisted of 80:20 ratio of solvent A to solvent B for 5 minutes, followed by a gradient starting at 80:20 (A to B) and finishing at 20:80 (A to B) over 20 minutes. The column was then washed with 100% solvent B for an additional 5 minutes. The product was eluted at a flow rate of 1 mL/min and monitored at a wavelength of 230 nm.

Preparative HLPC purifications were carried out on a Varian Pro Star preparative HPLC system, which consisted of a model 320 uniwavelength detector, a model 215 solvent delivery system, and a Microsorb Dynamax C-18 preparative column. The elution protocol consisted of 80:20 ratio of solvent A to solvent B for 5 minutes, followed by a gradient starting at 80:20 (A to B) and finishing at 20:80 (A to B) over 60 minutes. The column was then washed with 100% solvent B for an additional 10 minutes. The product was eluted at a flow rate of 30 mL/min and monitored at a wavelength of 230 nm. Preparative GPC purifications were carried out on a Waters HPLC system, which consisted of a model 486 tunable absorbance detector, a model 410 differential refractometer, an in-line degasser, a model 600 Pump, a model 600 controller, and a Polymer Labs PLgel MIXED-D preparative GPC column. The Waters model 600 pump was fitted with a 1.2 mL loop and a three directional recycling manifold that allowed for the product to be cycled back onto the column. All products were cycled over the column three times before separation using methanol as a solvent at a flow rate of 2.5 mL/min. Microwave reactions were performed using a Biotage Initiator Sixty instrument.

4.4.2. Synthesis

4.4.2.1. General Procedure for Dendrimer Growth. To a flame-dried round-bottom flask equipped with a magnetic stir bar (under argon atmosphere), the benzylidene protected anhydride, the hydroxyl-terminated dendrimer (generation 0 through 7), and 4-dimethylaminopyridine were all dissolved in a 3:2 ratio of CH_2Cl_2 and pyridine. After stirring at room temperature for over 12 h, approximately 2 mL of water was added and

the reaction was stirred for an additional 18 h in order to quench the excess anhydride. The product was isolated by diluting the mixture with CH_2Cl_2 (150 mL) and washing with 1 M $NaHSO_4$ (3 × 150 mL), saturated aqueous $NaCO_3$ (2 × 150 mL), and brine (150 mL). The organic layer was removed by rotary evaporation in vacuo. The product was then precipitated three times from a 9 : 1 hexanes : ethyl acetate mixture. Any residual solvent was removed in vacuo to yield white foam with a typical yield greater than 95%.

4.4.2.2. General Procedure for Deprotection of Benzylidene by Hydrogenolysis. To a flame-dried round-bottom flask equipped with a magnetic stir bar, the benzylidene protected dendrimer was dissolved in a 1 : 1 mixture of CH_2Cl_2 : MeOH. $Pd(OH)_2$ on Carbon (20%) was added and the flask was evacuated and back-filled with hydrogen three times (H_2 pressure: 1 atm). After vigorous stirring for 16 h, the reaction mixture was filtered through a celite plug in a fritted glass funnel and the filtrate was evaporated to dryness on a rotary evaporator in vacuo. The remaining residue was composed of the desired product, which was isolated as white foam in quantitative yields.

4.4.2.3. General Procedure for Deprotection of para-toluene sulfonyl ester (TSe) by DBU. To a flame-dried round-bottom flask equipped with a magnetic stir bar, the benzylidene protected dendrimer was dissolved in 5 mL of dichloromethane. 100 μL of 1,8-diazabicyclo[5.4.0]undec-7-ene (DBU) was added. The reaction was vigorously stirred overnight. The dichloromethane was removed by rotary evaporation in vacuo. The product was then precipitated three times from 9: 1 hexanes: ethyl acetate mixture. Any

residual solvent was removed in vacuo to yield white foam with a typical yield greater than 95%.

4.4.2.4. General Coupling Procedure. In a 5 mL scintillation vial equipped with a magnetic stir bar 3.5 equivalents of HBTU, 3.5 equivalents of HOBT, 3.0 equivalents of ligand **13** or ligand **14**, and the dendrimer bearing a single carboxylic acid were dissolved in 0.5 mL of DMF and 50 μL DIPEA. After stirring for 3 hours the entire reaction mixture was immediately injected on a recycling preparative GPC using methanol as the eluent. The high molecular weigh dendrimer was recycled three times on the preparative GPC column and separated from the DMF, reagents, and reaction by products. The high molecular weight dendrimer was collected in 1 mL aliquots and each aliquot was tested by MALDI-TOF MS for the desired mass. The aliquots containing the desired dendrimer were combined and the residual methanol was removed in vacuo to yield white foam with a typical yield between 55-75%. Each coupling product was injected onto an analytical HPLC column to determine purity. Each product was eluted over a 30 min duration using the solvent gradient described above.

TSe-G1-(O_2Bn)$_1$ (4.2). The generation growth was carried out as described above, specifically using para-toluene sulfonyl ethanol (**1**) (2.02 g, 10.0 mmol), benzylidene anhydride (8.65 g, 20.2 mmol, 2 equiv.) and DMAP (0.50 g, 4.10 mmol) all dissolved in 50 mL of dry CH_2Cl_2 and 25 mL of pyridine and stirred for 16 h at room temperature. Yield: 3.92 g, white foam (96%). ^{1}H NMR (600 MHz, $CDCl_3$): δ = 0.97 (s, 3H), 2.44 (s,

3H), 3.47 (t, 2H, J = 6 Hz), 3.60 (d, 2H, J = 11.4 Hz), 4.48 (t, 2H, J = 6 Hz), 4.53 (d, 2H, J = 11.4 Hz), 5.43 (s, 1H), 7.32 – 7.36 (m, 5H), 7.40 – 7.42 (m, 2H), 7.81 (d, 2H, J = 8.4 Hz). ^{13}C NMR (150 MHz, $CDCl_3$): δ = 17.04, 21.15, 41.98, 54.66, 57.53, 72.85, 101.25, 125.67, 127.72, 127.75, 128.53, 129.61, 135.55, 137.27, 144.63, 173.04. Calc.: $[M + H]^+$ ($C_{21}H_{25}O_6S_1$) m/z = 405.1372. Found ES MS: $[M + H]^+$ = 405.10, High Resolution ES MS: $[M + H]^+$ = 405.1359.

TSe-G1-(OH)$_2$ (4.3). Deprotection of TSe-G1-$(O_2Bn)_1$ (3.88 g, 9.60 mmol) in 150 mL of (1 : 1) CH_2Cl_2 : MeOH was carried out as above for 16 hours at room temperature under H_2 atmosphere. Yield: 3.02 g, white foam (99%). ^{1}H NMR (600 MHz, CD_3OD): δ = 1.03 (s, 3H), 2.47 (s, 3H), 3.53 (dd, 2H, J = 44.4, 10.8 Hz), 3.60 (t, 2H, J = 6.0 Hz), 4.39 (t, 2H, J = 6.0 Hz), 7.47 (d, 2H, J = 8.4 Hz), 7.82 (d, 2H, J = 11.4 Hz). ^{13}C NMR (150 MHz, CD_3OD): δ = 17.04, 21.57, 51.55, 55.88, 58.90, 65.65, 129.27, 131.19, 137.74, 146.68, 175.86. Calc.: $[M + H]^+$ ($C_{14}H_{21}O_6S_1$) m/z = 317.1059. Found ES MS: $[M + H]^+$ = 317.00, High Resolution ES MS: $[M + H]^+$ = 317.1068.

TSe-G2-(O$_2$Bn)$_2$ (4.4). The generation growth was carried out as described above, specifically using TSe-G1-$(OH)_2$ (2.90 g, 9.17 mmol), benzylidene anhydride (11.93 g, 27.49 mmol, 3 equiv.) and DMAP (0.50 g, 4.10 mmol) all dissolved in 50 mL of dry CH_2Cl_2 and 25 mL of pyridine and stirred for 16 h at room temperature. Yield: 6.53 g, white foam (98%). ^{1}H NMR (600 MHz, $CDCl_3$): δ = 0.96 (s, 6H), 1.08 (s, 3H), 2.38 (s, 3H), 3.10 (t, 2H, J = 6.0 Hz), 3.60 (d, 4H, J = 11.4 Hz), 4.18 – 4.22 (m, 6H), 4.56 (t, 4H,

J = 9.0 Hz), 5.42 (s, 2H), 7.29 – 7.33 (m, 8H), 7.39 – 7.41 (m, 4H), 7.68 (d, 2H, *J* = 8.4 Hz). ^{13}C NMR (150 MHz, $CDCl_3$): δ = 16.87, 17.27, 21.10, 42.14, 46.23, 54.17, 57.86, 64.74, 73.00, 73.07, 101.17, 125.66, 127.59, 127.71, 128.46, 129.55, 135.81, 137.31, 144.56, 171.56, 172.72. Calc.: $[M + H]^+$ ($C_{38}H_{45}O_{12}S_1$) m/z = 725.2632, $[M + NH_4]^+$ ($C_{38}H_{48}N_1O_{12}S_1$) m/z = 742.2897. Found ES MS: $[M + H]^+$ = 725.20, High Resolution ES MS: $[M + NH_4]^+$ = 742.2900.

TSe-G2-(OH)$_4$ (4.5). Deprotection of TSe-G2-(O_2Bn)$_2$ (4.98 g, 6.87 mmol) in 120 mL of (1 : 1) CH_2Cl_2 : MeOH was carried out as above for 16 hours at room temperature under H_2 atmosphere. Yield: 3.70 g, white foam (98%). ^{1}H NMR (600 MHz, CD_3OD): δ = 1.13 (s, 9H), 2.47 (s, 3H), 3.56 – 3.58 (m, 4H), 3.61 (t, 2H, *J* = 5.4 Hz), 3.64 – 3.66 (m, 4H), 4.09 (dd, 4H, *J* = 27.9, 10.8 Hz), 4.44 (t, 2H, *J* = 5.4 Hz), 7.48 (d, 2H, *J* = 7.8 Hz), 7.83 (d, 2H, *J* = 8.4 Hz). ^{13}C NMR (150 MHz, CD_3OD): δ = 15.38, 15.94, 19.72, 45.76, 49.91, 53.92, 57.75, 63.95, 64.25, 127.40, 129.41, 136.02, 144.82, 171.81, 173.94. Calc.: $[M + H]^+$ ($C_{24}H_{37}O_{12}S_1$) m/z = 549.2006. Found ES MS: $[M + H]^+$ = 549.10, High Resolution ES MS: $[M + H]^+$ = 549.1987.

TSe-G3-(O_2Bn)$_4$ (4.6). The generation growth was carried out as described above, specifically using TSe-G2-(OH)$_4$ (3.65 g, 6.65 mmol), benzylidene anhydride (17.5 g, 41.0 mmol, 6 equiv.) and DMAP (0.50 g, 4.10 mmol) all dissolved in 66 mL of CH_2Cl_2 and 33 mL of pyridine and stirred for 16 h at room temperature. Yield: 8.89 g, white foam (98%). ^{1}H NMR (600 MHz, $CDCl_3$): δ = 0.91 (s, 3H), 0.93 (s, 12H), 1.20 (s, 6H),

2.39 (s, 3H), 3.28 (t, 2H, J = 6.3 Hz), 3.58 (d, 8H, J = 11.4 Hz), 3.95 (dd, 4H, J = 27.0, 11.4 Hz), 4.31 – 4.34 (m, 10H), 4.56 (d, 8H, J = 12.0 Hz), 5.40 (s, 4H), 7.29 – 7.33 (m, 14H), 7.39 – 7.40 (m, 8H), 7.74 (d, 2H, J = 7.8 Hz). ^{13}C NMR (150 MHz, $CDCl_3$): δ = 16.39, 17.25, 21.12, 42.12, 45.85, 46.42, 54.13, 57.76, 64.68, 65.24, 72.98, 73.06, 101.22, 125.71, 127.60, 127.66, 128.39, 129.57, 135.82, 137.31, 144.53, 171.16, 171.36, 172.74. Calc.: $[M + Na]^+$ ($C_{72}H_{84}Na_1O_{24}S_1$) = 1387.4971, $[M + NH_4]^+$ ($C_{72}H_{88}N_1O_{24}S_1$) m/z = 1382.5417. Found MALDI-TOF MS: $[M + Na]^+$ = 1387.30, High Resolution ES MS: $[M + NH_4]^+$ = 1382.5404.

TSe-G3-(OH)$_8$ (4.7). Deprotection of TSe-G3-(O_2Bn)$_4$ (2.98 g, 2.18 mmol) in 100 mL of CH_2Cl_2 and MeOH (1 : 1) was carried out as above for 16 h at room temperature under H_2 atmosphere. Yield: 2.18 g, white foam (99%). ^{1}H NMR (600 MHz, CD_3OD): δ = 1.18 (s, 15H), 1.30 (s, 6H), 2.50 (s, 3H), 3.61 – 3.71 (m, 18H), 4.21 – 4.33 (m, 12H), 4.50 (t, 2H, J = 5.4 Hz), 7.51 (d, 2H, J = 7.8 Hz), 7.87 (d, 2H, J = 7.8 Hz). ^{13}C NMR (150 MHz, CD_3OD): δ = 15.42, 15.83, 16.35, 19.76, 45.88, 46.04, 49.91, 53.84, 57.94, 63.96, 64.30, 65.20, 127.40, 129.40, 136.03, 144.83, 171.46, 171.84, 174.04. Calc.: $[M + H]^+$ ($C_{44}H_{69}O_{24}S_1$) m/z = 1013.3900, $[M + NH_4]^+$ ($C_{44}H_{72}N_1O_{24}S_1$) m/z = 1030.4165. Found ES MS: $[M + NH_4]^+$ m/z = 1030.40, High Resolution ES MS: $[M + H]^+$ m/z = 1013.3929, $[M + NH_4]^+$ m/z = 1030.4172.

TSe-G4-(O_2Bn)$_8$ (4.8). The generation growth was carried out as described above, specifically using TSe-G3-(OH)$_8$ (2.18 g, 2.15 mmol), benzylidene anhydride (11.01 g,

25.8 mmol, 12 equiv.) and DMAP (0.50 g, 4.10 mmol) all dissolved in 40 mL of CH_2Cl_2 and 20 mL of pyridine and stirred for 16 h at room temperature. Yield: 5.58 g, white foam (98%). ^{1}H NMR (600 MHz, $CDCl_3$): δ = 0.95 (s, 24H), 1.05 (s, 6H), 1.09 (s, 3H) 1.23 (s, 12H), 2.41 (s, 3H), 3.37 (t, 2H, *J* = 6.0 Hz), 3.60 (dd, 16H, *J* = 11.4, 3.0 Hz), 4.10 – 4.14 (m, 12H), 4.35 – 4.41 (m, 18H), 4.59 (d, 16H, *J* = 12.6), 5.42 (s, 8H), 7.30 – 7.35 (m, 26H), 7.42 – 7.43 (m, 16H), 7.79 (d, 2H, *J* = 7.8 Hz). ^{13}C NMR (150 MHz, $CDCl_3$): δ = 16.52, 16.72, 17.22, 21.11, 42.10, 45.98, 46.06, 46.40, 54.15, 57.85, 64.61, 64.99, 65.63, 72.97, 73.03, 101.20, 125.72, 127.60, 127.66, 128.39, 129.59, 135.90, 137.41, 144.54, 170.94, 171.43, 172.73. Calc.: $[M + Na]^+$ ($C_{140}H_{164}Na_1O_{48}S_1$) m/z = 2668.0011, $[M + 3NH_4]^{3+}$ ($C_{140}H_{176}N_3O_{48}S_1$) m/z = 899.7048. Found MALDI-TOF MS: $[M + Na]^+$ m/z = 2668.83, High Resolution ES MS: $[M + 3NH_4]^{3+}$ m/z = 899.7111.

TSe-G4-(OH)$_{16}$ (4.9). Deprotection of TSe-G4-(O_2Bn)$_8$ (3.27 g, 1.24 mmol) in 120 mL of CH_2Cl_2 and MeOH (1 : 1) was carried out as above for 16 h at room temperature under H_2 atmosphere. Yield: 2.36 g, white foam (98%). ^{1}H NMR (600 MHz, CD_3OD): δ = 1.17 (s, 27H), 1.22 (s, 3H), 1.32 (s, 18H), 2.50 (s, 3H), 3.62 – 3.71 (m, 34H), 4.23 – 4.35 (m, 28H), 4.51 (t, 2H, *J* = 6.0 Hz), 7.52 (d, 2H, *J* = 7.8 Hz), 7.89 (d, 2H, *J* = 7.8 Hz). ^{13}C NMR (150 MHz, CD_3OD): δ = 15.48, 15.88, 16.22, 16.44, 19.83, 45.92, 46.06, 46.18, 49.91, 53.85, 57.98, 63.97, 64.29, 65.22, 65.55, 127.44, 129.44, 136.10, 144.91, 171.40, 171.91, 174.05. Calc.: $[M + Na]^+$ ($C_{84}H_{132}Na_1O_{48}S_1$) m/z = 1963.7507, $[M + NH_4]^+$ ($C_{84}H_{136}N_1O_{48}S_1$) m/z = 1958.7953. Found MALDI-TOF MS: $[M + Na]^+$ m/z = 1964.64, High Resolution ES MS: $[M + NH_4]^+$ m/z = 1958.7885.

TSe-G5-$(O_2Bn)_{16}$ (4.10). The generation growth was carried out as described above, specifically using TSe-G4-$(OH)_{16}$ (2.33 g, 1.20 mmol), benzylidene anhydride (12.31 g, 28.87 mmol, 24 equiv.) and DMAP (0.50 g, 4.10 mmol) all dissolved in 40 mL of CH_2Cl_2 and 20 mL of pyridine and stirred for 16 h at room temperature. Yield: 6.10 g, white foam (98%). ^{1}H NMR (500 MHz, $CDCl_3$): δ = 0.91 (s, 48H), 1.05 (s, 12H), 1.15 (s, 6H), 1.20 (s, 27H), 2.35 (s, 3H), 3.32 - 3.35 (m, 2H), 3.56 (dd, 32H, J = 11.4, 3.2 Hz), 4.07 – 4.15 (m, 28H), 4.32 – 4.38 (m, 34H), 4.55 (d, 32H, J = 11.5 Hz), 5.38 (s, 16H), 7.28 – 7.31 (m, 50H), 7.39 – 7.41 (m, 32H), 7.72 (d, 2H, J = 7.8 Hz). ^{13}C NMR (150 MHz, $CDCl_3$): δ = 16.48, 16.76, 16.84, 17.21, 42.07, 46.04, 46.37, 64.55, 64.76, 65.12, 72.93, 72.99, 101.16, 125.73, 127.64, 128.37, 129.58, 135.90, 137.45, 170.96, 171.40, 172.71 Calc.: $[M + Na]^+$ ($C_{276}H_{324}Na_1O_{96}S_1$) m/z = 5229.0090, $[M + H + 2NH_4]^{3+}$ ($C_{276}H_{333}N_2O_{96}S_1$) m/z = 1747.6986. Found MALDI-TOF MS: $[M + Na]^+$ m/z = 5232.48, High Resolution ES MS: $[M + H + 2NH_4]^{3+}$ m/z = 1747.6893.

TSe-G5-$(OH)_{32}$ (4.11). Deprotection of TSe-G5-$(O_2Bn)_{16}$ (2.55 g, 0.490 mmol) in 100 mL of CH_2Cl_2 and MeOH (1 : 1) was carried out as above for 16 h at room temperature under H_2 atmosphere. Yield: 1.84 g, white foam (99%). ^{1}H NMR (600 MHz, CD_3OD): δ = 1.17 (s, 48H), 1.28 (s, 3H), 1.33 (s, 27H), 1.34 (s, 12H), 1.37 (s, 6H), 2.51 (s, 3H), 3.62 – 3.71 (m, 66H), 4.27 – 4.38 (m, 60H), 4.54 (t, 2H, J = 5.4 Hz), 7.53 (d, 2H, J = 8.4 Hz), 7.89 (d, 2H, J = 8.4 Hz). ^{13}C NMR (150 MHz, CD_3OD): δ = 15.54, 16.03, 16.33, 16.53, 19.80, 46.06, 46.21, 49.91, 63.99, 64.28, 65.16, 65.45, 65.85, 127.46, 129.49, 136.15, 144.96, 171.46, 171.94, 174.07. Calc.: $[M + Na]^+$ ($C_{164}H_{260}Na_1O_{96}S_1$) m/z = 3820.5082,

$[M + 2NH_4]^{2+}$ ($C_{164}H_{268}N_2O_{96}S_1$) m/z = 1916.7936. Found MALDI-TOF MS: $[M + Na]^+$ m/z = 3823.46, High Resolution ES MS: $[M + 2NH_4]^{2+}$ m/z = 1916.7930.

BisPy Ligand (4.13). To a flame dried 100 mL round bottom flask *N*-boc-1,6-hexanediamine hydrochloride (1.0 g, 3.96 mmol), pyridine-2-carboxaldehyde (1.27 g, 11.86 mmol, 3 equiv.), and acetic acid (0.713 g, 11.87 mmol, 3 equiv) were dissolved in 25 mL dichloromethane and stirred for 20 minutes. The reducing agent sodium borohydride triacetate (2.93, 13.82 mmol, 3.5 equiv) was added and stirred for an additional 2 hours. The reaction was diluted with an additional 75 mL of dichloromethane and washed with 100 mL of 1 M NaOH. The organic layer was separated and dried over $MgSO_4$ and removed by rotary evaporation to produce a crude mixture containing compound **4.12**. The crude mixture of **4.12** was dissolved in 25 mL of 4 : 1 dichloromethane to trifluoroacetic acid and stirred for 3 hours. The solvent was removed by rotary evaporation and the crude mixture was dissolved in 10 mL of water. Five 2 mL aliquots were separately injected onto a preparative HPLC column. Compound **4.13** was elueted through the column over 60 minutes and the large peak between 18 and 23 minutes was collected. All samples containing ligand **4.13** were combined and the acetonitrile was removed by rotary evaporation. The remaining aqueous solution containing purified **4.13** was washed with 1 M NaOH. Ligand **4.13** was isolated after washing the aqueous layer three times with dichloromethane (100 mL). Yield: 0.69 g, yellowish-white wax (58%). ^{1}H NMR (600 MHz, $CDCl_3$): δ = 1.24 - 130 (m, 4H), 1.42 (quin, 2H, J = 7.2 Hz), 1.56 (quin, 2H, J = 7.2 Hz), 2.55 (t, 2H, J = 7.2 Hz), 2.65 (t, 2H,

J = 7.2 Hz), 3.82 (s, 4H), 7.14 – 7.16 (m, 2H), 7.55 (d, 2H, J = 7.8 Hz), 7.66 (dt, 2H, J = 7.8, 1.8 Hz), 8.54 (dd, 2H, J = 4.8, 1.2 Hz). ^{13}C NMR (150 MHz, $CDCl_3$): δ = 26.21, 26.59, 26.68, 33.32, 41.70, 53.93, 60.05, 121.35, 122.33, 135.84, 148.46, 159.68. Calc.: $[M + H]^+$ ($C_{18}H_{27}N_4$) m/z = 299.2236. Found ES MS: $[M + H]^+$ m/z = 299.10, High Resolution ES MS $[M + H]^+$ m/z = 299.2249.

ReBisPy Ligand (4.14). Compound **4.13** (0.200 g, 0.671 mmol) and $Re(H_2O)_3(CO)_3Br$ (0.325 g, 0.805mmol, 1.2 equiv) were added to a 10 mL Emry microwave vial and dissolved in 5 mL of methanol. The vial was heated to 110°C in a microwave and irradiated for 11 minutes. The methanol was removed by rotary evaporation, and the residue was dissolved in 10 mL of water. Five 2 mL aliquots were separately injected onto a preparative HPLC column. Compound **4.14** was elueted through the column over 60 minutes and the large peak between 25 and 30 minutes was collected. All samples containing ligand **4.14** were combined and the acetonitrile was removed by rotary evaporation. The remaining aqueous solution containing purified **4.14** was washed with 1 M NaOH. Ligand **4.14** was isolated after washing the aqueous layer ten times with dichloromethane (100 mL). Yield: 0.248 g, orange wax (65%). ^{1}H NMR (600 MHz, $CDCl_3$): δ = 1.43 - 1.54 (bm, 6H), 1.92 (bs, 2H), 2.05 (bs, 2H), 2.75 (t, 2H, J = 7.2 Hz), 3.73 (t, 2H, J = 8.4 Hz), 4.41 (d, 2H, J = 16.2 Hz), 5.76 (d, 2H, J = 16.2 Hz), 7.21 (t, 2H, J = 6.6 Hz), 7.81 – 7.88 (m, 4H), 8.65 (d, 2H, J = 5.5 Hz). ^{13}C NMR (150 MHz, $CDCl_3$): δ = 24.92, 25.91, 26.27, 32.83, 41.45, 66.71, 70.73, 124.52, 124.74, 139.84, 150.13,

160.91, 195.25, 195.48. Calc.: $[M]^+$ ($C_{21}H_{26}N_4O_3Re_1$) m/z = 569.1562. Found ES MS: $[M]^+$ m/z = 569.10, High Resolution ES MS $[M]^+$ m/z = 569.1560.

COOH-G5-$(O_2Bn)_{16}$ (4.15). The removal of the TSe protecting group was carried out as described above, specifically using TSe-G5-$(O_2Bn)_{16}$ (1.02 g, 0.196 mmol), and DBU (0.102 g, 100 μL, 0.670 mmol, 3.4 equiv.) were dissolved in 5 mL of CH_2Cl_2 and stirred for 16 hours. Yield: 0.965 g, white foam (98%). ^{1}H NMR (500 MHz, $CDCl_3$): δ = 0.91 (s, 48H), 1.04 (s, 12H), 1.14 (s, 6H) 1.22 (s, 27H), 3.55 (dd, 32H, *J* = 11.4, 2.7 Hz), 4.09 - 4.25 (m, 28H), 4.36 (m, 32H), 4.55 (d, 32H, *J* = 11.5 Hz), 5.39 (s, 16H), 7.28 – 7.32 (m, 48H), 7.39 – 7. 41 (m, 32H). ^{13}C NMR (150 MHz, $CDCl_3$): δ = 16.76, 16.88, 17.20, 42.09, 46.12, 46.40, 64.60, 64.88, 65.19, 72.93, 72.98, 101.18, 125.74, 127.66, 128.39, 137.41, 170.92, 171.53, 172.78 Calc.: $[M + Na]^+$ ($C_{267}H_{314}Na_1O_{94}$) m/z = 5046.9688. Found MALDI-TOF MS: $[M + Na]^+$ m/z = 5051.84.

COOH-G5-$(OH)_{32}$ (4.16). Deprotection of COOH-G5-$(O_2Bn)_{16}$ (0.903 g, 0.180 mmol) in 40 mL of CH_2Cl_2 and MeOH (1 : 1) was carried out as above for 16 h at room temperature under H_2 atmosphere. Yield: 0.644 g, white foam (99%). ^{1}H NMR (600 MHz, CD_3OD): δ = 1.17 (s, 48H), 1.32 – 1.36 (m, 45H), 3.62 – 3.71 (m, 64H), 4.26 - 4.35 (m, 60H). ^{13}C NMR (150 MHz, CD_3OD): δ = 15.53, 16.37, 16.52, 46.05, 46.18, 49.90, 63.96, 64.29, 65.11, 171.43, 171.93, 174.06. Calc.: $[M + Na]^+$ ($C_{155}H_{250}Na_1O_{94}$) m/z = 3638.4680, $[M + 3H]^{3+}$ ($C_{155}H_{253}O_{94}$) m/z = 1206.1672. Found MALDI-TOF MS: $[M + Na]^+$ m/z = 3640.95, High Resolution ES MS: $[M + 3H]^{3+}$ m/z = 1206.1639.

BisPy-G5-$(OH)_{32}$ (4.17). The amide coupling was carried out as describe above, specifically COOH-G5-$(OH)_{32}$ (0.100 g, 27.7 μmol), ligand **4.13** (25.2 mg, 84.4 μmol, 3 equiv.), HBTU (32.0 mg, 84.4 μmol, 3 equiv.), HOBT (11.4 mg, 84.4 μmol, 3 equiv.), and DIPEA (50 μL, 0.287 mmol, 10 equiv.) were weighed into a 5 mL scintillation vial and dissolved in 0.5 mL of DMF. After stirring for 3 hours the entire reaction mixture was immediately injected on a recycling preparative GPC using methanol as the eluent. Yield: 70.0 mg, white foam (65%). ^{1}H NMR (600 MHz, CD_3OD): δ = 1.17 (s, 48H), 1.33 – 1.40 (m, 45), 1.53 (bs, 2H), 1.62 (bs, 2H), 3.25 (m, 2H), 3.62 – 3.76 (m, 64H), 3.76 (m, 2H), 3.87 (bs, 4H) 4.27 – 4.37 (m, 60H), 7.33 (m, 2H), 7.66 (m, 2H), 7.85 (m, 2H), 8.48 (m, 2H). ^{13}C NMR (150 MHz, CD_3OD): δ = 15.39, 15.54, 16.36, 16.53, 16.83, 26.20, 26.59, 26.70, 33.32, 41.91, 46.06, 46.19, 49.92, 53.96, 59.93, 64.00, 64.28, 65.12, 65.41, 122.08, 123.06, 136.93, 147.56, 159.73, 171.43, 171.93, 174.06. Calc.: $[M + Na]^+$ ($C_{173}H_{274}N_4Na_1O_{93}$) m/z = 3918.6732, $[M + H + 2NH_4]^{3+}$ ($C_{173}H_{283}N_6O_{93}$) m/z = 1310.9200. Found MALDI-TOF MS: $[M + Na]^+$ m/z = 3919.24, High Resolution ES MS $[M + H + 2NH_4]^{3+}$ m/z = 1310.9194. HPLC: RT = 14.78 minutes.

$[ReBisPy-G5-(OH)_{32}]^+$ (4.18). The amide coupling was carried out as describe above, specifically COOH-G5-$(OH)_{32}$ (0.100 g, 27.7 μmol), ligand **4.14** (54.7 mg, 84.4 μmol, 3 equiv.), HBTU (32.0 mg, 84.4 μmol, 3 equiv.), HOBT (11.4 mg, 84.4 μmol, 3 equiv.), and DIPEA (50 μL, 0.287 mmol, 10 equiv.) were weighed into a 5 mL scintillation vial and dissolved in 0.5 mL of DMF. After stirring for 3 hours the entire reaction mixture was immediately injected on a recycling preparative GPC using methanol as the eluent.

Yield: 65.5 mg, white foam (57%). ^{1}H NMR (600 MHz, CD_3OD): δ = 1.18 (s, 48H), 1.33 - 135 (m, 45H), 1.55 (bs, 4H), 1.69 (bs, 2H), 2.03 (bs, 2H), 3.25 (bm, 2H), 3.62 – 3.76 (m, 64H), 3.76 (bm, 2H), 4.27 – 4.35 (m, 60H), 7.37 – 7.39 (m, 2H), 7.60 - 7.61 (m, 2H), 7.71 – 7.73 (bm, ~1H), 7.95 – 7.97 (m, 2H), 8.88 – 8.89 (m, 2H). ^{13}C NMR (150 MHz, CD_3OD): δ = 15.55, 16.34, 16.53, 16.83, 25.48, 25.87, 26.15, 28.76, 41.91, 46.06, 46.19, 49.92, 53.96, 64.00, 64.28, 65.14, 65.44, 66.73, 67.06, 70.04, 122.84, 125.03, 139.80, 151.23, 160. 53, 171.46, 171.94, 174.08, 195.65. Calc.: $[M]^+$ ($C_{176}H_{274}N_4O_{96}Re_1$) m/z = 4166.6239, $[M + 2NH_4]^{3+}$ ($C_{176}H_{282}N_6O_{96}Re_1$) m/z = 1400.8976. Found MALDI-TOF MS: $[M]^+$ m/z = 4168.35, High Resolution ES MS $[M + 2NH_4]^{3+}$ m/z = 1400.8998. HPLC: RT = 16.19 minutes.

TSe-G6-$(O_2Bn)_{32}$ (4.19). The generation growth was carried out as described above, specifically using TSe-G5-$(OH)_{32}$ (1.75 g, 0.461 mmol), benzylidene anhydride (9.43 g, 22.11 mmol, 48 equiv.) and DMAP (0.50 g, 4.10 mmol) all dissolved in 40 mL of CH_2Cl_2 and 20 mL of pyridine and stirred for 16 h at room temperature. Yield: 4.73 g, white foam (99%). ^{1}H NMR (600 MHz, $CDCl_3$): δ = 0.89 (s, 96H), 1.05 (s, 24H), 1.17 – 1.20 (bm, 60H), 1.26 – 1.28 (bm, 9H), 2.32 (s, ~3H), 3.30 (bs, ~2H), 3.53 – 3.55 (m, 64H), 4.07 – 4.21 (m, 56H), 4.32 – 4.42 (m, 70H), 4.50 - 4.53 (m, 64H), 5.38 (s, 32H), 7.30 – 7.41 (bm, 162H), 7.72 (bs, 2H). ^{13}C NMR (150 MHz, $CDCl_3$): δ = 16.81, 16.97, 17.18, 42.04, 46.00, 46.36, 64.48, 65.21, 72.88, 101.09, 125.75, 127.63, 128.35, 137.50, 170.95, 171.39, 172.70 Calc.: $[M + Na]^+$ ($C_{548}H_{644}Na_1O_{192}S_1$) m/z = 10351.0248. Found MALDI-TOF MS: $[M + Na]^+$ m/z = 10354.61.

TSe-G6-(OH)$_{64}$ (4.20). Deprotection of TSe-G6-(O_2Bn)$_{32}$ (2.74 g, 0.265 mmol) in 100 mL of CH_2Cl_2 and MeOH (1 : 1) was carried out as above for 16 h at room temperature under H_2 atmosphere. Yield: 1.97 g, white foam (99%). ^{1}H NMR (600 MHz, CD_3OD): δ = 1.17 (s, 96H), 1.34 – 1.38 (m, 96H), 2.52 (s, ~3H), 3.63 – 3.72 (m, 130), 4.28 – 4.38 (m, 124H), 4.56 (bs, 2H), 7.56 (d, 2H, *J* = 7.8 Hz), 7.90 (d, 2H, *J* = 7.8 Hz). ^{13}C NMR (150 MHz, CD_3OD): δ = 15.61, 16.45, 16.63, 46.05, 46.19, 49.91, 64.02, 64.27, 65.07, 127.50, 129.50, 171.47, 171.98, 174.09. Calc.: $[M + Na]^+$ ($C_{324}H_{516}Na_1O_{192}S_1$) m/z = 7534.0232, $[M + 4NH_4]^{4+}$ ($C_{324}H_{532}N_4O_{192}S_1$) m/z = 1895.7927. Found MALDI-TOF MS: $[M + Na]^+$ m/z = 7539.10, High Resolution ES MS $[M + 4NH_4]^{4+}$ m/z = 1895.7939.

COOH-G6-(O_2Bn)$_{32}$ (4.21). The removal of the TSe protecting group was carried out as described above, specifically using TSe-G6-(O_2Bn)$_{32}$ (1.05 g, 0.102 mmol), and DBU (0.102 g, 100 μL, 0.670 mmol, 6.6 equiv.) dissolved in 5 mL of CH_2Cl_2 and stirred for 16 hours. Yield: 1.01 g, white foam (98%). ^{1}H NMR (600 MHz, $CDCl_3$): δ = 0.89 (s, 96H), 1.05 (s, 24H), 1.10 – 1.25 (m, 69H), 3.53 – 3.55 (m, 64H), 4.07 - 4.18 (m, 60), 4.18 – 4.36 (m, 64H), 4.50 – 4.53 (m, 64H), 5.38 (s, 32H), 7.30 – 7.42 (m, 160H). ^{13}C NMR (150 MHz, $CDCl_3$): δ = 16.80, 16.96, 17.17, 42.04, 46.00, 46.34, 64.50, 72.88, 101.10, 125.75, 127.63, 128.36, 137.49, 170.85, 171.05, 171.40, 172.73. Calc.: $[M + Na]^+$ ($C_{539}H_{634}Na_1O_{190}$) m/z = 10168.9846. Found MALDI-TOF MS: $[M + Na]^+$ m/z = 10171.96.

COOH-G6-$(OH)_{64}$ (4.22). Deprotection of COOH-G6-$(O_2Bn)_{32}$ (0.950 g, 93.6 μmol) in 40 mL of CH_2Cl_2 and MeOH (1 : 1) was carried out as above for 16 h at room temperature under H_2 atmosphere. Yield: 0.665 g, white foam (97%). ^{1}H NMR (600 MHz, CD_3OD): δ = 1.17 (s, 96H), 1.34 – 1.40 (m, 93H), 3.63 – 3.65 (m, 64H), 3.70 – 3.72 (m, 64H), 4.28 – 4.38 (m, 124H). ^{13}C NMR (150 MHz, CD_3OD): δ = 15.60, 16.45, 16.62, 46.05, 46.19, 49.91, 64.00, 64.28, 171.97, 171.98, 174.08. Calc.: $[M + Na]^+$ ($C_{315}H_{506}Na_1O_{190}$) m/z = 7351.9830, $[M + 4H]^{4+}$ ($C_{315}H_{510}O_{190}$) m/z = 1833.2561. Found MALDI-TOF MS: $[M + Na]^+$ m/z = 7355.45, High Resolution ES MS $[M + 4H]^{4+}$ m/z = 1833.2645.

BisPy-G6-$(OH)_{64}$ (4.23). The amide coupling was carried out as describe above, specifically COOH-G6-$(OH)_{64}$ (0.100 g, 13.6 μmol), ligand **4.13** (20.3 mg, 68.2 μmol, 5 equiv.), HBTU (25.8 mg, 68.2 μmol, 5 equiv.), HOBT (9.2 mg, 68.2 μmol, 5 equiv.), and DIPEA (50 μL, 0.287 mmol, 21 equiv.) were weighed into a 5 mL scintillation vial and dissolved in 0.5 mL of DMF. After stirring for 3 hours the entire reaction mixture was immediately injected on a recycling preparative GPC using methanol as the eluent. Yield: 71.0 mg, white foam (69%). ^{1}H NMR (600 MHz, CD_3OD): δ = 1.18 (s, 96H), 1.34 – 1.40 (m, 99H), 1.55 (bs, 2H), 1.65 (bs, ~2H), 3.63 - 3.75 (m, 128H), 3.89 (bs, 4H), 4.28 - 4.36 (m, 124H), 7.26 – 7.36 (bm, 2H), 7.61 – 7.69 (bm, 2H), 7.78 – 7.88 (bm, 2H), 8.479 (bs, 2H). ^{13}C NMR (150 MHz, CD_3OD): δ = 15.61, 16.45, 16.63, 46.05, 46.17, 46.19, 49.92, 53.96, 64.02, 64.26, 65.05, 137.08, 147.90, 171.34, 171.45, 171.97, 174.08. Calc.: $[M + Na]^+$ ($C_{333}H_{530}N_4Na_1O_{189}$) m/z = 7632.1882, $[M + H + 3NH_4]^{4+}$ ($C_{333}H_{543}N_7O_{189}$) m/z =

1916.0774. Found MALDI-TOF MS: $[M + Na]^+$ m/z = 7625.34, High Resolution ES MS $[M + H + 3NH_4]^{4+}$ m/z = 1916.0768. HPLC: RT = 14.66 minutes.

$[ReBisPy\text{-}G6\text{-}(OH)_{64}]^+$ (4.24). The amide coupling was carried out as describe above, specifically COOH-G6-$(OH)_{64}$ (0.100 g, 13.6 μmol), ligand **4.14** (44.2 mg, 68.2 μmol, 5 equiv.), HBTU (25.8 mg, 68.2 μmol, 5 equiv.), HOBT (9.2 mg, 68.2 μmol, 5 equiv.), and DIPEA (50 μL, 0.287 mmol, 21 equiv.) were weighed into a 5 mL scintillation vial and dissolved in 0.5 mL of DMF. After stirring for 3 hours the entire reaction mixture was immediately injected on a recycling preparative GPC using methanol as the eluent. Yield: 64.3 mg, white foam (60%). ^1H NMR (600 MHz, CD_3OD): δ = 1.18 (s, 96H), 1.34 – 1.42 (m, 99H), 1.55 (bs, 4H), 1.65 (bs, 2H), 3.63 – 3.75 (m, 128H), 4.28 – 4.36 (m, 126H), 7.36 – 7.42 (bs, 2H), 7.62 – 7.65 (bm, 2H), 7.95 – 8.00 (bm, 2H), 8.89 (bs, 2H). ^{13}C NMR (150 MHz, CD_3OD): δ = 15.61, 16.45, 16.63, 46.06, 46.19, 49.92, 53.96, 64.03, 64.27, 65.06, 171.47, 171.98, 174.10. Calc.: $[M]^+$ ($C_{336}H_{530}N_4O_{192}Re_1$) m/z = 7880.1389, $[M + 3NH_4]^{4+}$ ($C_{336}H_{542}N_7O_{192}Re_1$) m/z = 1983.5605. Found MALDI-TOF MS: $[M]^+$ m/z = 7888.81, High Resolution ES MS $[M + H + 2NH_4]^{4+}$ m/z = 1983.5621. HPLC: RT = 15.09 minutes.

TSe-G7-$(O_2Bn)_{64}$ (4.25). The generation growth was carried out as described above, specifically using TSe-G6-$(OH)_{64}$ (1.86 g, 0.248 mmol), benzylidene anhydride (10.55 g, 24.74 mmol, 100 equiv.) and DMAP (0.50 g, 4.10 mmol) all dissolved in 40 mL of CH_2Cl_2 and 20 mL of pyridine and stirred for 36 h at room temperature. Yield: 5.01 g,

white foam (98%). ^{1}H NMR (600 MHz, $CDCl_3$): δ = 0.85 (s, 192H), 0.95 (s, 48H), 1.15 – 1.30 (bm, 141H), 2.30 (bs, ~3H), 3.50 (bs, 128H), 4.06 – 4.34 (bm, 254H), 4.52 (bs, 128H), 5.33 (s, 64H), 7.28 (bs, 192H), 7.39 (bs, 130H), 7.68 (bs, ~2H). ^{13}C NMR (150 MHz, $CDCl_3$): δ = 16.04, 16.53, 16.85, 17.15, 17.23, 42.00, 45.95, 46.30, 64.42, 72.85, 101.03, 125.78, 127.62, 128.34, 137.59, 171.00, 171.39, 172.69. Calc.: $[M + Na]^+$ ($C_{1092}H_{1284}Na_1O_{384}S_1$) m/z = 20595.0565. Found MALDI-TOF MS: $[M + Na]^+$ m/z = 20605.44.

TSe-G7-(OH)$_{128}$ (4.26). Deprotection of TSe-G7-$(O_2Bn)_{64}$ (2.96 g, 0.144 mmol) in 100 mL of CH_2Cl_2 and MeOH (1 : 1) was carried out as above for 36 h at room temperature under H_2 atmosphere. Yield: 2.05 g, white foam (95%). ^{1}H NMR (600 MHz, CD_3OD): δ = 1.18 (s, 192H), 1.35 – 1.41 (bm, 189H), 2.52 (s, ~3H), 3.63 – 3.72 (m, 262H), 4.28 – 4.38 (m, 250H), 7.58 (bs, 2H), 7.92 (bs, 2H). ^{13}C NMR (150 MHz, CD_3OD): δ = 15.69, 16.58, 16.74, 46.05, 46.17, 49.91, 64.06, 64.27, 64.98, 171.50, 172.01, 174.11. Calc.: $[M + Na]^+$ ($C_{644}H_{1028}Na_1O_{384}S_1$) m/z = 14961.0533. Found MALDI-TOF MS: $[M + Na]^+$ m/z = 14969.61.

COOH-G7-$(O_2Bn)_{64}$ (4.27). The removal of the TSe protecting group was carried out as described above, specifically using TSe-G7-$(O_2Bn)_{64}$ (1.01 g, 49.1 μmol), and DBU (0.102 g, 100 μL, 0.670 mmol, 13.6 equiv.) dissolved in 5 mL of CH_2Cl_2 and stirred for 16 hours. Yield: 0.981 g, white foam (98%). ^{1}H NMR (600 MHz, $CDCl_3$): δ = 0.85 (s, 192H), 0.93 (s, 48H), 1.15 – 1.25 (bm, 141H), 3.51 (bs, 128H), 4.05 – 4.28 (bm, 122H),

4.29 – 4.34 (bs, 130H), 4.51 (bs, 128H), 5.33 (s, 64H), 7.27 – 7.30 (bm, 192H), 7.38 – 7.41 (bm, 128H). ^{13}C NMR (150 MHz, $CDCl_3$): δ = 16.53, 16.84, 17.06, 17.14, 17.23, 17.58, 42.01, 45.96, 46.13, 46.30, 64.43, 72.85, 101.04, 125.78, 127.62, 128.34, 137.58, 171.00, 171.39, 172.71 Calc.: $[M + Na]^+$ ($C_{1083}H_{1274}Na_1O_{382}$) m/z = 20413.0163. Found MALDI-TOF MS: $[M + Na]^+$ m/z = 20423.01.

COOH-G7-(OH)$_{128}$ (4.28). Deprotection of COOH-G7-(O_2Bn)$_{128}$ (0.925 g, 45.4 μmol) in 40 mL of CH_2Cl_2 and MeOH (1 : 1) was carried out as above for 16 h at room temperature under H_2 atmosphere. Yield: 0.662 g, white foam (99%). ^1H NMR (600 MHz, CD_3OD): δ = 1.19 (s, 192H), 1.35 – 1.40 (bm, 189H), 3.63 – 3.72 (bm, 258H), 4.29 – 7.39 (m, 250H). ^{13}C NMR (150 MHz, CD_3OD): δ = 15.70, 16.18, 16.58, 16.74, 46.06, 46.18, 49.91, 64.02, 64.28, 65.01, 171.50, 172.01, 174.12. Calc.: $[M]^+$ ($C_{635}H_{1018}O_{382}$) m/z = 14756.0234. Found MALDI-TOF MS: $[M]^+$ m/z = 14760.90.

BisPy-G7-(OH)$_{128}$ (4.29). The amide coupling was carried out as describe above, specifically COOH-G7-(OH)$_{128}$ (0.100 g, 6.78 μmol), ligand **4.13** (20.2 mg, 67.8 μmol, 10 equiv.), HBTU (25.7 mg, 67.8 μmol, 10 equiv.), HOBT (9.2 mg, 67.8 μmol, 10 equiv.), and DIPEA (50 μL, 0.287 mmol, 42 equiv.) were weighed into a 5 mL scintillation vial and dissolved in 0.5 mL of DMF. After stirring for 12 hours the entire reaction mixture was immediately injected on a recycling preparative GPC using methanol as the eluent. Yield: 73.0 mg, white foam (72%). ^1H NMR (600 MHz, CD_3OD): δ = 1.19 (s, 192H), 1.34 – 1.44 (bm, 189H), 3.63 – 3.72 (m, 258H), 4.28 – 4.38

(m, 250H), 7.29 – 7.39 (bm, ~2H), 7.58 – 7.70 (bm, ~2H), 7.78 – 7.89 (bm, ~2H), 8.45 – 8.55 (bm, ~2H). ^{13}C NMR (150 MHz, CD_3OD): δ = 15.69, 16.58, 16.73, 46.05, 46.17, 49.91, 64.06, 64.26, 64.96, 171.38, 171.49, 172.01, 174.11. Calc.: $[M + Na]^+$ ($C_{653}H_{1042}N_4Na_1O_{381}$) m/z = 15059.2183. Found MALDI-TOF MS: $[M + Na]^+$ m/z = 15064.45. HPLC: RT = 14.27 minutes.

TSe-G8-$(O_2Bn)_{128}$ (4.30). The generation growth was carried out as described above, specifically using TSe-G7-$(OH)_{128}$ (1.90 g, 0.127 mmol), benzylidene anhydride (10.83 g, 25.40 mmol, 200 equiv.) and DMAP (0.50 g, 4.10 mmol) all dissolved in 40 mL of CH_2Cl_2 and 20 mL of pyridine and stirred for 72 hours at room temperature. Yield: 4.95 g, white foam (95%). %). ^{1}H NMR (600 MHz, $CDCl_3$): δ = 0.80 (s, 384H), 1.08 (s, 96H), 1.17 (bs, 285H), 2.30 (s, ~3H, v. small), 3.44 (bs, 256H), 4.04 – 4.30 (bm, 508H), 4.46 (bs, 256H), 5.33 (s, 128H), 7.26 (bs, 384H), 7.36 (bs, 258H). ^{13}C NMR (150 MHz, $CDCl_3$): δ = 16.86, 17.11, 17.22, 41.95, 45.89, 46.24, 64.34, 72.75, 100.93, 125.82, 127.60, 128.30, 137.68, 171.05, 171.40, 172.67. Calc.: $[M]^+$ ($C_{2180}H_{2564}O_{768}S_1$) m/z = 41060.1301. Found MALDI-TOF MS: $[M]^+$ m/z = 41043.82.

TSe-G8-$(OH)_{256}$ (4.31). Deprotection of TSe-G8-$(O_2Bn)_{128}$ (2.45 g, 59.67 μmol) in 100 mL of CH_2Cl_2 and MeOH (1 : 1) was carried out as above for 36 h at room temperature under H_2 atmosphere. Yield: 1.70 g, white foam (96%). ^{1}H NMR (600 MHz, CD_3OD): δ = 1.19 (s, 384H), 1.33 – 1.40 (bm, 381H), 2.52 (s, ~3H, v. small), 3.63 – 3.72 (m, 538H), 4.29 – 4.40 (m, 486H), 7.58 (bs, 2H, v. small), 7.89 (bs, 2H, v. small). ^{13}C NMR (150

MHz, CD_3OD): δ = 15.80, 16.72, 16.88, 46.04, 49.91, 64.09, 64.27, 64.98, 171.56, 172.05, 174.14. Calc.: $[M + Na]^+$ ($C_{1284}H_{2052}Na_1O_{768}S_1$) m/z = 29815.1135. Found MALDI-TOF MS: $[M + Na]^+$ m/z = 29883.51.

COOH-G8-$(O_2Bn)_{128}$ (4.32). The removal of the TSe protecting group was carried out as described above, specifically using TSe-G8-$(O_2Bn)_{128}$ (0.783 g, 19.1 μmol), and DBU (0.102 g, 100 μL, 0.670 mmol, 35.1 equiv.) dissolved in 5 mL of CH_2Cl_2 and stirred for 16 hours. Yield: 0.742 g, white foam (95%). ^1H NMR (600 MHz, $CDCl_3$): δ = 0.80 (s, 384H), 0.92 (s, 96H), 1.30 -1.40 (bm, 285H), 3.44 – 3.51 (m, 256H), 4.04 - 4.34 (bm, 508H), 4.46 (bs, 256H), 5.33 (s, 128H), 7.27 (bs, 384H), 7.38 (bs, 256H). ^{13}C NMR (150 MHz, $CDCl_3$): δ = 16.85, 17.11, 17.22, 41.95, 45.89, 46.23, 64.37, 72.75, 100.94, 125.82, 127.61, 128.32, 137.67, 171.06, 171.40, 172.69. Calc.: $[M]^+$ ($C_{2171}H_{2554}O_{766}$) m/z = 40878.0899. Found MALDI-TOF MS: $[M + Na]^+$ m/z = 40964.32.

COOH-G8-$(OH)_{256}$ (4.33). Deprotection of COOH-G8-$(O_2Bn)_{128}$ (0.650 g, 15.9 μmol) in 100 mL of CH_2Cl_2 and MeOH (1 : 1) was carried out as above for 36 h at room temperature under H_2 atmosphere. Yield: 0.452 g, white foam (96%). ^1H NMR (600 MHz, CD_3OD): δ = 1.19 (s, 384H), 1.30 – 1.40 (bm, 380H), 3.64 – 3.72 (bm, 518H), 4.30 – 4.40 (bm, 502H). ^{13}C NMR (150 MHz, CD_3OD): δ = 15.80, 16.72g, 16.77, 16.88, 46.04, 46.16, 49.92, 64.10, 64.25, 64.91, 171.57, 172.07, 174.15. Calc.: $[M]^+$ ($C_{1275}H_{2042}O_{766}$) m/z = 29610.0835. Found MALDI-TOF MS: $[M]^+$ m/z = 29617.60.

4.5. References

(1) Haag, R.; Kratz, F. *Angewandte Chemie-International Edition* **2006**, *45*, 1198-1215.
(2) Duncan, R. *Nature Reviews Drug Discovery* **2003**, *2*, 347-360.
(3) Duncan, R. *Nature Reviews Cancer* **2006**, *6*, 688-701.
(4) Twaites, B.; Alarcon, C. D.; Alexander, C. *Journal of Materials Chemistry* **2005**, *15*, 441-455.
(5) Duncan, R. *Anti-Cancer Drugs* **1992**, *3*, 175-210.
(6) Maeda, H.; Seymour, L. W.; Miyamoto, Y. *Bioconjugate Chemistry* **1992**, *3*, 351-362.
(7) Gillies, E. R.; Frechet, J. M. J. *Journal of the American Chemical Society* **2002**, *124*, 14137-14146.
(8) Matsumura, Y.; Maeda, H. *Cancer Research* **1986**, *46*, 6387-6392.
(9) Maeda, H.; Wu, J.; Sawa, T.; Matsumura, Y.; Hori, K. *Journal of Controlled Release* **2000**, *65*, 271-284.
(10) Seymour, L. W. *Critical Reviews in Therapeutic Drug Carrier Systems* **1992**, *9*, 135-187.
(11) Frechet, J. M. J. *Science* **1994**, *263*, 1710-1715.
(12) Esfand, R.; Tomalia, D. A. *Drug Discovery Today* **2001**, *6*, 427-436.
(13) Tomalia, D. A.; Naylor, A. M.; Goddard, W. A. *Angewandte Chemie-International Edition* **1990**, *29*, 138-175.
(14) Frechet, J. M. J.; Tomalia, D. A. *Dendrimers and Other Dendritic Polymers*; John Wiley & Sons, Ltd.: West Sussex, 2001.
(15) Newkome, G. R.; Moorefield, C. N.; Vogtle, F. *Dendritic Macromolecules: Concepts, Synthesis, Perspectives*; VCH: Weinheim, Germany, 1996.
(16) Ihre, H. R.; Padilla De Jesus, O. L.; Szoka, F. C. J.; Frechet, J. M. J. *Bioconjugate Chemistry* **2002**, *13*, 443-452.
(17) Ihre, H.; Hult, A.; Soderlind, E. *Journal of the American Chemical Society* **1996**, *118*, 6388-6395.
(18) Ihre, H.; Hult, A.; Frechet, J. M. J.; Gitsov, I. *Macromolecules* **1998**, *31*, 4061-4068.
(19) Ihre, H.; Padilla De Jesus, O. L.; Fréchet, J. M. J. *JACS* **2001**, *123*, 5908-5917.
(20) De Jesus, O. L. P.; Ihre, H. R.; Gagne, L.; Frechet, J. M. J.; Szoka, F. C. *Bioconjugate Chemistry* **2002**, *13*, 453-461.
(21) Banerjee, S. R.; Wei, L. H.; Levadala, M. K.; Lazarova, N.; Golub, V. O.; O'Connor, C. J.; Stephenson, K. A.; Valliant, J. F.; Babich, J. W.; Zubieta, J. *Inorganic Chemistry* **2002**, *41*, 5795-5802.
(22) Stephenson, K. A.; Zubieta, J.; Banerjee, S. R.; Levadala, M. K.; Taggart, L.; Ryan, L.; McFarlane, N.; Boreham, D. R.; Maresca, K. P.; Babich, J. W.; Valliant, J. F. *Bioconjugate Chemistry* **2004**, *15*, 128-136.
(23) James, S.; Maresca, K. P.; Allis, D. G.; Valliant, J. F.; Eckelman, W.; Babich, J. W.; Zubieta, J. *Bioconjugate Chemistry* **2006**, *17*, 579-589.

(24) Liley, M. J.; Johnson, T.; Gibson, S. E. *Journal of Organic Chemistry* **2006**, *71*, 1322-1329.
(25) Abram, U.; Alberto, R. *J Brazil Chem Soc* **2006**, *17*, 1486-1500.

Chapter 5. *In Vivo* Evaluation of Tecnetium-99m Labeled Aliphatic Polyester Dendrimers.

Abstract

A series of aliphatic polyester dendrons were previously prepared with a core bis-pyridyl ligand known to strongly chelate to various isotopes of Tc and Re. Metalation with radioactive technetium-99m (^{99m}Tc) was accomplished at the core of each dendrimer from generation 5 through 7. This resulted in precise, site-specific radiolabeling of each dendrimer. The radiolabeled dendrimers were used as radioactive tracers, tracked *in vivo* by single photon emission computed tomography (SPECT). This series of radiolabeled dendrimers was injected into healthy rats, and their biodistribution was recorded in real time using SPECT. It was found that these structures were cleanly and rapidly eliminated from the bloodstream via the kidneys. No uptake in any organs or tissues was observed. This data was corroborated by a quantitative biodistribution study involving *ex-vivo* harvesting of individual organs and tissues. The quantitative biodistribution results were in excellent agreement with the data obtained from SPECT. This chapter has been reproduced in part with permission from *Journal of the American Chemical Society* **2008**, ja-2008-078175. Copyright 2006 American Chemical Society.

5.1. Introduction

Since the pioneering work of Ringsdorf[1, 2] and Kopecek,[3, 4] the field of macromolecular therapeutics has received continually increasing attention.[5-8, 9] The advantages of conjugating small-molecule drugs to water soluble, non-toxic, biocompatible polymers have been repeatedly documented,[9-11] and include improved drug solubility, longer blood circulation time, decreased toxicity to healthy cells and tissues, and the possibility to deliver drug payloads specifically to disease sites via both passive[12-14] and active targeting methods.[15, 16] Within this area, the dendritic polymer architecture holds significant potential due to a number of decisive advantages. The controlled, step-wise synthetic protocols used in dendrimer synthesis enable the formation of precisely-defined structures that can be modified at their core, interior branch points, and periphery, allowing the introduction of therapeutic agents, targeting moieties, and solubilizing functionalities as necessary. Additionally, the monodisperse nature of dendritic polymers enables facile characterization and eliminates reproducibility issues that may arise when using traditional, polydisperse macromolecular therapeutics that contain polymer fractions with greatly differing molecular weights.[17]

Amongst the wide array of dendrimer structures that have been reported over the past four decades, several have been heavily investigated for biological/therapeutic applications.[17] The commercially available polyamidoamine (PAMAM) and polypropyleneimine (PPI) dendrimers have been most widely studied, especially in gene delivery, as MRI contrast agents, and as covalent drug conjugates.[18] The more biocompatible peptide-based dendrimers have also been demonstrated to exhibit

promising characteristics as components of vaccines, as well as antiviral and antibacterial agents.[19] In addition, polyester dendrimers have been applied to tissue engineering and surgical closure materials, where they have been used as degradable photocrosslinkers for repairing corneal wounds.[20] More recently, aliphatic polyester dendrimers based on the 2,2-bis(hydroxymethyl)-propanoic acid (bis-MPA) building block have been studied as potential drug-delivery agents.[21, 22] These poly(2,2-bis(hydroxymethyl)-propanoic acid) (PMPA) dendrimer structures, initially reported by Ihre and Hult,[23, 24] exhibit excellent aqueous solubility, low in-vivo toxicity, biocompatibility, and biodegradability, while being relatively easy to fabricate via convergent[24] or divergent methods.[25] Thus, these structures have been modified to incorporate various therapeutic agents within their interior,[26] and on their periphery.[17, 21, 27, 28] Furthermore, peripheral functionalization of PMPA polyester dendrimers with high molecular weight poly(ethylene oxide) (PEO) chains has been found to result in long blood residence times for the dendrimer-PEO conjugates.[29] Recently, Fréchet and co-workers have demonstrated that "bow-tie" PMPA dendrimer conjugates with doxorubicin (DOX) exhibit high tumor uptake and greatly diminished cytotoxicity (relative to free DOX).[29, 30] These compounds were found to completely eradicate colon carcinoma in mice after a single intravenous injection.[31] The use of PMPA dendrimer structures in therapeutic applications is therefore becoming more prominent.

In these, and all other examples of macromolecular therapeutic agents, biodistribution studies that detail both pharmacokinetics and pharmacodynamics are critical in assessing the efficacy of the therapeutic agent. Typically, this is accomplished

using iodine-125 (^{125}I) to radioiodinate phenol-functionalized derivatives of the target therapeutic agent.[29, 32-34] However, introduction of the requisite radioiodinated phenols can result in enhanced liver uptake,[31] providing an inaccurate biodistribution picture of the target. Additionally, the biodistribution studies of ^{125}I-labeled compounds can only be accomplished using an *ex-vivo* radioactivity measurement within harvested organs, or the "cut and count" methodology, which is laborious and animal intensive. Conversely, radioimaging agents are routinely used in diagnostic medicine to locate, highlight, and follow sites of inflammation and disease, as well as to monitor organ function *in-vivo* and in real-time.[35] The high spatial and temporal resolution of radioimaging methodologies makes them extremely useful in diagnostic medicine.

Of all the known radionuclides, the γ-emitting ^{99m}Tc is the most commonly used isotope in diagnostic medicine due to its ideal half-life (6 h), a γ-energy (140 keV) that is sufficient to penetrate internal organs but low enough to prevent a high-dose burden to patients, and the commercial availability of ^{99}Mo/^{99m}Tc-generators at relatively low cost.[36] Specifically, these properties of ^{99m}Tc make it the preferred radionuclide in single photon emission computed tomography (SPECT), a radioimaging methodology that enables real-time, in-vivo determination of the path that a γ-emitting radionuclide traverses post injection into a human or animal subject. While a number of clinically useful chelators for ^{99m}Tc have been developed and applied to the imaging of tumors, organs, vasculature, and numerous other tissues,[36] this radionuclide's use in determining the pharmacokinetics and pharmacodynamics of macromolecular drug delivery agents has received very little attention. To the best of our knowledge, only two prior

publications involving the chelation of ^{99}Tc within dendrimers have been reported, but neither extends the dendrimer-^{99}Tc complexes to radioimaging.[37, 38] In addition, the multi-site, poorly controlled binding of the radionuclide within these reported dendrimers diminishes their clinical applicability and overall utility in diagnostic imaging.

In order to prepare a clinically relevant ^{99m}Tc-labeled dendrimer for SPECT imaging, it was hypothesized that a single, strongly-binding ligand for the radionuclide would have to be placed at the core of a high-generation dendrimer. This would ensure that radiolabeling occurs in a well-defined, site-specific manner, and at only a single point within the dendrimer framework. Furthermore, by introducing the radionuclide at the site-isolated core of the dendrimer, the overall size, shape, polarity, and mode of interaction of the dendrimer periphery with its external environment should not be appreciably affected. Therefore, the biodistribution of the radiolabeled dendrimer would exactly match that of an unlabeled analog.

Herein, we describe the labeling of these ligand-bearing dendrimers with ^{99m}Tc in high radiochemical yield, and preliminary *in-vivo* SPECT imaging results obtained with a series of high-generation radiolabeled dendrimers. This work represents early stages in the development of a dendrimer family that can house a therapeutic payload, be targeted to specific disease sites through peripheral modification, and can be monitored in real time upon injection into, perfusion through, and elimination from living patients.

5.2. Results and Discussion

5.2.1. Radiochemistry

The preparation of site-specifically radiolabeled dendrimers that could be followed by SPECT imaging involved the introduction of the ^{99m}Tc within the core-bound bis-pyridyl ligand. This was accomplished by first converting sodium pertechnetate ($Na^{99m}TcO_4$) "milked" from the $^{99}Mo/^{99m}Tc$-generator to the tris-aquo species $[^{99m}Tc(CO)_3(H_2O)_3]^+$, bearing easily labile H_2O ligands.[39-41] For this step, we employed a modified procedure based on the elegant work of Alberto and co-workers,[42] which involved dissolving boranyl carbonate ($K_2[BH_3{\bullet}CO_2]$), sodium carbonate (Na_2HCO_3), Na/K-tartrate, and Borax ($Na_2B_4O_7{\bullet}10H_2O$) in 1 mL of saline solution containing approximately 925 MBq (25 mCi) of sodium pertechnetate ($Na^{99m}TcO_4$). The solution was heated by microwave irradiation at 130°C for 3 minutes,[43] quantitatively converting the $Na^{99m}TcO_4$ to $[^{99m}Tc(CO)_3(H_2O)_3]^+$. The reaction was cooled and acidified with aqueous HCl to a pH between 4 and 6. An aqueous solution containing 1 mg of the BisPy-G5-$(OH)_{32}$ dendron was added to the reaction vial and the mixture was again heated by microwave irradiation at 130°C for an additional 5 minutes to give $[^{99m}$TcBisPy-G5-$(OH)_{32}]^+$ (Scheme 5.1). This entire procedure was completed within 10 minutes. *Caution*: extreme care must be used when working with radioactive materials, and all work must be performed in designated facilities that are licensed for radiochemistry.

Scheme 5.1. Radiolabeling of the BisPy-G5-$(OH)_{32}$ dendron to form [^{99m}TcBisPy-G5-$(OH)_{32}$]$^{+}$.

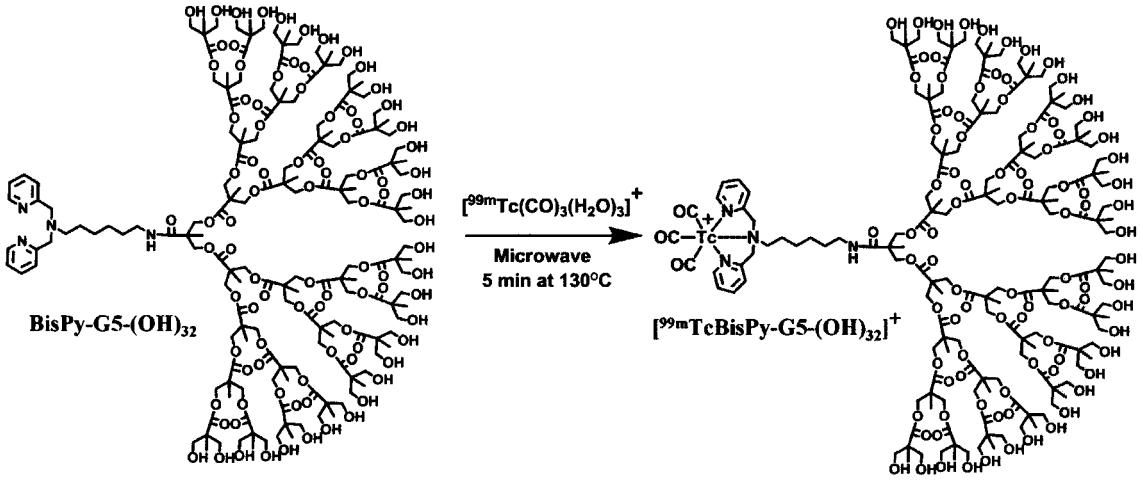

Using this protocol, incorporation of ^{99m}Tc within the BisPy-G5-$(OH)_{32}$ dendron to form [^{99m}TcBisPy-G5-$(OH)_{32}$]$^{+}$ was accomplished in 89 ± 0.6 % radiochemical yield (RCY) over three labeling experiments. The remaining 10% of radioactive material was comprised of unbound [^{99m}Tc$(CO)_3(H_2O)_3$]$^{+}$ and other ^{99m}Tc salts loosely bound by the numerous oxygen lone pairs throughout the dendron. Given that it was imperative to isolate each dendron to greater than 99% radiochemical purity in order to produce a viable imaging agent, it was necessary to remove all of the weakly bound ^{99m}Tc salts. This was accomplished by adding a large excess of histidine (200 μL of a 10.0 mM solution), which serves as a ligand that produces soluble, low molecular weight complexes with the weakly-bound ^{99m}Tc species. The resulting mixture was heated by microwave irradiation to 150°C for 5 min and then passed through three size-exclusion

chromatography (SEC) HiTrap desalting cartridges (GE Healthcare), connected in series, to achieve complete separation of the high-generation dendrimers from the low molecular weight histidine-^{99m}Tc complexes. This procedure enabled the complete removal of all weakly bound ^{99m}Tc species within the sample, and allowed isolation of the dendrimers in high radiochemical purity.

High performance liquid chromatography equipped with a gamma-detector was used to monitor the conversion of BisPy-G5-$(OH)_{32}$ to $[^{99m}$TcBisPy-G5-$(OH)_{32}]^+$. The HPLC chromatograms in Figure 5.1 show that BisPy-G5-$(OH)_{32}$ had a retention time (RT) of 14.66 min, the rhenium standard $[$ReBisPy-G5-$(OH)_{32}]^+$ had a retention time of 16.19 min, and the technetium-labeled dendrimer $[^{99m}$TcBisPy-G5-$(OH)_{32}]^+$ eluted at 16.49 min. Both BisPy-G5-$(OH)_{32}$ and $[$ReBisPy-G5-$(OH)_{32}]^+$ were monitored using a UV-Vis detector, while the $[^{99m}$TcBisPy-G5-$(OH)_{32}]^+$ was monitored by a gamma detector. The difference of 0.30 min between the rhenium standard, $[$ReBisPy-G5-$(OH)_{32}]^+$, and the radioactive dendrimer, $[^{99m}$TcBisPy-G5-$(OH)_{32}]^+$, corresponds to the travel time between the UV-Vis detector and the gamma detector within the HPLC instrument. From this data, it is clear that introduction of the radionuclide within the core bis-pyridyl ligand of the G5 dendrimer significantly affects its interaction with the stationary phase, resulting in a large retention time difference. However, the close match between the Re standard and the radiolabeled dendrimer, along with the absence of any other γ-emitting species, confirms that the radiolabeling chemistry is efficient and highly specific to the core ligand.

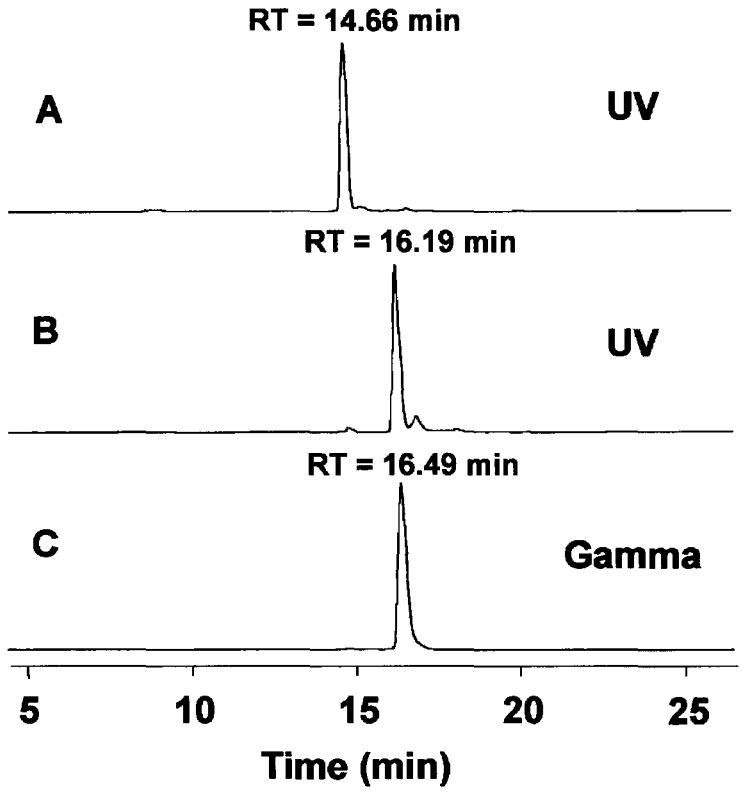

Figure 5.1. HPLC Chromatograms of BisPy-G5-$(OH)_{32}$ (A), $[ReBisPy\text{-}G5\text{-}(OH)_{32}]^+$ (B), and $[^{99m}TcBisPy\text{-}G5\text{-}(OH)_{32}]^+$ (C).

The radiolabeling conditions developed for G5 were then used to produce $[^{99m}TcBisPy\text{-}G6\text{-}(OH)_{64}]^+$ and $[^{99m}TcBisPy\text{-}G7\text{-}(OH)_{128}]^+$ in 70 ± 1 % and 53 ± 2 % radiochemical yields, respectively. The exact structures of these two compounds are given in Figure 5.2. The decrease in radiochemical yield indicates that accessibility to the bis-pyridyl ligand within the dendron becomes hindered with increasing generation. The HPLC chromatograms for the G6 dendrimer series show similar trends to the G5 series (Figure 5.3). Again, the unmetalated ligand-bearing dendrimer had the shortest retention time, while the rhenium standard was detected 0.3 minutes before the ^{99m}Tc-

labeled dendrons. It should be noted, however, that the retention times of the two metalated G6 compounds are more than one minute shorter than the corresponding G5 dendrimers. This indicates that the effect of core metalation on retention time decreases with increasing generation, as would be expected from the enhanced site-isolation of the ligand located at the core. This trend continued in the seventh generation (Figure 5.4), where the retention time of the ^{99m}Tc-labeled dendrimer decreased by almost another minute. Here the retention time difference between the unmetalated and metalated dendrimers corresponded only to the difference in travel time between the UV-Vis and gamma detectors, indicating that the actual elution times for the two compounds were identical. Therefore, at G7, the need for a Re standard to identify the radiolabeled compound was eliminated. Figure 5.5 shows a plot of retention time as a function of dendrimer generation for the unmetalated and radiolabeled dendrimers (before and after correction for the difference in travel time between the two detectors), clearly demonstrating the convergence of retention times at the seventh generation. Again, these differences in retention time indicate that the metalated ligand becomes completely encapsulated within the dendrimer core only at the seventh generation, while at lower generations metalation of the core has an impact on the dendrimer's interactions with its surrounding environment.

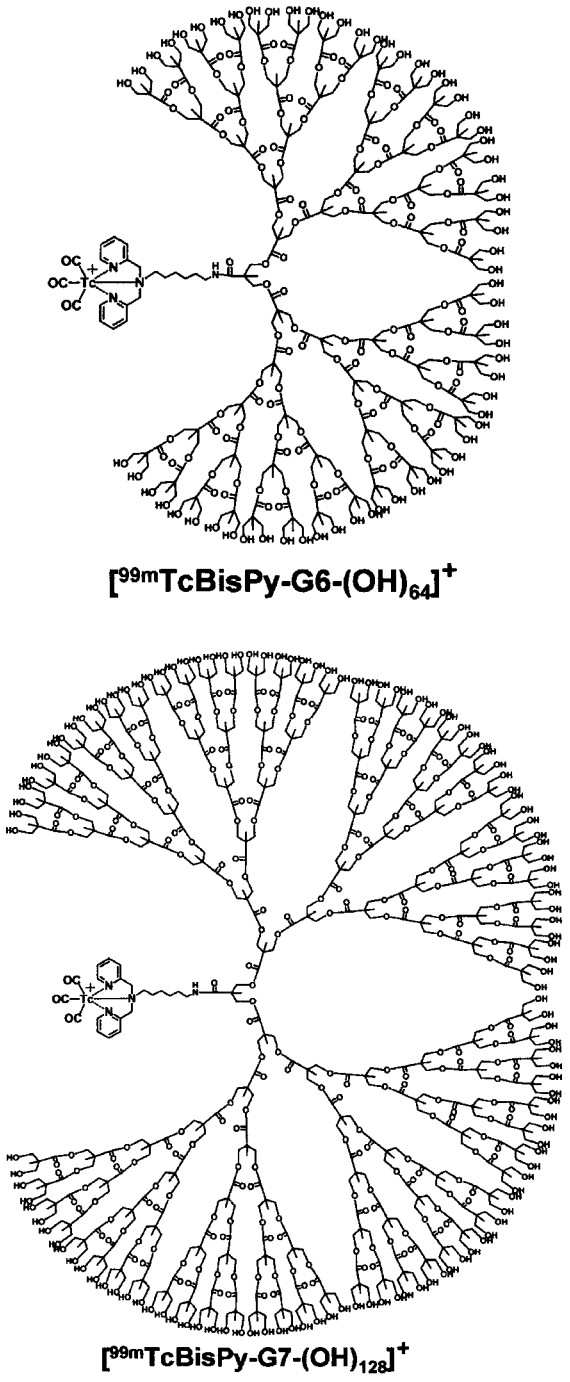

Figure 5.2. Exact structures of the two highest generation ^{99m}Tc-labeled dendrimers, $[^{99m}$TcBisPy-G6-$(OH)_{64}]^+$, and $[^{99m}$TcBisPy-G7-$(OH)_{128}]^+$.

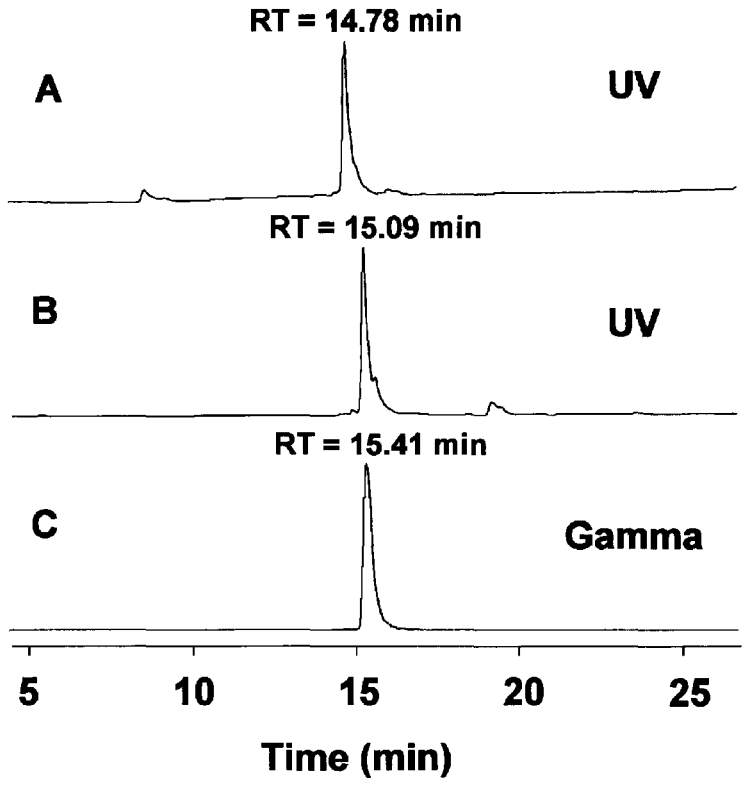

Figure 5.3. HPLC Chromatograms of BisPy-G6-$(OH)_{64}$ (A), $[ReBisPy\text{-}G6\text{-}(OH)_{64}]^+$ (B), and $[^{99m}TcBisPy\text{-}G6\text{-}(OH)_{64}]^+$ (C).

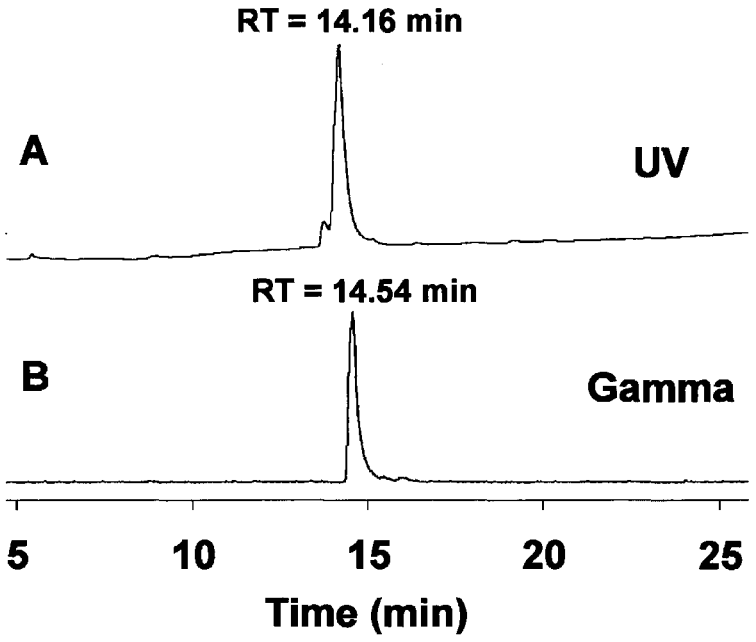

Figure 5.4. HPLC Chromatograms of BisPy-G7-$(OH)_{128}$ (A), and $[^{99m}$TcBisPy-G7-$(OH)_{128}]^+$ (B).

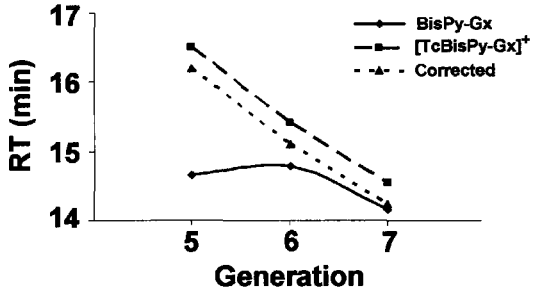

Figure 5.5. HPLC retention times (RT) plotted as a function of dendrimer generation for G5, G6, and G7 dendrons before (solid line) and after (dashed line) introduction of the radionuclide ^{99m}Tc. The dotted line represents data that has been corrected for the time required to traverse the distance between the UV-Vis detector and the gamma detector within the HPLC instrument.

5.2.2. Single Photon Emission Computed Tomography (SPECT) Imaging.

SPECT imaging was accomplished using a Gamma Medica Ideas X-SPECT preclinical small animal imaging system. An aliquot of each of the radiolabeled dendrimers, dissolved in 1 mL of saline solution, was injected into the tail vein of anesthetized adult male Copenhagen rats having an average weight of 275 g. The injected radiation dose amounted to approximately 37 MBq, or 1 mCi, per experiment. The location of these dendrimers as they traversed through the circulation and into various organs/tissues of the animals was determined using a dual-head detector system equipped with high-resolution parallel beam collimators, having a reconstruction field of view of 125 x 125 x 125 mm, with 3-4 mm spatial resolution. Individual images were collected every 10 s for the first 15 min (900 s) of the dynamic scan, followed by one image every 60 s for the next 45 min post injection. The acquired images could either be analyzed individually or assembled into a movie showing the progression of radioactivity as a function of time.

Figure 5.6. shows the individual SPECT images, at 30 s intervals, from the first 15 min post injection of $[^{99m}$TcBisPy-G7-$(OH)_{128}]^+$. From these images, the dendritic radiotracer can be seen rapidly moving through the tail vein and immediately into the heart and lungs within the first few seconds of the experiment. Between 30 and 60 s post injection, radiation was observed in the kidneys and indicated that the dendrimer was beginning to filter out of the blood. This was almost immediately followed by detection of radioactivity in the bladder (between 120 and 150 s), which served as the final repository of the dendrimer. Very little signal was observed localizing in any other

organs or tissues throughout the experiment, with only a low level of highly dispersed radiation across the entire body being detectable. As can be seen from Figure 5.6, the dendrimer is almost completely removed from the blood within 10 min post injection, and the kidneys transfer it to the bladder almost quantitatively after 15 min.

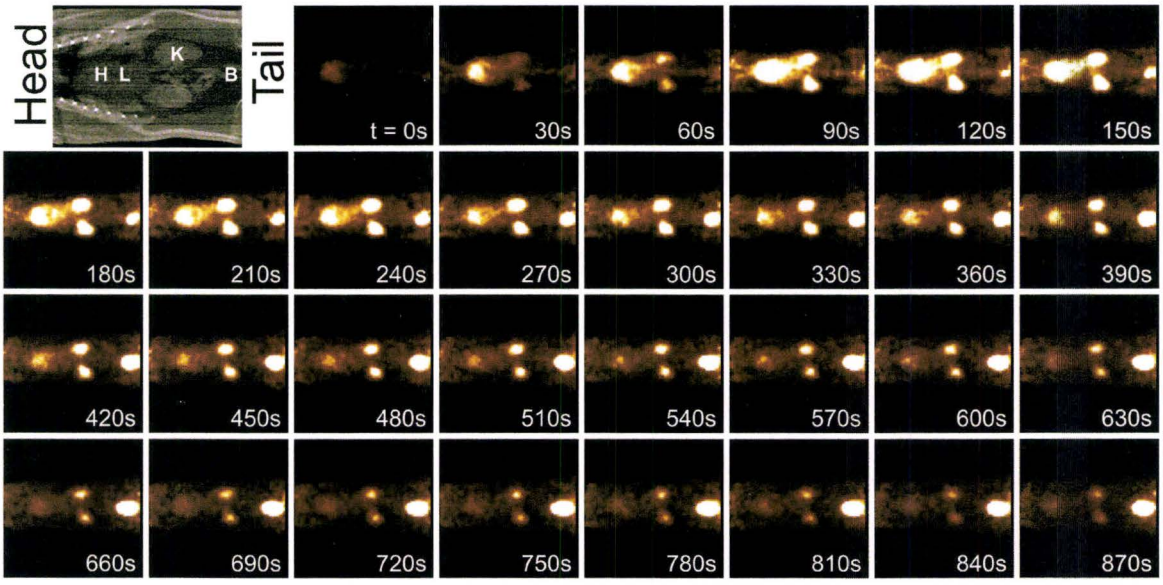

Figure 5.6. Dynamic SPECT images of $[^{99m}$TcBisPy-G7-$(OH)_{128}]^+$ taken from time 0 to 15 minutes with an image every 30 seconds.

Scintigraphic imaging coupled with X-ray imaging provides two-dimensional "snapshots" that track the motion of the dendritic radiotracer across different areas of the animal's body. However, this top-down projection makes it difficult to definitively determine which organs the radiotracer is located in, as different organs may overlap (i.e., one on top of another). To determine accurate anatomical localization of the dendritic radiotracers, precisely coregistered volumetric X-ray computed tomography (CT) data

was obtained using the same small-animal scanner used for the dynamic scan (above). Reconstructed SPECT and CT images were then coregistered and interpolated, covering the same field of view, so that images could be fused. Four of these 3-D images, showing the animal's skeleton and locations of highest radioactivity over the course of the first 15 min of the experiment, are depicted in Figure 5.7. It is clear from these images that the radioactivity is mainly centered in the kidneys and bladder, with no involvement of any organs that may spatially coincide in the top-down projection (i.e., the liver). These images are therefore consistent with our interpretation of the dynamic SPECT data, where the majority of the radioactivity emanated from the vicinity of the kidneys and the bladder.

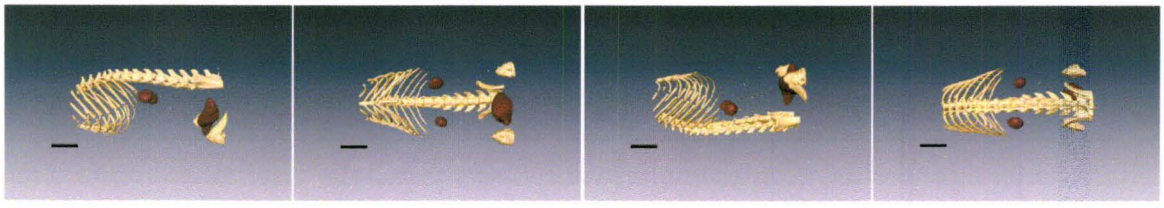

Figure 5.7. Fused SPECT and CT images of $[^{99m}$TcBisPy-G7-$(OH)_{128}]^+$ taken over 15 min. Scale bar corresponds to 1 cm.

Dynamic SPECT images were also collected for the fifth and sixth generation dendrimers, $[^{99m}$TcBisPy-G5-$(OH)_{32}]^+$ and $[^{99m}$TcBisPy-G6-$(OH)_{64}]^+$, respectively. The individual SPECT images depicting the path of these molecules post injection into the tail vein are depicted in Figure 5.8 and Figure 5.9.

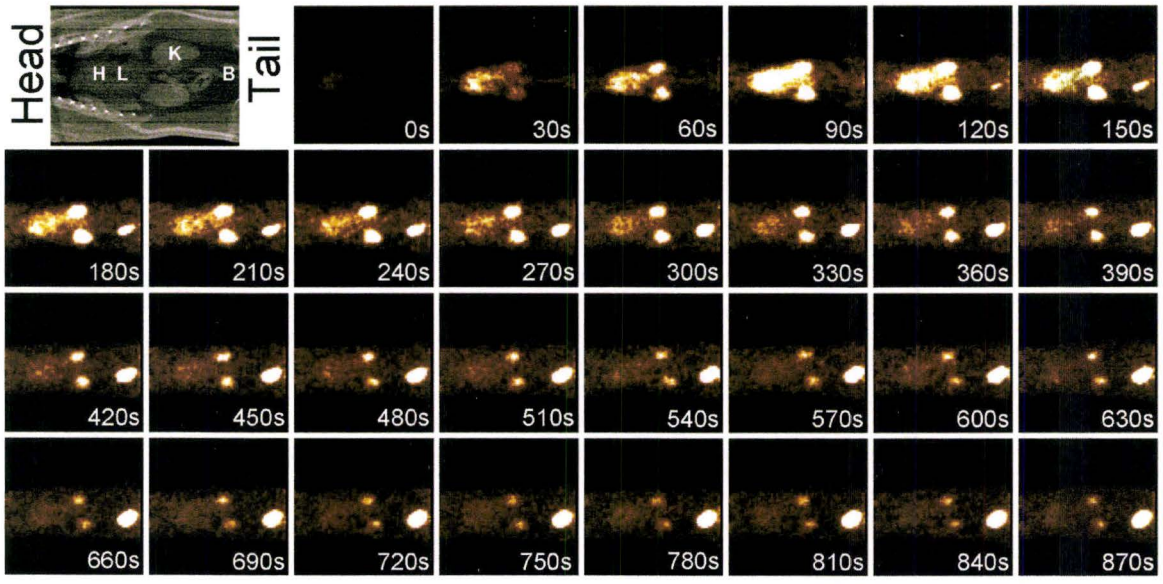

Figure 5.8. Dynamic SPECT images of $[^{99m}TcBisPy\text{-}G5\text{-}(OH)_{32}]^+$ taken from time 0 to 15 minutes with an image every 30 seconds.

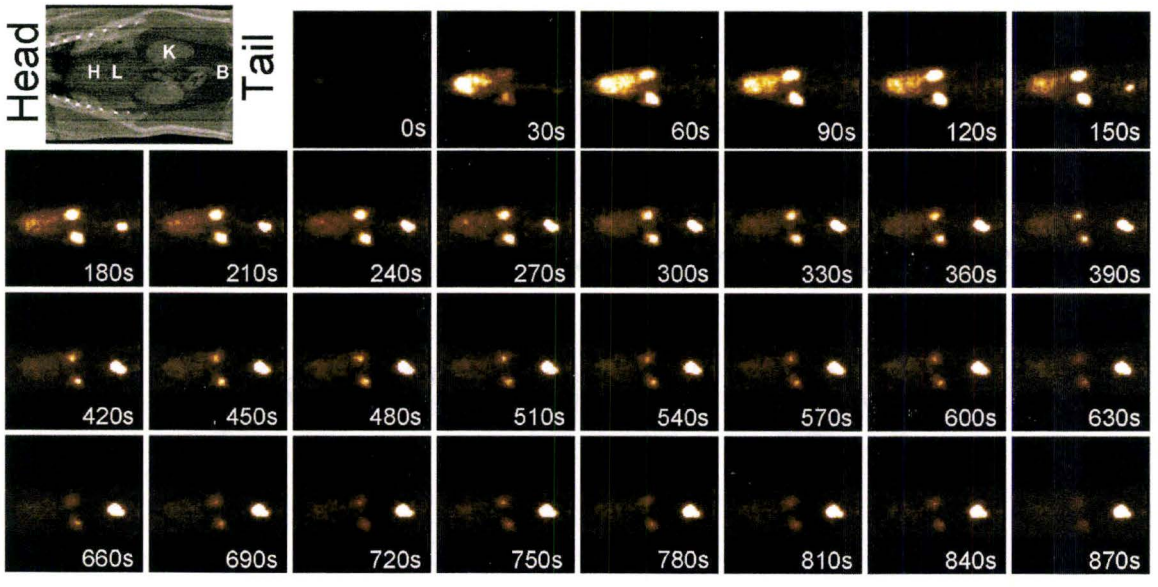

Figure 5.9. Dynamic SPECT images of $[^{99m}TcBisPy\text{-}G6\text{-}(OH)_{64}]^+$ taken from time 0 to 15 minutes with an image every 30 seconds.

Qualitatively, the data for G5 and G6 is very similar to what is described above for G7. More quantitative information was obtained by plotting the amount of radiation emanating from specific organs over the course of the experiment. Figure 5.10 depicts the relative amount of gamma radiation measured as a function of time from regions of interest (ROI) around the heart/lungs (these two organs are too small and close in proximity to be distinguished), kidneys, and bladder, for each dendrimer generation, normalized to the point of maximum intensity. The near exact coincidence of these curves indicates that the path taken by the three dendrimers, from the tail vein to the bladder, was practically identical. The observed rapid clearance of all the dendrimers is a result of the molecular weight of each dendrimer (4.1, 7.8, and 15.2 kDa for G5, G6, and G7, respectively) being well below the renal filtration cutoff of 40-60 kDa. Similarly, the measured hydrodynamic radii of these dendrimers, being well below 3 nm (Chapter 4), are smaller than the known radius of the renal pores (5 nm),[44] again consistent with the observed rapid clearance. By fitting the decay profiles, from the maximum intensity point onward, to monoexponential decay functions, it was possible to extract an organ clearance half-life ($t_{1/2}$) for the heart/lungs and the kidneys. As demonstrated in Figure 5.11, the clearance half-life of $[^{99m}$TcBisPy-G6-$(OH)_{64}]^+$ from the kidneys was 112 ± 2 s . A complete table of calculated values is provided in Table 5.1.

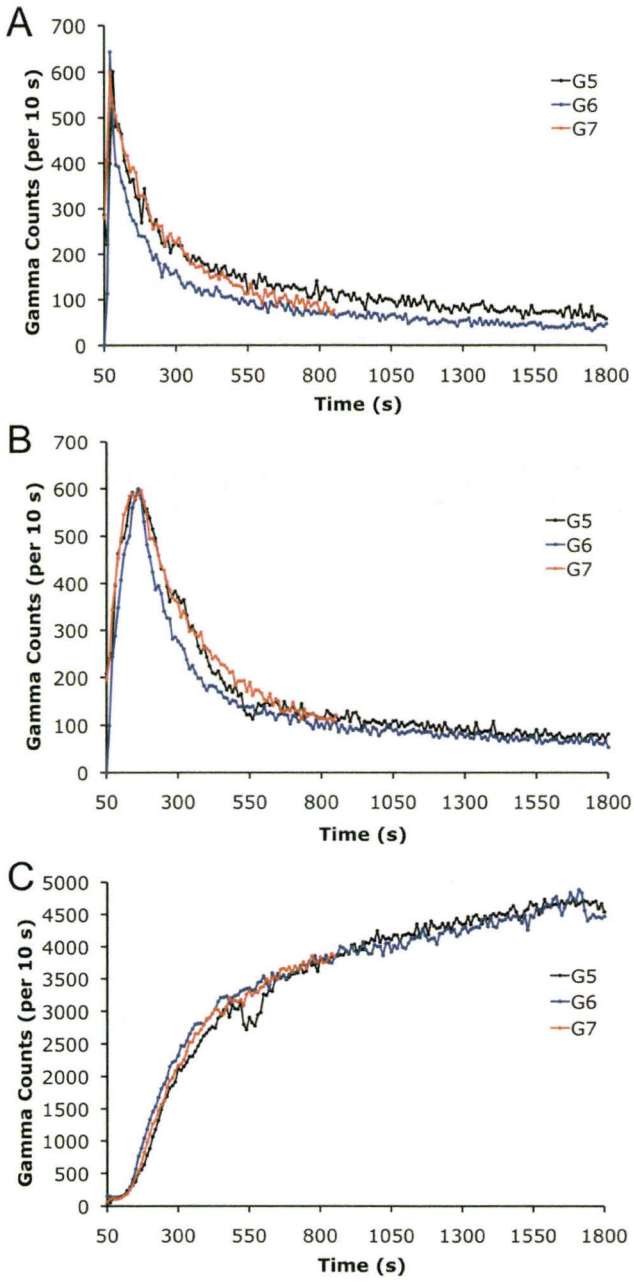

Figure 5.10. Time-activity plots for gamma radiation emanating from the heart/lungs (A), kidneys (B), and bladder (C) for $[^{99m}\text{TcBisPy-G5-(OH)}_{32}]^{+}$ (black curves), $[^{99m}\text{TcBisPy-G6-(OH)}_{64}]^{+}$ (blue curves), and $[^{99m}\text{TcBisPy-G7-(OH)}_{128}]^{+}$ (red curves). For the G7 dendrimer, data was only collected over the first 14 minutes post injection.

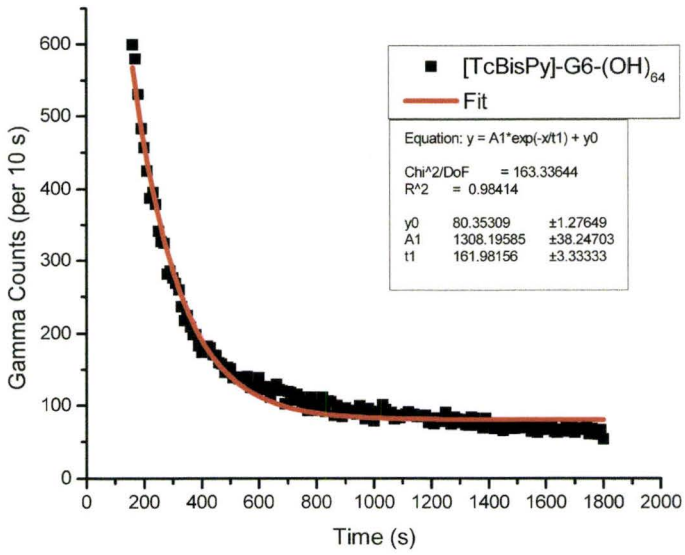

Figure 5.11. Monoexponential decay fitting for the determination of kidney clearance half-life of $[^{99m}$TcBisPy-G6-$(OH)_{64}]^+$.

Table 5.1. Clearance half-lives calculated from monoexponential decay fits of time-activity curves for G5 to G7 dendrimers.

Dendrimer Generation	Clearance Half-Life (s)	
	Heart/Lungs	Kidneys
5	147 ± 5	136 ± 3
6	102 ± 4	112 ± 2
7	126 ± 4	147 ± 4

5.2.3 Quantitative Biodistribution Studies.

To corroborate and confirm the accuracy of the *in vivo*, real-time data obtained by SPECT analysis, a detailed biodistribution study was also performed using the "cut and count" methodology with the radiolabeled G7 dendrimer, $[^{99m}$TcBisPy-G7-$(OH)_{128}]^+$. Using the same adult male Copenhagen rats, biodistribution data was collected by harvesting the organs and tissues of five animals at time points of 5, 15, 60, 120 and 360 min post injection of the radiolabeled dendrimer via the tail vein. The organs/tissues that

were harvested from each rat included blood (via heart puncture), heart, lungs, liver, adrenals, kidneys, muscle, stomach, small intestine, caecum, large intestine, testes, brain, bone, adipose tissue, spleen, trachea/thyroid, skin and eyes. The harvested tissues were weighed and the radioactivity within each organ/tissue was quantified using a multi-detector well counter. The complete data set is presented in tabular form in Figure 5.12 (A: percent dose injected per organ; B: percent dose injected per gram of organ). This data is in full agreement with the SPECT analysis, indicating that the dendrimer is rapidly cleared from the animals via the kidneys. Greater than 95 % of the injected dose is eliminated within the first 5 min, and nearly 99 % of the dendrimer is cleared within 15 min. Over the course of the first hour, a small amount of accumulation was found in the digestive tract, including the stomach and small intestine, but these organs showed complete clearance at the 360 min time point. After the full six hours of the experiment, only traces of radioactivity were found to remain in the animals.

Complete and rapid elimination of drug carriers upon delivery of the therapeutic payload is a critical aspect to their successful clinical implementation. Here, we have demonstrated that it is possible to prepare, characterize, and radiolabel a series of high-generation PMPA dendrimers. Furthermore, it is possible to track these macromolecular radiotracers *in-vivo* and in real-time using dynamic SPECT imaging, showing that these dendrimer structures are indeed rapidly cleared from the rat bloodstream. Although the short circulation time of the structures investigated here make them unsuitable for drug delivery applications in their present form, it has already been demonstrated that PEGylation of the PMPA dendrimer periphery dramatically increases blood circulation

time. Therefore, these studies serve as the basis for future investigation of analogous dendrimers that will be peripherally modified with agents to improve circulation time (i.e., PEG), as well as to target the dendrimers to specific sites of interest by decoration with a variety of small molecules, sugars, peptides, nucleic acids, and other biologically relevant molecules. Furthermore, the introduction of chemotherapeutic agents within the interior of these structures (carboranes, camptothecin, doxorubicin, etc.), as well as radiotherapeutic agents within the core bis-pyridyl ligand (^{186}Re, and ^{188}Re)[45, 46] will potentially enable their use in a wide spectrum of therapeutic methodologies.

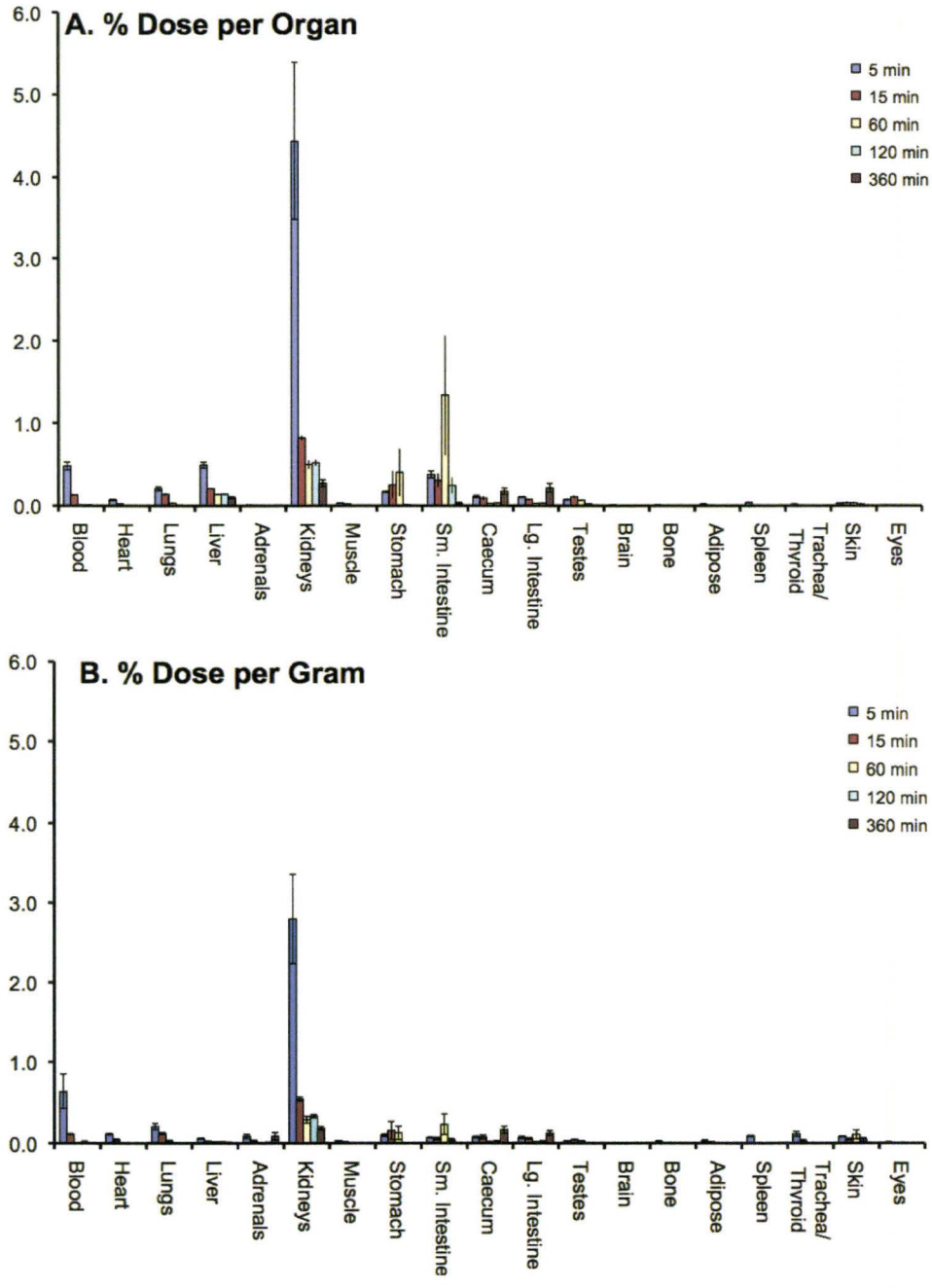

Figure 5.12. Biodistribution of $[^{99m}TcBisPy\text{-}G7\text{-}(OH)_{128}]^{+}$ in healthy adult male copenhagen rats showing percent dose per organ (A) and percent dose per gram of organ (B) at five time points post injection: 5, 15, 60, 120, and 360 min (5 mice per time point).

5.3. Conclusion

Using ^{99m}Tc, radiolabeling conditions were optimized for BisPy-G5-$(OH)_{32}$, BisPy-G6-$(OH)_{64}$, and BisPy-G7-$(OH)_{128}$. It was found that the radiochemical yield decreased with increasing generation, indicating that steric bulk around the core diminishes reactivity. However, the difference in HPLC retention times of the metalated and unmetalated species decreased with generation as a result of improved site isolation of the core functionality. Radiolabeling of the G5 to G7 dendrimers with ^{99m}Tc enabled them to be visualized in real time as they traversed the bloodstream and organs of healthy rats after injection through the tail vein. It was found that all three dendrimer generations were rapidly and efficiently removed from the bloodstream via the kidneys, and excreted through the bladder within 15 minutes post injection. The clearance half lives for the kidneys and heart/lungs were all below 150 s. The SPECT-CT data was corroborated with a quantitative biodistribution study involving ex-vivo harvesting of various organs and determining the radioactivity within the organs as a function of time post injection. The data from this study indicated rapid clearance through the kidneys, with practically complete elimination of the dendrimers within 15 min. Clearly, this study shows that PMPA dendrimers up to the seventh generation are not retained within any organs of the Copenhagen rats used in this study. The work described here benchmarks the behaviour of these dendrons in vivo, and enables further investigations of their targeting via surface functionalization with a variety of biologically relevant molecules.

5.4. Experimental

5.4.1. Materials and Characterization

Analytical HPLC was performed using a Varian Pro Star model 330 PDA detector, model 230 solvent delivery system, a Bio-Rad IN/US γ-detector and a Varian C-18 nucleosil column. The mobile phase consisted of mixtures of H_2O with 0.1% TFA (solvent A) and acetonitrile with 0.1% TFA (solvent B). The elution protocol consisted of 80:20 ratio of solvent A to solvent B for 5 minutes, followed by a gradient starting at 80:20 (A to B) and finishing at 20:80 (A to B) over 20 minutes. The column was then washed with 100% solvent B for an additional 5 minutes. The product was eluted at a flow rate of 1 mL/min and monitored at a wavelength of 230 nm. Microwave reactions were performed using a Biotage Initiator Sixty instrument. $^{99m}TcO_4^-$ was eluted from a $^{99}Mo/^{99m}Tc$ generator. *Caution.* ^{99m}Tc is a γ-emitter (E_γ = 140 keV, $t_{½}$ = 6h), which should only be used in a licensed and appropriately shielded facility.

5.4.2. SPECT-CT Imaging.

Adult male copenhagen rats (average weight of 275 g) were anesthetized with isoflurane gas. Approximately 37 MBq or 1 mCi of technetium labeled dendron (G-5, G-6, or G-7) was diluted to 1.0 mL saline solution. A bolus injection of this solution was performed intravenously via tail vein. The animals were placed in the supine position on a standard bed of a Gamma Medica Ideas X-SPECT preclinical imaging system. Image acquisition was performed using a dual-head detector system (125 x 125 x 125 mm

reconstruction field of view) with 3-4 mm spatial resolution. Images were collected every 30 seconds for 15 minutes (900 seconds), and every 60 seconds for an addition 45 minutes post injection. Three dimensional images were collected using this dual modality system composed of a CT and SPECT. The CT consists of a 10 x 10 cm detector and a 75 kvp x-ray tube which rotates 360 degrees around the specimen/animal. The resolution of the CT images was 155 μm. The fused SPECT-CT imaging was performed using a low-energy, high resolution collimator over a total of 64 angles around the body (32 angles per detector). Projection data were reconstructed using a filtered back-projection algorithim into a three-dimensional representation of the radioactive dendron distribution. Three dimensional SPECT/CT images of $[^{99m}TcBisPy\text{-}G_7]\text{-}(OH)_{128}^{+}$ were collected over 15 minutes (900 seconds) post injection.

5.4.3 Biodistribution in Healthy Rats.

Adult male copenhagen rats (average weight of 275 g) were injected intravenously via tail vein with 100 μL saline solution of 370 kBq (10.0 μCi) of $[^{99m}TcBisPy\text{-}G_7\text{-}(OH)_{128}]^{+}$. Five rats were sacrificed at each time point of 5, 15, 60, 120 and 360 minutes. The following tissue was harvested, weighed, and the radioactivity was quantified; blood (via heart puncture), heart, lungs, liver, adrenals, kidneys, muscle, stomach, small intestine, stomach, caecum, large intestine, testes, brain, bone, adipose, spleen, trachea/thyroid, skin and eyes. All animal experiments were carried out in accordance with the guidelines set out by the Canadian Council on Animal Care and were approved by the Animal Research Ethics Board of McMaster University.

5.4.4 Synthesis

5.4.4.1. General Radiolabeling Procedure

To a 10 mL Emry microwave vial equipped with a septum 8.5 mg boranyl carbonate ($K_2[BH_3{\bullet}CO_2]$), 4.0 mg sodium carbonate (Na_2HCO_3), 15.0 mg Na/K-tartrate, and 3.0 mg Borax ($Na_2B_4O_7{\bullet}10H_2O$) were added. The vial was sealed and purged with argon gas for 15 minutes. Approximately 925 MBq (25 mCi) of sodium pertechnetate ($Na^{99m}TcO_4$) in 1 mL saline was added to the vial. The reaction was heated in a microwave at 130°C for 3 minutes converting the $Na^{99m}TcO_4$ to $[^{99m}Tc(CO)_3(H_2O)_3]^+$. The reaction was allowed to cool to room temperature when 100 µL of 2.63 M HCl was added to acidify the reaction, bringing the pH between 4.0 and 6.0. A solution of 1-2 mg of dendrimer dissolved in 0.1 mL of water and syringed into the reaction vial. The vial was again heated by microwave at 130°C for an additional 5 minutes. Histidine (200 µL, 200 mM) was added and was heated in a microwave at 150°C for 5 minutes to remove loosely bound technetium. HPLC was used to confirm the conversion of $Na^{99m}TcO_4$ to $[^{99m}Tc(CO)_3(H_2O)_3]^+$and finally the incorporation into the dendrimer. The reaction was allowed to cool to room temperature and the solution was passed through a size exclusion separation package to remove radioactive salts and buffer.

$[^{99m}$TcBisPy-G5-$(OH)_{32}]^+$. The radiolabeling was carried out as mentioned above, specifically boranyl carbonate ($K_2[BH_3{\bullet}CO_2]$) (8.5 mg, 62.5 µmol), sodium carbonate (Na_2HCO_3) (4.0 mg, 37.4 µmol), 15.0 mg Na/K-tartrate (15 mg, 71.4 µmmol), and borax

($Na_2B_4O_7 \bullet 10H_2O$) (3.0 mg, 7.87 μmol) were added to a 10 mL Emry microwave vial. Following a purge with argon gas, approximately 925 MBq (25 mCi) of sodium pertechnetate ($Na^{99m}TcO_4$) in 1 mL saline was added to the vial. The reaction was heated in a microwave at 130°C for 3 minutes. The reaction was allowed to cool to room temperature when 100 μL of 2.63 M HCl was added to the reaction. The dendrimer BisPy-G5-$(OH)_{32}$ (1.0 mg, 257 nmol) was dissolved in 0.1 mL of water, and added to the reaction vial. The vial was heated by microwave at 130°C for 5 minutes. Histidine (200 μL, 200 mM) was added and the reaction was heated in a microwave at 150°C for 5 minutes. The reaction was cooled and passed through a size exclusion separation package to remove radioactive salts and buffer. A small aliquot was injected onto a HPLC equipped with a gamma detector. The reaction was completed three times. Radiochemical Yield (RCY) = 89 ± 0.58 %. HPLC: RT = 16.49 minutes.

[^{99m}TcBisPy-G6-$(OH)_{64}$]$^+$. The radiolabeling was carried out as mentioned above, specifically boranyl carbonate ($K_2[BH_3 \bullet CO_2]$) (8.5 mg, 62.5 μmol), sodium carbonate (Na_2HCO_3) (4.0 mg, 37.4 μmol), 15.0 mg Na/K-tartrate (15 mg, 71.4 μmmol), and borax ($Na_2B_4O_7 \bullet 10H_2O$) (3.0 mg, 7.87 μmol) were added to a 10 mL Emry microwave vial. Following a purge with argon gas, approximately 925 MBq (25 mCi) of sodium pertechnetate ($Na^{99m}TcO_4$) in 1 mL saline was added to the vial. The reaction was heated in a microwave at 130°C for 3 minutes. The reaction was allowed to cool to room temperature when 100 μL of 2.63 M HCl was added to the reaction. The dendrimer BisPy-G6-$(OH)_{64}$ (2.0 mg, 263 nmol) was dissolved in 0.1 mL of water, and added to the

reaction vial. The vial was heated by microwave at 130°C for 5 minutes. Histidine (200 μL, 200 mM) was added and the reaction was heated in a microwave at 150°C for 5 minutes. The reaction was cooled and passed through a size exclusion separation package to remove radioactive salts and buffer. A small aliquot was injected onto a HPLC equipped with a gamma detector. The reaction was completed three times. Radiochemical Yield (RCY) = 70 ± 1.12 %. HPLC: RT = 15.41 minutes.

[^{99m}TcBisPy-G7-(OH)$_{128}$]$^{+}$. The radiolabeling was carried out as mentioned above, specifically boranyl carbonate ($K_2[BH_3{\bullet}CO_2]$) (8.5 mg, 62.5 μmol), sodium carbonate (Na_2HCO_3) (4.0 mg, 37.4 μmol), 15.0 mg Na/K-tartrate (15 mg, 71.4 μmmol), and borax ($Na_2B_4O_7{\bullet}10H_2O$) (3.0 mg, 7.87 μmol) were added to a 10 mL Emry microwave vial. Following a purge with argon gas, approximately 925 MBq (25 mCi) of sodium pertechnetate ($Na^{99m}TcO_4$) in 1 mL saline was added to the vial. The reaction was heated in a microwave at 130°C for 3 minutes. The reaction was allowed to cool to room temperature when 100 μL of 2.63 M HCl was added to the reaction. The dendrimer BisPy-G7-(OH)$_{128}$ (3.0 mg, 200 nmol) was dissolved in 0.1 mL of water, and added to the reaction vial. The vial was heated by microwave at 130°C for 5 minutes. Histidine (200 μL, 200 mM) was added and the reaction was heated in a microwave at 150°C for 5 minutes. The reaction was cooled and passed through a size exclusion separation package to remove radioactive salts and buffer. A small aliquot was injected onto a HPLC equipped with a gamma detector. The reaction was completed three times. Radiochemical Yield (RCY) = 53 ± 2.31 %. HPLC: RT = 14.54 minutes.

5.5 References

(1) Bader, H.; Ringsdorf, H.; Schmidt, B. *Angewandte Makromolekulare Chemie* **1984**, *123*, 457-485.
(2) Ringsdorf, H. *Journal of Polymer Science Part C-Polymer Symposium* **1975**, 135-153.
(3) Kopecek, J. *Polym. Med.* **1977**, *7*, 191-221.
(4) Kopecek, J.; Kopeckova, P.; Minko, T.; Lu, Z. R. *European Journal of Pharmaceutics and Biopharmaceutics* **2000**, *50*, 61-81.
(5) Haag, R.; Kratz, F. *Angewandte Chemie-International Edition* **2006**, *45*, 1198-1215.
(6) Twaites, B.; Alarcon, C. D.; Alexander, C. *Journal of Materials Chemistry* **2005**, *15*, 441-455.
(7) Duncan, R. *Nature Reviews Drug Discovery* **2003**, *2*, 347-360.
(8) Duncan, R. *Nature Reviews Cancer* **2006**, *6*, 688-701.
(9) Park, J. H.; Lee, S.; Kim, J.; Park, K.; Kim, K.; Kwon, I. C. *Progress in Polymer Science* **2008**, *33*, 113-137.
(10) Kopecek, J.; Kopeckova, P.; Minko, T.; Lu, Z. R.; Peterson, C. M. *Journal of Controlled Release* **2001**, *74*, 147-158.
(11) Jensen, K. D.; Nori, A.; Tijerina, M.; Kopeckova, P.; Kopecek, J. *Journal of Controlled Release* **2003**, *87*, 89-105.
(12) Maeda, H.; Wu, J.; Sawa, T.; Matsumura, Y.; Hori, K. *Journal of Controlled Release* **2000**, *65*, 271-284.
(13) Maeda, H.; Seymour, L. W.; Miyamoto, Y. *Bioconjugate Chemistry* **1992**, *3*, 351-362.
(14) Matsumura, Y.; Maeda, H. *Cancer Research* **1986**, *46*, 6387-6392.
(15) Lu, Z. R.; Shiah, J. G.; Sakuma, S.; Kopeckova, P.; Kopecek, J. *Journal of Controlled Release* **2002**, *78*, 165-173.
(16) Khandare, J.; Minko, T. *Progress in Polymer Science* **2006**, *31*, 359-397.
(17) Gillies, E. R.; Frechet, J. M. J. *Drug Discovery Today* **2005**, *10*, 35-43.
(18) Cheng, Y.; Gao, Y.; Rao, T.; Li, Y.; Xu, T. *Comb Chem High T Scr* **2007**, *10*, 336-349.
(19) Crespo, L.; Sanclimens, G.; Pons, M.; Giralt, E.; Royo, M.; Albericio, F. *Chem. Rev.* **2005**, *105*, 1663-1681.
(20) Grinstaff, M. W. *Chem-Eur J* **2002**, *8*, 2838-2846.
(21) Ihre, H. R.; De Jesus, O. L. P.; Szoka, F. C.; Frechet, J. M. J. *Bioconjugate Chem* **2002**, *13*, 443-452.
(22) De Jesus, O. L. P.; Ihre, H. R.; Gagne, L.; Frechet, J. M. J.; Szoka, F. C. *Bioconjugate Chem* **2002**, *13*, 453-461.
(23) Ihre, H.; Hult, A.; Soderlind, E. *Journal of the American Chemical Society* **1996**, *118*, 6388-6395.
(24) Ihre, H.; Hult, A.; Frechet, J. M. J.; Gitsov, I. *Macromolecules* **1998**, *31*, 4061-4068.

(25) Ihre, H.; De Jesus, O. L. P.; Frechet, J. M. J. In *J Am Chem Soc*, 2001; Vol. 123, pp 5908-5917.
(26) Parrott, M. C.; Marchington, E. B.; Valliant, J. F.; Adronov, A. *J Am Chem Soc* **2005**, *127*, 12081-12089.
(27) Lee, C. C.; MacKay, J. A.; Frechet, J. M. J.; Szoka, F. C. *Nat Biotechnol* **2005**, *23*, 1517-1526.
(28) Malik, N.; Evagorou, E. G.; Duncan, R. *Anti-Cancer Drugs* **1999**, *10*, 767-776.
(29) Gillies, E. R.; Dy, E.; chet, J. M. J. F.; Szoka, F. C. *Mol Pharm* **2005**, *2*, 129-138.
(30) Gillies, E. R.; Frechet, J. M. J. *J Am Chem Soc* **2002**, *124*, 14137-14146.
(31) Lee, C. C.; Gillies, E. R.; Fox, M. E.; Guillaudeu, S. J.; Frechet, J. M. J.; Dy, E.; Szoka, F. C. *Proceedings of the National Academy of Sciences of the United States of America* **2006**, *103*, 16649.
(32) Larwood, D. J.; Szoka, F. C. *Journal of Labelled Compounds & Radiopharmaceuticals* **1984**, *21*, 603-614.
(33) Lee, C. C.; Yoshida, M.; Frechet, J. M. J.; Dy, E. E.; Szoka, F. C. *Bioconjugate Chem* **2005**, *16*, 535-541.
(34) Malik, N.; Wiwattanapatapee, R.; Klopsch, R.; Lorenz, K.; Frey, H.; Weener, J. W.; Meijer, E. W.; Paulus, W.; Duncan, R. *J Control Release* **2000**, *65*, 133-148.
(35) Britz-Cunningham, S. H.; Adelstein, S. J. *Journal of Nuclear Medicine* **2003**, *44*, 1945-1961.
(36) Abram, U.; Alberto, R. *J Brazil Chem Soc* **2006**, *17*, 1486-1500.
(37) Stephan, H.; Spies, H.; Johannsen, B.; Gloe, K.; Gorka, M.; Vogtle, F. *Eur J Inorg Chem* **2001**, 2957-2963.
(38) Agashe, H.; Babbar, A.; Jain, S.; Sharma, R.; Mishra, A.; Asthana, A.; Garg, M.; Dutta, T.; Jain, N. *Nanomedicine: Nanotechnology, Biology and Medicine* **2007**, *3*, 120-127.
(39) Waibel, R.; Alberto, R.; Willuda, J.; Finnern, R.; Schibli, R.; Stichelberger, A.; Egli, A.; Abram, U.; Mach, J. P.; Pluckthun, A.; Schubiger, P. A. *Nature Biotechnology* **1999**, *17*, 897-901.
(40) Alberto, R.; Schibli, R.; Egli, A.; Schubiger, A. P.; Abram, U.; Kaden, T. A. *Journal of the American Chemical Society* **1998**, *120*, 7987-7988.
(41) Alberto, R.; Schibli, R.; Schubiger, A. P.; Abram, U.; Pietzsch, H. J.; Johannsen, B. *Journal of the American Chemical Society* **1999**, *121*, 6076-6077.
(42) Alberto, R.; Ortner, K.; Wheatley, N.; Schibli, R.; Schubiger, A. P. *Journal of the American Chemical Society* **2001**, *123*, 3135-3136.
(43) Causey, P. W.; Besanger, T. R.; Scfaffer, P.; Valliant, J. F. *Inorganic Chemistry* **2008**, *In Press*.
(44) Deen, W. M.; Bohrer, M. P.; Brenner, B. M. *Kidney International* **1979**, *16*, 353-365.
(45) Lambert, B.; de Klerk, J. M. H. *Nuclear Medicine Communications* **2006**, *27*, 223-229.
(46) Cyr, J. E.; Pearson, D. A.; Wilson, D. M.; Nelson, C. A.; Guaraldi, M.; Azure, M. T.; Lister-James, J.; Dinkelborg, L. M.; Dean, R. T. *Journal of Medicinal Chemistry* **2007**, *50*, 1354-1364.

Chapter 6: Concluding Remarks and Future Directions

6.1. Concluding Remarks

The two main objectives of this thesis were to develop dendrimers for cancer therapy and to study the biodistribution of these macromolecules in vivo.

The development of dendrimers as potential candidates for cancer therapy was accomplished and detailed in chapter 2. The synthesis and properties of a number of carborane containing aliphatic-polyester dendrimers were investigated for boron neutron capture therapy (BNCT). By utilizing a bifunctional carborane derivative bearing an acid group and a benzyl ether protected alcohol, the incorporation of 4, 8, or 16 carboranes within a dendrimer framework was accomplished. Further dendronization of the macromolecular periphery was used to impart aqueous solubility, and produce three dendrimers with a range of molecular weight (8 – 18 kDa) and boron concentration (5 – 9 wt %). This family of dendrimers has proven to be extremely versatile, allowing complete control over location and number of carborane moieties, as well as overall aqueous solubility. These structures simultaneously combine all the required properties for BNCT including biocompatibility, water solubility, biodegradability, and low toxicity and could therefore serve as potential candidates for BNCT.

An exciting phenomenon was explored with three carborane containing aliphatic-polyester dendrimers in chapter 3. These macromolecular structures were found to exhibit a reversible precipitation at elevated temperatures in aqueous solution. Cloud point temperatures were studied as a function of dendrimer generation, as well as the number

of heating/cooling cycles. In addition, the affect of pH on the cloud point of these materials was investigated. It was found that under mildly acidic conditions, dendrimer cloud points were unaffected. However, under basic conditions, the dendrimers were found to degrade, causing a disappearance of the thermal transition and precipitation of smaller dendrimer fragments.

Monitoring how aliphatic-polyester dendrimers traverse though biological tissue was the second objective of this thesis and was illustrated in chapter 4 and 5. The synthesis of high-generation dendrons, using toluene sulfonyl ethyl (TSe) ester, provided the ability to make dendrons that can be modified at their core carboxylic acid functionality via amidation chemistry. Taking advantage of this core functionality, a bis-pyridyl ligand was introduced within the dendritic structure and provided the necessary precursors for the chelation of radioactive technetium-99m. Radioactive labeling with ^{99m}Tc enabled generation-5, generation-6 and generation-7 dendrimers to be visualized, in real time, using single photon emission computed tomography (SPECT). All three dendrimer generations were rapidly and efficiently removed from the bloodstream via the kidneys, and excreted through the bladder of healthy rats. The SPECT data was corroborated with a quantitative biodistribution study involving ex-vivo harvesting of various organs and determining the radioactivity within the organs as a function of time post injection. The data from this study indicated rapid clearance through the kidneys, with practically complete elimination of the dendrimers within 15 min. Although the elimination of these materials was rather quick, the work described here benchmarks the

behaviour of these dendrons *in vivo*, and enables further investigations of their targeting via surface functionalization with a variety of biologically relevant molecules.

6.2. Future Directions

First and foremost, utilizing the chemistry demonstrated in this thesis one could incorporate carborane cages within a dendrimer capable of chelating a radioactive label such as ^{99m}Tc. This would provide a macromolecular structure that 1) passively targets diseased tissue via the EPR effect, 2) be tracked and imaged *in vivo*, and finally 3) be used to treat diseased tissue by way of boron neutron capture therapy. The development of such a material could lead to breakthrough materials used for multiple applications.

Another area of research would have to focus on increasing the size of these dendrimers. The dendrimer size presents a major issue since material less than 5 nm are rapidly eliminated by the kidneys. The largest dendrimer presented in this work was only 2.8 nm. Therefore, bulk must be added to these materials to insure that they have long circulation times *in vivo*. Increasing the overall size of these materials could be accomplished by further dendronization or by covalent attachment of biocompatible polymers such as poly(ethylene glycol), (PEG) to the dendrimer surface.

An area not yet explored in this work is to exploit the multifunctionality of these dendrimers by attaching multiple targeting vectors to their periphery. The addition of small targeting molecules would allow for active targeting of the dendrimer to diseased tissue. This would also increase the dendrimer accumulation within diseased tissue and cellular internalization.

Finally, dendrimers only represents one type of architecture used in polymer chemistry. By exploring linear polymers, graft polymers, branched polymers, hyper-branched polymers and dendronized polymer, novel and facile methods of incorporating these properties within different polymeric structures can be achieved.